ICOSAHEDRAL SYMMETRY And Its Application To Possible Models of the Fullerene Molecule C_{60}

Hajar Haji Abu Bakar

M.Sc

Thesis submitted for the degree of

Doctor of Philosophy

Department of Mathematics

The City University

London

July 1993

Contents

Plate I

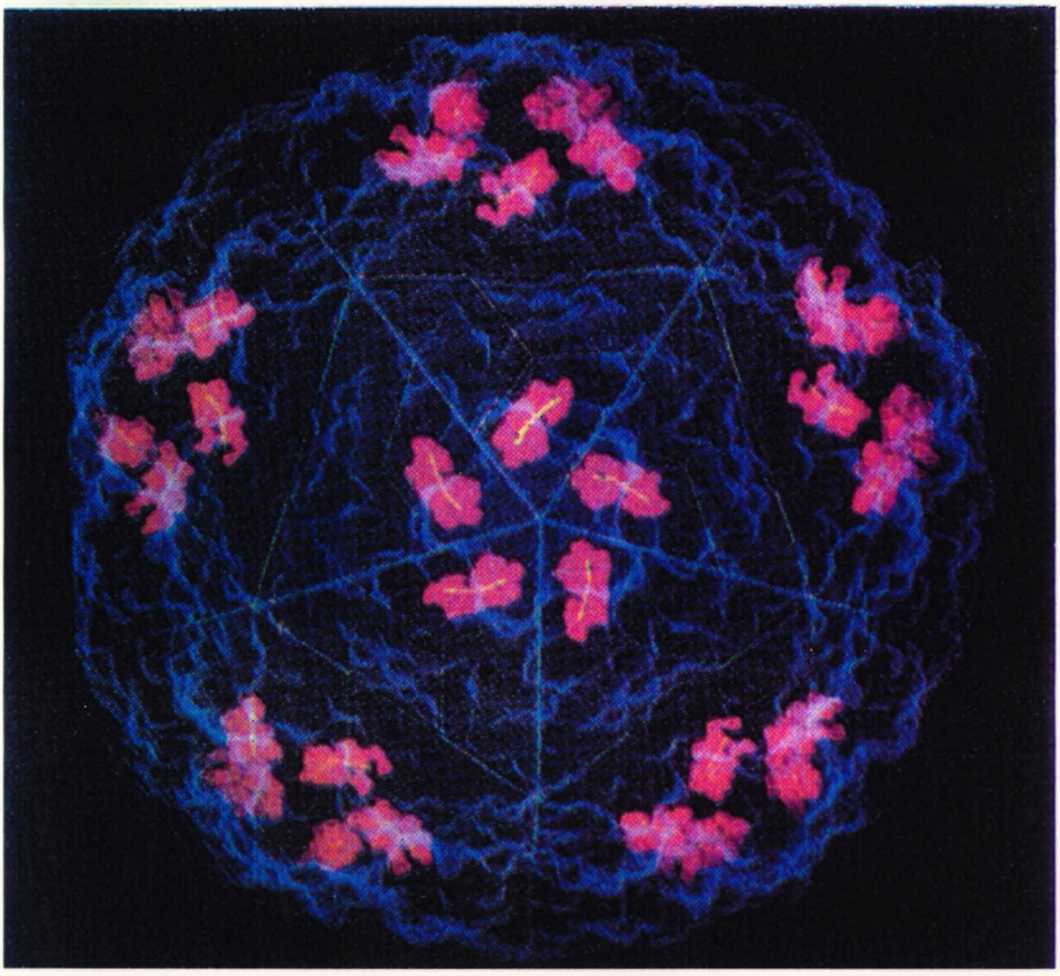

Virus blocker viewed from the vertex perspective of a regular icosahedron [26].

List of Tables

List of Figures

Acknowledgements

The author wishes to express sincere gratitude to her main supervisor, Professor M.A. Jaswon, for his unceasing encouragement and excellent supervision in the preparation of this work; and to Dr. T.E. Stanley, deputy who provided brilliant guidance on Group Theory and valuable editorial comments on my drafts.

Acknowledgements are due to *University of Malaya* (JPA/UM) for sponsoring this research; to my dearest **mum and dad** without whose patient encouragement, this thesis could never have been completed; to all my siblings, Ir. Abdul Halim, Mislamah, Abdullah and Khalijah, for the helpful interest at all times; and to SERC and City University funds for the completion of this manuscript.

Thanks are due to Dr. M.A. Villeret for providing such a superb model of the buckyball, which she obtained at the Spring Meeting of the Materials Research Society and for a wonderful companionship; last but not least, thanks are due to Professor P.G. Daniels as Head of the Department for helpful advice during my difficult moments.

Abstract

A convenient rectangular cartesian coordinate system is constructed for the regular icosahedron. This allows us to write down the coordinates of every vertex, so enabling the direction-ratios of all the symmetry axes to be obtained. Our results afford a fresh approach to various geometrical features of the icosahedron and of the icosahedral group.

The circumsphere of a regular icosahedron may be converted into possible models for the spherical carbon molecule C_{60} (the buckyball), by expanding the 12 vertex points into 12 regular spherical pentagons of equal size. We examine quantitatively the changing pentagonal-hexagonal pattern as the pentagon size expands up to the possible maximum, at which stage the circumsphere is entirely covered with pentagons i.e. is the circumsphere of a regular dodecahedron. Arguments are given for a unique choice model which conforms to the chemical data.
Prolate spheroid models for C_{70} and C_{80} are also considered.

Introduction

The regular icosahedron is one of the five Platonic solids known to the early Greeks. However it attracted little attention until the nineteenth century, when 5–fold symmetry axes were found to be inadmissible in mathematical crystallography. Despite this the icosahedral point-group is sometimes listed as a supplement to the classical crystallographic point-groups since it forms a natural extension of these point-groups. It may be mentioned that the German mathematician Felix Klein [21] wrote a monograph on the icosahedron, but its orientation appears to be algebraic rather than geometrical.

The icosahedron was introduced into crystal physics in 1952, when F.C. Frank [22] pointed out that this configuration provides an efficient method of close-packing for atoms which would be favoured on energetic grounds. More than thirty years later [23], the existence of icosahedral configurations in an aluminium-manganese alloy was inferred from the appearance of X-ray diffraction patterns exhibiting 5–fold symmetry features. These could not be produced by a crystalline medium, but one might envisage icosahedral clusters having a short-range order ($\sim 10^4 - 10^5\,\mathring{A}$) which does not build up into any long-range order, so forming a quasi-crystalline medium intermediate between a crystal and an amorphous solid. Quasicrystals of various composition have been fabricated since then, but no generally accepted theory of their structure has yet emerged [24]–[25]. It is of course well known that some virus structures adopt the icosahedral configuration, e.g. as appears in Plate I (following Table of Contents).

This thesis divides naturally into two main parts. Part I treats icosahedral symmetry (covering also the dodecahedron) by methods of algebraic geometry. Part II uses the methods and results of Part I essentially to examine the buckyball model of C_{60}, i.e. the spherical carbon molecule now known as fullerene, discovered by

Kroto and Smalley [27]–[28] in 1985. The buckyball is often depicted as a truncated icosahedron, with the vertices replaced by regular pentagons. An equivalent, but mathematically more convenient picture, is to regard it as the circumsphere of the icosahedron, with the 12 vertices expanded into 12 spherical pentagons. These automatically carve out 20 spherical hexagons from the 20 spherical triangles on the original circumsphere, so yielding the familiar football pattern. This point of view enables us to determine the coordinates of any pentagonal vertex (i.e. of any carbon atom) referred to rectangular cartesian axes embedded in the icosahedron. Two independent parameters enter into the coordinates: the circumsphere radius R and the pentagon shallowness f. A computer program then calculates the ratio $d(6{:}6)$ / $d(6{:}5)$ of the two characteristic C–C bond lengths as a function of f, running from $f \simeq 0$ (vanishingly small pentagons) to $f = 0.141$ (vanishingly small hexagons), keeping R fixed. Our results are used to examine various features of the buckyball model, in particular how its radius varies with bond length yielding excellent agreement with the experimental data.

If we input the graphite data $d(6{:}5) = d(6{:}6) = 1.420$ $\mathring{A}$ into the model, it provides a pattern of 20 perfectly regular hexagons on the circumsphere accomodated by 12 perfectly regular pentagons yielding a surprisingly close approximation to the observed buckyball radius. It appears that the first stage of buckyball formation involves a graphite pattern for the hexagons, which are then distorted from regularity by physical factors [29] dependent upon the curvature of the π-orbitals in C_{60} as compared with graphite. Models of C_{70} and C_{80} may be constructed building upon that for C_{60}. These are prolate spheroids for which the axial ratios can be readily calculated. A useful schematic method for exhibiting the pentagon-hexagon patterns in these fullerenes is presented.

The main original contribution of this thesis is in Part II. This part provides a fresh mathematical analysis of the buckyball so that we are able to predict the observed dimensions of the buckyball in terms of operative C–C bond lengths. Building upon this, we construct models for C_{70} and C_{80} using a new method of pattern representation. Much of Part I may be regarded as preparatory for the work of Part II. In the first place, it includes a general review of the field. Also we introduce a convenient rectangular coordinate system into the icosahedron, which allows us to

assign direction-ratios to various symmetry axes operative in the buckyball. The regular dodecahedron is discussed from a similar point of view to that of the regular icosahedron, which provides a model for the hypothetical molecule C_{20}.

To summarise, this thesis places the buckyball model of C_{60} on a rigorous mathematical foundation by relating it more closely to the underlying regular icosahedron.

Part I

ICOSAHEDRAL SYMMETRY

Chapter 1

The Five Regular Solids

1.1 Introduction

For many decades the five regular solids have been prominent aesthetic figures in pure and applied mathematical research as well as the subjects of interest to artists, architects, chemists and crystallographers. Playing a key role in Plato's cosmology, the five regular solids comprise the regular tetrahedron, the cube and octahedron, the regular icosahedron and dodecahedron; they are also conventionally known as the five Platonic solids.

Physical features corresponding to these solids are displayed in Table 1.1. Note that the cube and octahedron are complementary to each other since the number of vertices is interchangeable with the number of faces. By the same reasoning, the regular icosahedron and dodecahedron are also complementary to each other. Furthermore, the centroid, O, for these four solids is in fact the centre of symmetry of the solid since any vertex can be inverted into the symmetrically opposite vertex through O. However, the tetrahedron is self-complementary and its centroid is not a centre of symmetry. We observe that its centroid joins any vertex into the centroid of the opposite face, which makes it special as a foundation for further development in the analysis of fullerene C_{28}–chemical name for the carbon molecule having 28

Regular Solids	V	F	E	p (*number of sides in a face*)	q (*number of edges meeting in a vertex*)	$\{p,q\}$
Tetrahedron	4	4	6	3	3	{3,3}
Cube	8	6	12	4	3	{4,3}
Octahedron	6	8	12	3	4	{3,4}
Icosahedron	12	20	30	3	5	{3,5}
Dodecahedron	20	12	30	5	3	{5,3}

Table 1.1: $\{p,q\}$ signifies a regular solid with $\{p\}$-gon faces and q edges meeting in a vertex. Note that p, q are interchanged for the cube and octahedron i.e. they are complementary solids. The same property holds for the icosahedron and dodecahedron. Here V denotes the number of vertices, F the number of faces and E the number of edges of a regular solid.

atoms. More important, the regular icosahedron deserves special mention as it effectively provides a basis for further studies of fullerene C_{60}–known to be the most stable carbon molecule among the fullerides.

1.2 Spheres Related To The Regular Solids

Within each regular polyhedron the centroid, O, is the common centre of three spheres:

1. The circumsphere which passes through all the vertices. This has a radius

$$R = l \, csc \, \phi \tag{1.2.1}$$

where $2\ l$ = edge length of polyhedron
and $2\ \phi$ = angle subtended at O by an edge.

2. The midsphere which touches all the edges at their midpoints. This has a radius

$$R_{md} = R \cos \phi = l \cot \phi \tag{1.2.2}$$

3. The insphere which touches all the faces at their centres. For the $\{p,q\}$ solid this has a radius given by

$$R_{in}^2 = l^2 \left(\csc^2 \phi - \csc^2 \frac{\pi}{p} \right) = l^2 \left(\cot^2 \phi - \cot^2 \frac{\pi}{p} \right). \tag{1.2.3}$$

To prove these formulae we imagine the solid as built up from F equal pyramids, each based upon a face of the solid and sharing a common apex at O. Any $\{p,q\}$ face is a regular polygon $C_1 \ldots C_p$, centre C, with $\mid C_1C_2 \mid = 2\ l$ and $C_1\widehat{C}C_2 = \frac{2\pi}{p}$ as depicted in Figure 1.1. Also, associated with the edge C_1C_2 there exists a triangular side face C_1OC_2 of the pyramid with $\mid OC_1 \mid = \mid OC_2 \mid = R$ and $C_1\widehat{O}C_2 = 2\ \phi$ as depicted in Figure 1.2 which immediately yields formulae (1.2.1), (1.2.2) above. A useful figure associated with the pyramid is the Schläfli tetrahedron OC_1MC

depicted in Figure 1.3, where OC marks the normal from O onto $C_1 \ldots C_p$ being therefore at right angles to both CM and CC_1, i.e.

$$\begin{aligned} R_{in}^2 &= \mid OC \mid^2 = \mid OC_1 \mid^2 - \mid CC_1 \mid^2 \\ &= R^2 - l^2 \csc^2 \frac{\pi}{p} \\ &= l^2 \left(\csc^2 \phi - \csc^2 \frac{\pi}{p} \right) \end{aligned} \tag{1.2.4}$$

from Figure 1.1 (a) or equivalently

$$\begin{aligned} R_{in}^2 &= \mid OC \mid^2 = \mid OM \mid^2 - \mid CM \mid^2 \\ &= R_{md}^2 - l^2 \cot^2 \frac{\pi}{p} \\ &= l^2 \left(\cot^2 \phi - \cot^2 \frac{\pi}{p} \right) \end{aligned} \tag{1.2.5}$$

as noted above.

We now prove the Coxeter formula [1]

$$\cos \phi = \cos \frac{\pi}{p} \csc \frac{\pi}{q} \tag{1.2.6}$$

and its complementary formula

$$\cos \psi = \cos \frac{\pi}{q} \csc \frac{\pi}{p} \tag{1.2.7}$$

where $\pi - 2\psi$ is the dihedral angle of $\{p,q\}$. Choosing any vertex P as pole vertex we observe that OP defines a q-fold symmetry axis for $\{p,q\}$. This means that P has q neighbouring vertices $A_1 \ldots A_q$ (Figure 1.4) forming a $\{q\}$ polygon intersected at its centre A by OP.

If so

$$\mid AA_1 \mid = \frac{\frac{1}{2} \mid A_1 A_2 \mid}{\sin \frac{\pi}{q}} \tag{1.2.8}$$

(a) Note that

$| CC_1 | = \frac{1}{2} | C_1C_2 | \csc \frac{\pi}{p}$

i.e. $c = l \csc \frac{\pi}{p}$.

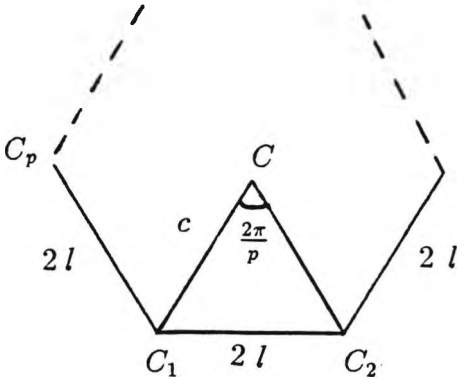

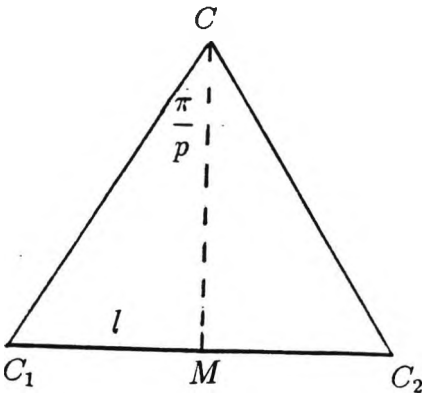

(b) Note

$| CM | = | C_1M | \cot \frac{\pi}{p} = l \cot \frac{\pi}{p}$

$\Longrightarrow$ area of $\triangle C_1CC_2 = l^2 \cot \frac{\pi}{p}$.

Figure 1.1: Base plane of pyramid C_1, C_2, ... C_p.

(a) $| OC_1 | = l \csc \phi$ i.e. $R = l \csc \phi$,

(b) $| OM | = | C_1M | \cot \phi$ i.e. $R_{md} = l \cot \phi$.

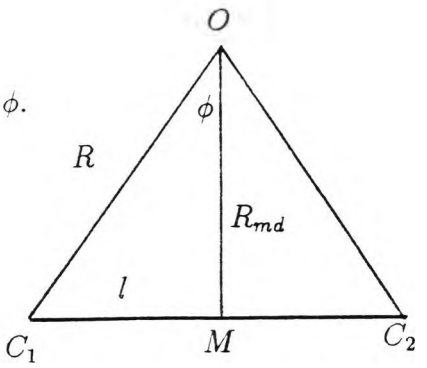

Figure 1.2: Side-face of pyramid $OC_1C_2 \ldots C_p$.

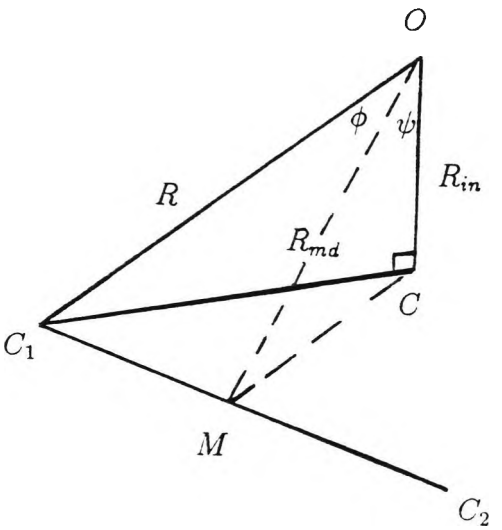

Note that

(a) $| OC |^2 = | OC_1 |^2 - | CC_1 |^2$

i.e. $R_{in}^2 = R^2 - l^2 \csc^2 \frac{\pi}{p}$

from Figure 1.1 (a),

OR (b) $| OC |^2 = | OM |^2 - | CM |^2$,

see equation (1.2.5).

Figure 1.3: Schläfli tetrahedron of $\{p,q\}$.

(a) q symmetry axis OP generates
a $\{q\}$-gon $A_1 \ldots A_q$,

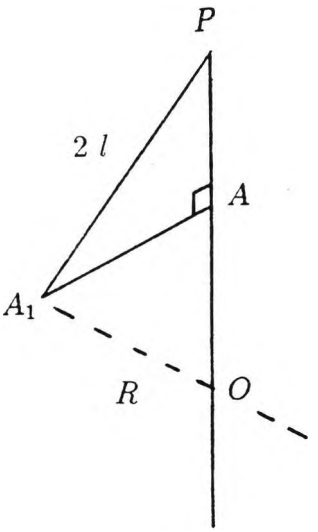

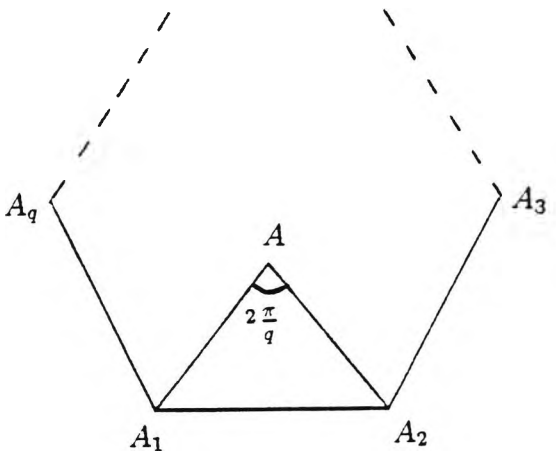

Note that
(b) $| AA_1 | = \frac{1}{2} | A_1A_2 |$ csc $\frac{\pi}{q}$
as indicated in Figure 1.1 (a)
with p replaced by q.

Figure 1.4: $\{q\}$-gon associated with vertex P of $\{p,q\}$.

from Figure 1.4 (b) where

$$| A_1A_2 | = 4\, l \cos \frac{\pi}{p} \tag{1.2.9}$$

bearing in mind that PA_1, PA_2 are two neighbouring edges of a face i.e. of a $\{p\}$ polygon (Figure 1.5). Reference to Figure 1.6 shows that

$$\sin 2\phi = \frac{| AA_1 |}{| OA_1 |} = \frac{\frac{1}{2} \bullet 4\, l \cos \frac{\pi}{p}}{\sin \frac{\pi}{q}} \bullet \frac{\sin \phi}{l} \tag{1.2.10}$$

since $| OA_1 | = R$

$$\Longrightarrow \cos \phi = \frac{\cos \frac{\pi}{p}}{\sin \frac{\pi}{q}} \tag{1.2.11}$$

as stated earlier in (1.2.6). Formula (1.2.7) follows from the complementary nature of ϕ, ψ so that utilising formula (1.2.11) provides

$$\begin{aligned} \sin^2 \phi &= 1 - \frac{\cos^2 \frac{\pi}{p}}{\sin^2 \frac{\pi}{q}} \\ &= \frac{\sin^2 \frac{\pi}{q} - \cos^2 \frac{\pi}{p}}{\sin^2 \frac{\pi}{q}} \\ &= \frac{k^2}{\sin^2 \frac{\pi}{q}} \qquad ; k^2 = \sin^2 \frac{\pi}{q} - \cos^2 \frac{\pi}{p}, \end{aligned} \tag{1.2.12}$$

i.e.

$$\sin \phi = \frac{k}{\sin \frac{\pi}{q}} . \tag{1.2.13}$$

If so,

$$R = \frac{l}{\sin \phi} = \frac{l}{k} \sin \frac{\pi}{q} , \; R_{md} = \frac{l}{k} \cos \frac{\pi}{p} \tag{1.2.14}$$

Note that

$A_1\widehat{P}A_2 = \pi - \frac{2\pi}{p}$ from Figure 1.1 (a),

$\Longrightarrow \mid A_1A_2 \mid = 2\,PA_1 \mid \sin\left(\frac{\pi}{2} - \frac{\pi}{p}\right)$

$\equiv 2 \bullet 2\,l \cos\frac{\pi}{p} = 4\,l \cos\frac{\pi}{p}$ showing

that $\mid AA_1 \mid = \frac{1}{2} \bullet 4\,l \cos\frac{\pi}{p} \csc\frac{\pi}{q}$.

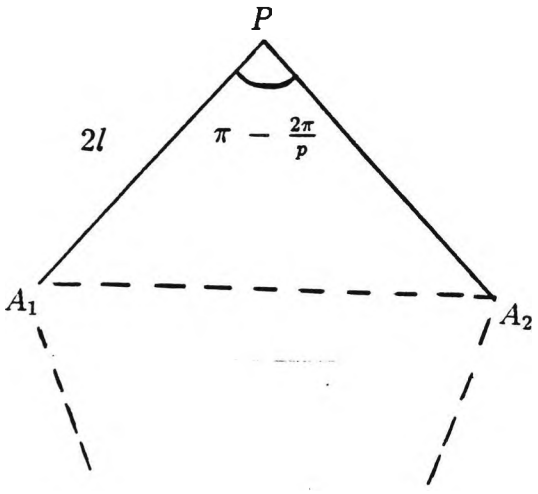

Figure 1.5: Face of $\{p,q\}$ defined p edges PA_1, PA_2.

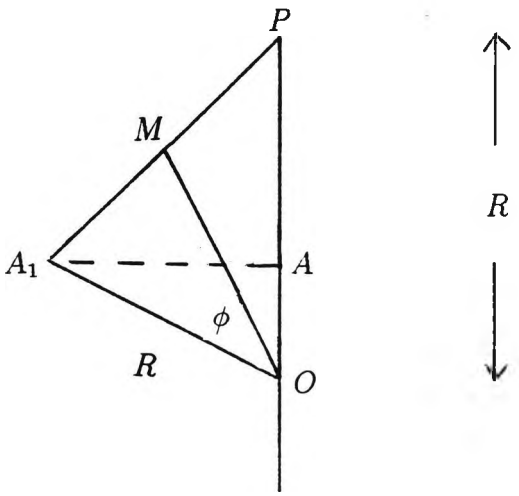

Figure 1.6: Elevation of PA_1A showing $A_1\widehat{O}M = \phi$ which is half of the angle subtended by an edge at the centre, O, so that $\sin 2\phi = \frac{|AA_1|}{|OA_1|}$.

Also,

$$R_{in}^2 = l^2 \left(\frac{1}{\sin^2 \phi} - \frac{1}{\sin^2 \frac{\pi}{p}} \right) = l^2 \left(\frac{\sin^2 \frac{\pi}{q}}{k^2} - \frac{1}{\sin^2 \frac{\pi}{p}} \right)$$

$$= \frac{l^2}{k^2 \sin^2 \frac{\pi}{p}} \left(\sin^2 \frac{\pi}{q} \sin^2 \frac{\pi}{p} - k^2 \right)$$

$$= \frac{l^2}{k^2 \sin^2 \frac{\pi}{p}} \left(\cos^2 \frac{\pi}{p} \cos^2 \frac{\pi}{q} \right)$$

$$= \frac{l^2}{k^2} \cot^2 \frac{\pi}{p} \cos^2 \frac{\pi}{q} \tag{1.2.15}$$

which implies

$$R_{in} = \frac{l}{k} \cot \frac{\pi}{p} \cos \frac{\pi}{q} \tag{1.2.16}$$

Finally, from Figure 1.3

$$\cos \psi = \frac{R_{in}}{R_{md}} = \frac{l}{k} \cot \frac{\pi}{p} \cos \frac{\pi}{q} \bullet \frac{k}{l \cos \frac{\pi}{p}}$$

$$= \frac{\cos \frac{\pi}{q}}{\sin \frac{\pi}{p}} \tag{1.2.17}$$

showing that ϕ, ψ, R, R_{md}, R_{in} for $\{p,q\}$ are all known in terms of p and q.

The value of k for each $\{p,q\}$ is given in Table 1.2 since it will be needed in the following section.

1.3 Surface Area And Volume Of $\{p,q\}$

A $\{p\}$–gon is made up of p isosceles triangles each of area $l^2 \cot \frac{\pi}{p}$ (Figure 1.1), so that a $\{p\}$–gon has the surface area $pl^2 \cot \frac{\pi}{p}$.

$\{p,q\}$	$\sin^2\frac{\pi}{q} - \cos^2\frac{\pi}{p} = \sin^2\frac{\pi}{p} - \cos^2\frac{\pi}{q}$	k^2	$\sim k$
$\{3,3\}$	$\sin^2\frac{\pi}{3} - \cos^2\frac{\pi}{3} = \frac{3}{4} - \frac{1}{4}$	$\frac{1}{2}$	0.707107
$\{4,3\}$	$\sin^2\frac{\pi}{3} - \cos^2\frac{\pi}{4} = \frac{3}{4} - \frac{1}{2}$	$\frac{1}{4}$	0.500000
$\{3,4\}$	$\sin^2\frac{\pi}{4} - \cos^2\frac{\pi}{3} = \frac{1}{2} - \frac{1}{4}$	$\frac{1}{4}$	0.500000
$\{3,5\}$	$\sin^2\frac{\pi}{5} - \cos^2\frac{\pi}{3} = \frac{(5-\sqrt{5})}{8} - \frac{1}{4}$	$\frac{(3-\sqrt{5})}{8}$	0.309017
$\{5,3\}$	$\sin^2\frac{\pi}{3} - \cos^2\frac{\pi}{5} = \frac{3}{4} - \frac{(3+\sqrt{5})}{8}$	$\frac{(3-\sqrt{5})}{8}$	0.309017

Table 1.2: Approximate value of k for each $\{p,q\}$. Note that $k^2\{p,q\} = k^2\{q,p\}$.

Therefore

$$S = \text{surface area of } \{p,q\}$$

$$= F \bullet pl^2 \cot \frac{\pi}{p} \tag{1.3.1}$$

from which

$$V = \text{volume of } \{p,q\}$$

$$= S \bullet \frac{R_{in}}{3}. \tag{1.3.2}$$

Formula (1.3.2) may be rewritten in the useful form

$$\frac{S}{V} = \frac{3}{R_{in}} \tag{1.3.3}$$

which compares with the value

$$\frac{4\,\pi\sigma^2}{\frac{4}{3}\,\pi\sigma^3} = \frac{3}{\sigma} \tag{1.3.4}$$

for a sphere of radius σ.

There exists a surface-equivalent sphere to $\{p,q\}$ with radius σ defined by

$$4\,\pi\sigma^2 = S \;\; i.e. \;\; \sigma = \sqrt{\frac{S}{4\pi}}. \tag{1.3.5}$$

Now

$$\frac{\frac{4}{3}\,\pi\,\sigma^3}{V} = \frac{\frac{4}{3}\,\pi\,\sigma^3}{4\,\pi\,\sigma^2} \bullet \frac{S}{V} = \frac{\sigma}{3} \bullet \frac{3}{R_{in}}$$

$$= \frac{\sigma}{R_{in}} \tag{1.3.6}$$

where σ/R_{in} is computed in Appendix A. We find $\sigma/R_{in} > 1$ for each $\{p,q\}$, showing that the surface-equivalent sphere always has a greater volume than that of the corresponding $\{p,q\}$.

Similarly there exists a volume-equivalent sphere to $\{p,q\}$, with radius ρ defined by

$$\frac{4}{3}\pi\rho^3 = V, \quad i.e. \quad \rho = \left(\frac{3V}{4\pi}\right)^{1/3}. \tag{1.3.7}$$

Now

$$\frac{4\pi\rho^2}{S} = \frac{4\pi\rho^2}{\frac{4}{3}\pi\rho^3} \bullet \frac{V}{S} = \frac{3}{\rho} \bullet \frac{R_{in}}{3}$$

$$= \frac{R_{in}}{\rho} \tag{1.3.8}$$

where this ratio is also computed in Appendix A. We find $R_{in}/\rho < 1$ for each $\{p,q\}$ showing that volume-equivalent sphere has a smaller surface area than that of the corresponding $\{p,q\}$.

Our two conclusions can be summarized as follows:

- for a given *surface area*, the sphere has a *greater volume* than any $\{p,q\}$;
- for a given *volume*, the sphere has a *smaller surface* area than any $\{p,q\}$.

[2. Polya and Szego]

Tables of $\frac{S}{l^2}$, $\frac{V}{l^3}$, $\frac{R_{in}}{l}$, $\frac{\sigma}{l}$, $\frac{\rho}{l}$, $\frac{\sigma}{R_{in}}$, $\frac{R_{in}}{\rho}$ are given in Appendix A for further verification of these corresponding results.

Chapter 2

The Regular Icosahedron

2.1 Rectangular Coordinate System

As already mentioned, the centroid O of every regular solid (except the tetrahedron) serves as a centre of symmetry for the solid i.e. it inverts any vertex P into the symmetrically opposite vertex P' (Figure 2.1). In the case of a regular icosahedron this suggests that a convenient rectangular coordinate system may be constructed with O as origin and OP as the z-axis (Figure 2.2). As regard the x, y-axes, we note that P has five nearest neighbouring vertices forming a regular pentagon A_1, A_2, ..., A_5 with centre A as depicted in Figure 2.3. Clearly PP' is normal to the pentagon and passes through its centre A. If so the x-axis can be chosen to pass through O parallel to AA_1 (Figure 2.4), and the y-axis then passes through O at right angles to OX.

Since $\angle A_1AA_2 = \frac{2\pi}{5}$, it follows from the isosceles triangle A_1AA_2 (Figure 2.5) that

$$| A_1A_2 | = 2 | AA_1 | \sin\frac{\pi}{5}, \quad i.e. \quad 2l = 2a \sin\frac{\pi}{5} \tag{2.1.1}$$

where

$$\begin{aligned} | A_1A_2 | &= \text{edge length of icosahedron} \equiv 2l = | PA_1 |, \text{ etc.} \\ | AA_1 | &= \text{circumradius of pentagon} \equiv a \end{aligned} \tag{2.1.2}$$

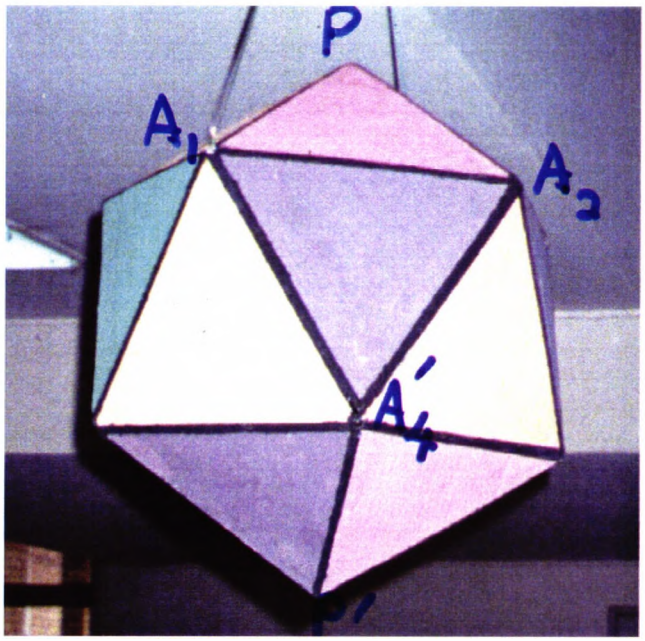

Figure 2.1: Photoprint of a regular icosahedron showing the inversion of pole vertex P into opposite P'.

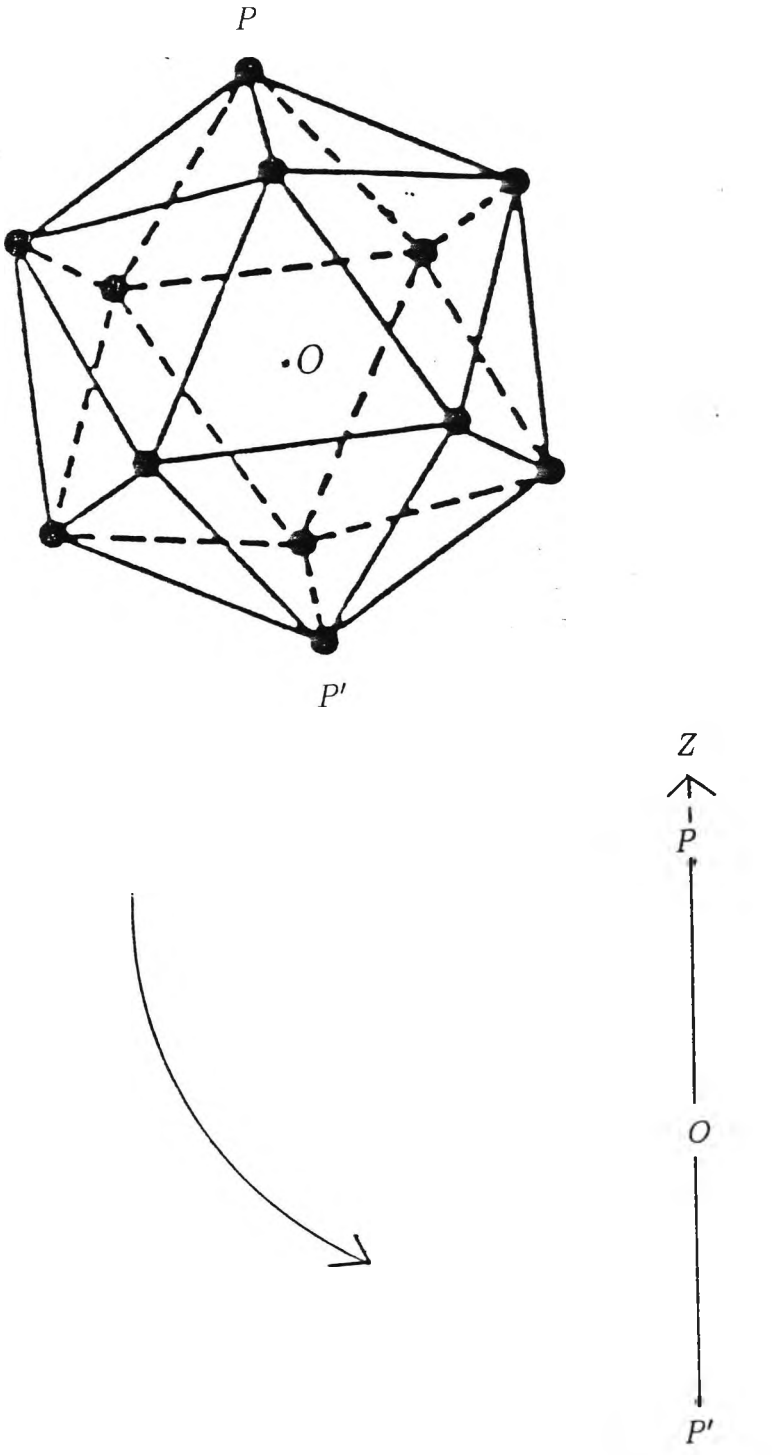

Figure 2.2: Choice of OP as the z-axis for the rectangular coordinate system of the regular icosahedron, alongside its 'wire' model [3].

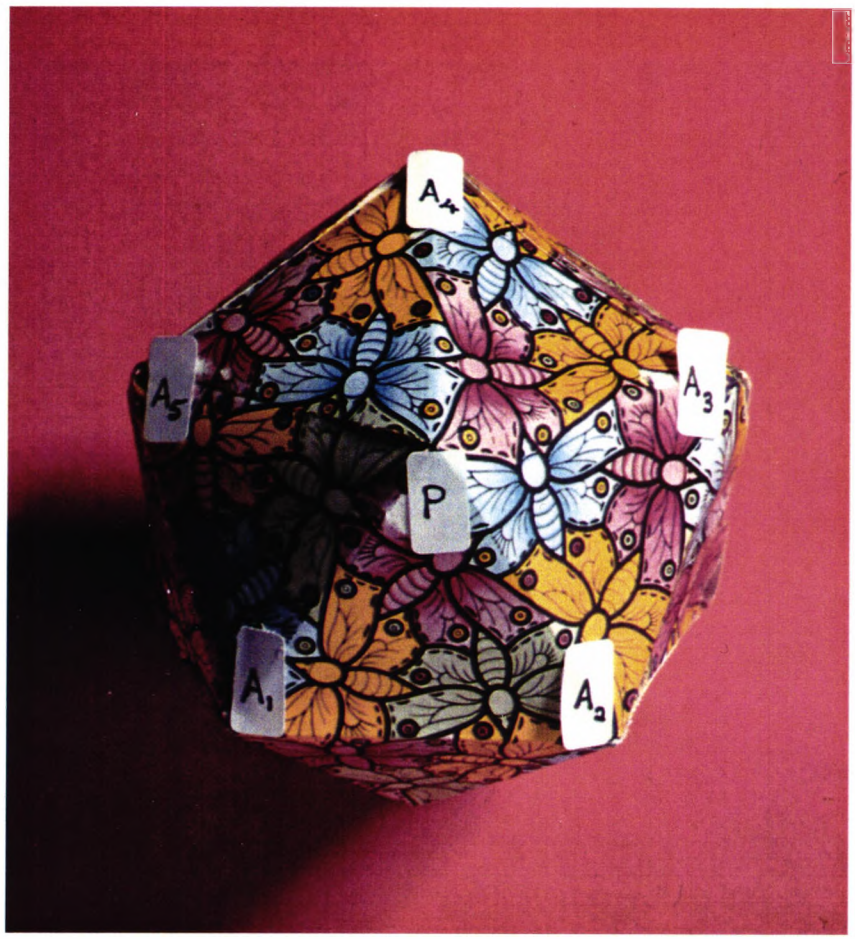

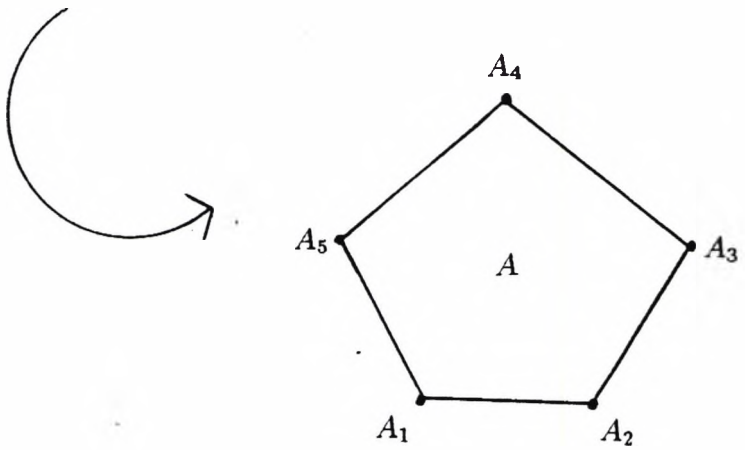

Figure 2.3: Icosahedral pentagon with centre A viewed along PP'.

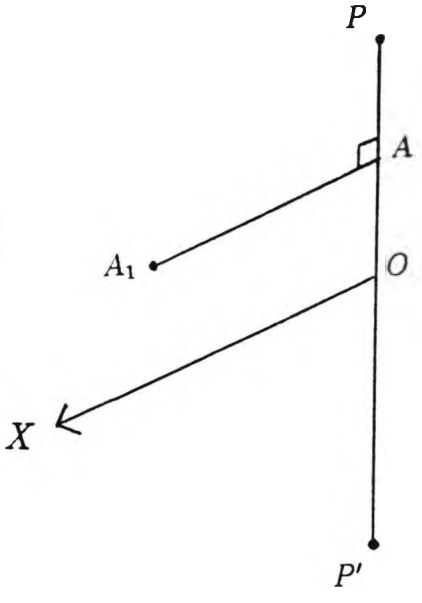

Figure 2.4: Choice of z-axis and x-axis in relation to OP, AA_1 respectively.

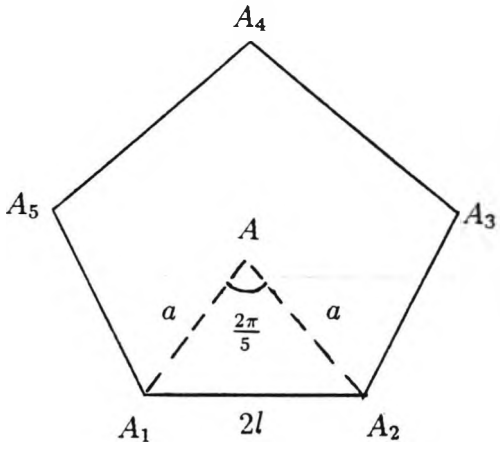

Figure 2.5: Isosceles triangle A_1AA_2 in the A-pentagon with centre A, formed by 5 edges emanating from P.

which implies

$$a = \frac{l}{\sin\frac{\pi}{5}} = l\csc\frac{\pi}{5} \tag{2.1.3}$$

Within the A-plane, all vertices may be conveniently represented by the complex vectors

$$\vec{AA_1} = a\,e^{i0},\ \vec{AA_2} = a\,e^{2i\pi/5},\ldots \tag{2.1.4}$$

which may be readily broken down into x, y components. However, it remains to compute their z-coordinates. By reference to Figure 2.6

$$\begin{aligned} |\,AP\,|^2 &= |\,A_1P\,|^2 - |\,A_1A\,|^2 \\ &= 4l^2 - a^2 \\ &= 4\left(a\sin\frac{\pi}{5}\right)^2 - a^2 \\ &= a^2\left(4\sin^2\frac{\pi}{5} - 1\right) \end{aligned} \tag{2.1.5}$$

We prove (see Appendix B) that

$$\left(4\sin^2\frac{\pi}{5} - 1\right)^{1/2} = 2\cos\frac{2\pi}{5} = \tau^{-1} > 0 \tag{2.1.6}$$

where τ is the golden mean and τ satisfies the quadratic equation

$$\tau^2 - \tau - 1 = 0. \tag{2.1.7}$$

Now all the vertices lie on a circumsphere, as mentioned earlier, with centre O, radius R so that (Figure 2.7)

$$\begin{aligned} R^2 = |\,OP\,|^2 &= (|\,OA\,| + |\,AP\,|)^2 \\ &= |\,OA\,|^2 + 2\,|\,OA\,|\,|\,AP\,| + |\,AP\,|^2 \end{aligned} \tag{2.1.8}$$

and also

$$R^2 = | OA_1 | = | OA |^2 + | AA_1 |^2 = | OA |^2 + a^2 \tag{2.1.9}$$

Equating (2.1.8) and (2.1.9) for R^2 and utilising $| AP |^2$, $| AP |$ gives

$$| OA | = a \frac{(1 - 2 \sin^2 \frac{\pi}{5})}{(4 \sin^2 \frac{\pi}{5} - 1)^{1/2}} = \frac{a}{2} \tag{2.1.10}$$

i.e. z–coordinate of A_1, A_2, ..., A_5. An alternative expression of $| OA |$ is

$$a \left(\sin^2 \frac{\pi}{5} - \sin^2 \frac{\pi}{10} \right)^{1/2} = \frac{a}{2} \tag{2.1.11}$$

as also may be readily verified in Appendix B.

Using (2.1.4), (2.1.10) we obtain the x, y, z coordinates of each vertex as listed in Table 2.1. Since x, y, z inverts into -x, -y, -z we immediately obtain the coordinates of A'_1, A'_2, ..., A'_5, centre A'. These vertices form a regular pentagon rotated by an angle $\frac{\pi}{5}$ to the A-pentagon (Figure 2.7), and separated from it by the distance

$$| AA' | = 2 | OA | = a \equiv | AA_1 | \tag{2.1.12}$$

as illustrated in Figure 2.8. Now

$$\begin{aligned} R &= | OA | + | AP | \\ &= a \frac{\left(1 - 2 \sin^2 \frac{\pi}{5}\right)}{\left(4 \sin^2 \frac{\pi}{5} - 1\right)^{1/2}} + a \left(4 \sin^2 \frac{\pi}{5} - 1\right)^{1/2} \\ &= a \frac{2 \sin^2 \frac{\pi}{5}}{\left(4 \sin^2 \frac{\pi}{5} - 1\right)^{1/2}} \end{aligned} \tag{2.1.13}$$

Substituting (2.1.3) into R, we have

$$R = l \frac{2 \sin \frac{\pi}{5}}{\left(4 \sin^2 \frac{\pi}{5} - 1\right)^{1/2}}$$

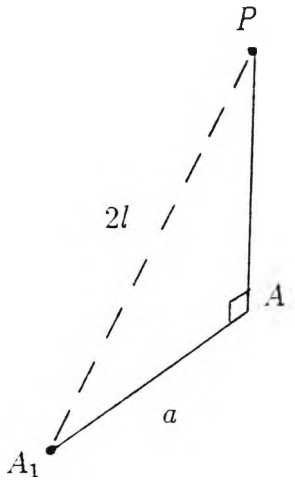

Figure 2.6: The orthogonal projection of P on its pentagonal plane is associated with the relation $\mid A_1P \mid^2 - \mid A_1A \mid^2 = \mid AP \mid^2$, ... such that $4\,l^2 - a^2 = \mid AP \mid^2$, ...

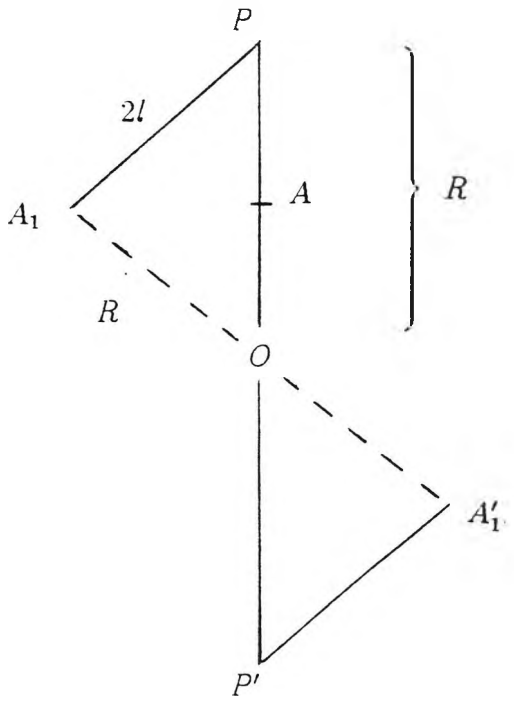

Figure 2.7: Transformation of the vertex A_1 into its corresponding inverse A_1'.

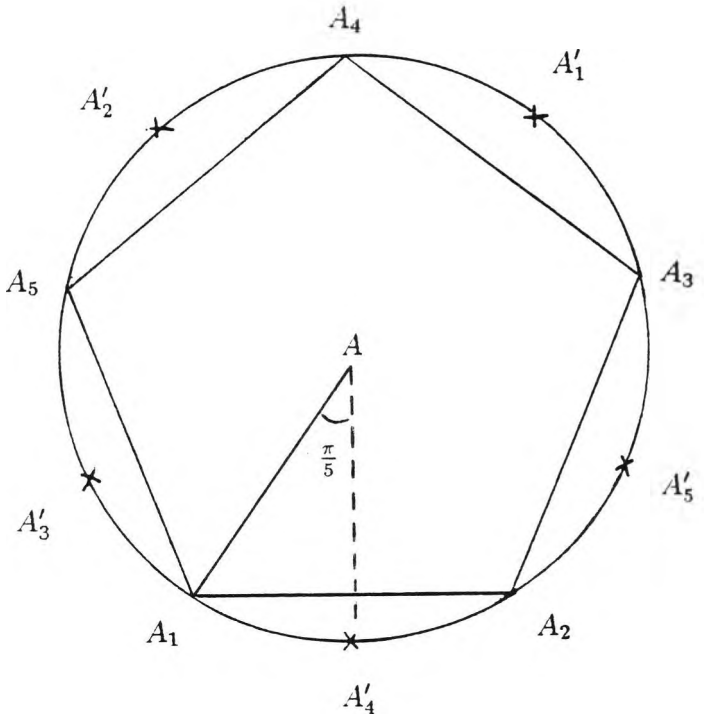

Figure 2.8: The vertices $A'_1 \ldots$ mark the orthogonal projection of $A_1 \ldots$ onto the A-pentagonal plane. Note that the pentagon $A'_1 \ldots, A'_5$ is rotated through $\frac{\pi}{5}$ relative to $A_1 \ldots, A_5$, showing that the inverse pentagon $A'_1 \ldots, A'_5$ is rotated by $\frac{\pi}{5}$ relative to $A_1 \ldots, A_5$.

Vertices	X, Y, Z	*Inverse Vertices*
P	$(0, 0, R)$ $a\left(0, 0, \frac{\sqrt{5}}{2}\right)$	P'
A_1	$(a, 0, \mid OA \mid)$ $a\left(1, 0, \frac{1}{2}\right)$	A_1'
A_2	$\left(a\cos\frac{2\pi}{5}, a\sin\frac{2\pi}{5}, \mid OA \mid\right)$ $a\left(\cos\frac{2\pi}{5}, \sin\frac{2\pi}{5}, \frac{1}{2}\right)$	A_2'
A_3	$\left(a\cos\frac{4\pi}{5}, a\sin\frac{4\pi}{5}, \mid OA \mid\right)$ $a\left(-\cos\frac{\pi}{5}, \sin\frac{\pi}{5}, \frac{1}{2}\right)$	A_3'
A_4	$\left(a\cos\frac{6\pi}{5}, a\sin\frac{6\pi}{5}, \mid OA \mid\right)$ $a\left(-\cos\frac{\pi}{5}, -\sin\frac{\pi}{5}, \frac{1}{2}\right)$	A_4'
A_5	$\left(a\cos\frac{8\pi}{5}, a\sin\frac{8\pi}{5}, \mid OA \mid\right)$ $a\left(\cos\frac{2\pi}{5}, -\sin\frac{2\pi}{5}, \frac{1}{2}\right)$	A_5'

Table 2.1: Coordinates Of The Vertices. Note that $a = l \csc\frac{\pi}{5}$ while $\mid OA \mid$, R are effectively provided by formulae (2.1.10), (2.1.13).

which gives the Coxeter formula

$$R = \frac{l}{k} \sin \frac{\pi}{5} \tag{2.1.14}$$

on noting from Table 1.2 that

$$\begin{aligned} k &= \left(\sin^2 \frac{\pi}{q} - \cos^2 \frac{\pi}{p}\right)^{1/2} = \left(\sin^2 \frac{\pi}{5} - \cos^2 \frac{\pi}{3}\right)^{1/2} \\ &= \left(\sin^2 \frac{\pi}{5} - \frac{1}{4}\right)^{1/2} = \frac{\left(4 \sin^2 \frac{\pi}{5} - 1\right)^{1/2}}{2} \end{aligned} \tag{2.1.15}$$

Since

$$\sin^2 \frac{\pi}{5} = \frac{5 - \sqrt{5}}{8},$$

we deduce from (2.1.15) that

$$k = \left(\frac{3 - \sqrt{5}}{8}\right)^{1/2}$$

from which

$$\begin{aligned} R &= l \sqrt{\frac{5 - \sqrt{5}}{3 - \sqrt{5}}} \\ &= l \sqrt{\frac{10 + 2\sqrt{5}}{4}} \\ &= l \sqrt{\frac{5 + \sqrt{5}}{2}} \end{aligned} \tag{2.1.16}$$

2.2 Symmetry Elements

Table 2.2 lists the direction-ratios (drs) of the six 5-fold symmetry axes $(PP')_5$, $(A_1A_1')_5$, ..., $(A_5A_5')_5$ utilising an obvious symbolism. Since each axis joins x, y, z

to -x, -y, -z, these drs are immediately obtained from the coordinates of P, A_1, ..., A_5 and multiplying (if necessary) by an appropriate factor. In particular, the axis $(PP')_5$ is derived as follows:

$$(PP')_5 = \Big(x(P) - x(P'), y(P) - y(P'), z(P) - z(P') \Big)$$

$$= 2\Big(x(P), y(P), z(P) \Big) \qquad (2.2.1)$$

Similarly Tables 2.3, 2.4 and 2.5 lists the drs of the fifteen 2-fold axes $(PA_1)_2$, ..., $(A_1A_2)_2$, ..., $(A_1A_4')_2$, ... which pass through the midpoints of the edges PA_1, ... A_1A_2, ... A_1A_4', ...

Finally Table 2.6, 2.7 lists the drs of the ten 3-fold axes $(PA_1A_2)_3$, ... $(A_1A_2A_4')_3$, ... which pass through the centroids of the faces PA_1A_2, ..., $A_1A_2A_4'$, ...

Rotations through $\frac{2\pi}{5}$, $\frac{4\pi}{5}$, $\frac{6\pi}{5}$, $\frac{8\pi}{5}$, $\frac{10\pi}{5}$ $(= 2\pi)$ about $(PP')_5$ transform the icosahedron into equivalent orientations keeping O fixed, and similarly for all the 5-fold axes. Accordingly these contribute $6 \times 4 = 24$ *operations* to the icosahedral group $\{532\}$. Here $\{532\}$ is the crystallographic point group symbolism for the group of symmetry rotations of the icosahedron. Also a rotation through $\frac{2\pi}{2}$ $(= \pi)$ about each 2–fold axis contributes $15 \times 1 = 15$ *operations* to $\{532\}$. Finally, rotations through $\frac{2\pi}{3}$, $\frac{4\pi}{3}$ about each 3-fold axis contributes $10 \times 2 = 20$ *operations* to $\{532\}$. Supplementing these by the unit operations ($\frac{10\pi}{5} = \frac{4\pi}{2} = \frac{6\pi}{3}$) for each axis yields $24 + 15 + 20 + 1 = 60$ *operations* included in the icosahedral group.

It is interesting to look at the subgroups of $\{532\}$ utilising drs of the symmetry axes so providing fresh interplay between geometrical and algebraic aspects. We may readily verify from the Tables that $(PP')_5$ is orthogonal to $(A_1A_4')_2$, $(A_2A_4')_2$, $(A_2A_5')_2$, $(A_3A_5')_2$ and $(A_3A_1')_2$ which demonstrates the existence of a dihedral subgroup $\{52\}$ within $\{532\}$. Similarly we may verify that $(PA_1A_2)_3$ is orthogonal to $(A_3A_4)_2$, $(A_4A_5)_2$ and $(A_3A_5')_2$ thus demonstrating the existence of a dihedral subgroup $\{32\}$ within $\{532\}$. Furthermore, the three 2–fold axes $(A_2A_3)_2$, $(PA_5)_2$ and $(A_1A_4')_2$ form an orthogonal triad so demonstrating the existence of a dihedral subgroup $\{22\}$ i.e. the V-group, within $\{532\}$. We find that $(PA_1A_2)_3$ is equally

The 5–fold symmetry axes	$X : Y : Z$
$(PP')_5$	$0 : 0 : 2R$ $0 : 0 : 1$
$(A_1A_1')_5$	$2a : 0 : 2 \mid OA \mid$ $2 : 0 : 1$
$(A_2A_2')_5$	$2a\cos\frac{2\pi}{5} : 2a\sin\frac{2\pi}{5} : 2 \mid OA \mid$ $2\cos\frac{2\pi}{5} : 2\sin\frac{2\pi}{5} : 1$
$(A_3A_3')_5$	$2a\cos\frac{4\pi}{5} : 2a\sin\frac{4\pi}{5} : 2 \mid OA \mid$ $-2\cos\frac{\pi}{5} : 2\sin\frac{\pi}{5} : 1$
$(A_4A_4')_5$	$2a\cos\frac{6\pi}{5} : 2a\sin\frac{6\pi}{5} : 2 \mid OA \mid$ $-2\cos\frac{\pi}{5} : -2\sin\frac{\pi}{5} : 1$
$(A_5A_5')_5$	$2a\cos\frac{8\pi}{5} : 2a\sin\frac{8\pi}{5} : 2 \mid OA \mid$ $2\cos\frac{2\pi}{5} : -2\sin\frac{2\pi}{5} : 1$

Table 2.2: Direction-ratios of the 5–fold symmetry axes. A simplified form of drs is given in the second row of each corresponding 5–fold axes respectively. Again $\mid OA \mid$ and a are as illustrated in Table 2.1.

2-fold symmetry axes	$X : Y : Z$
$(PA_1)_2$	$a : 0 : R + \mid OA \mid$ $1 : 0 : 2\cos\frac{\pi}{5}$
$(PA_2)_2$	$a\cos\frac{2\pi}{5} : a\sin\frac{2\pi}{5} : R + \mid OA \mid$ $\cos\frac{2\pi}{5} : \sin\frac{2\pi}{5} : 2\cos\frac{\pi}{5}$
$(PA_3)_2$	$a\cos\frac{4\pi}{5} : a\sin\frac{4\pi}{5} : R + \mid OA \mid$ $-\cos\frac{\pi}{5} : \sin\frac{\pi}{5} : 2\cos\frac{\pi}{5}$
$(PA_4)_2$	$a\cos\frac{6\pi}{5} : a\sin\frac{6\pi}{5} : R + \mid OA \mid$ $-\cos\frac{\pi}{5} : -\sin\frac{\pi}{5} : 2\cos\frac{\pi}{5}$
$(PA_5)_2$	$a\cos\frac{8\pi}{5} : a\sin\frac{8\pi}{5} : R + \mid OA \mid$ $\cos\frac{2\pi}{5} : -\sin\frac{2\pi}{5} : 2\cos\frac{\pi}{5}$

Table 2.3: Direction-ratios of P type 2–fold symmetry axes e.g. $(PA_1)_2$ signifies the 2–fold axis joining the mid-point of PA_1 to the mid-point of the inverse edges $P'A'_1$.

2–fold symmetry axes	$X : Y : Z$
$(A_1A_2)_2$	$a + a\cos\frac{2\pi}{5} : a\sin\frac{2\pi}{5} : 2 \mid OA \mid$ $1 + \cos\frac{2\pi}{5} : \sin\frac{2\pi}{5} : 1$
$(A_2A_3)_2$	$a\cos\frac{2\pi}{5} + a\cos\frac{4\pi}{5} : a\sin\frac{2\pi}{5} + a\sin\frac{4\pi}{5} : 2 \mid OA \mid$ $\cos\frac{2\pi}{5} - \cos\frac{\pi}{5} : \sin\frac{2\pi}{5} + \sin\frac{\pi}{5} : 1$
$(A_3A_4)_2$	$a\cos\frac{4\pi}{5} + a\cos\frac{6\pi}{5} : a\sin\frac{4\pi}{5} + a\sin\frac{6\pi}{5} : 2 \mid OA \mid$ $-2\cos\frac{\pi}{5} : 0 : 1$
$(A_4A_5)_2$	$a\cos\frac{6\pi}{5} + a\cos\frac{8\pi}{5} : a\sin\frac{6\pi}{5} + a\sin\frac{8\pi}{5} : 2 \mid OA \mid$ $-\cos\frac{\pi}{5} + \cos\frac{2\pi}{5} : -\sin\frac{\pi}{5} - \sin\frac{2\pi}{5} : 1$
$(A_5A_1)_2$	$a\cos\frac{8\pi}{5} + a : a\sin\frac{8\pi}{5} : 2 \mid OA \mid$ $\cos\frac{2\pi}{5} + 1 : -\sin\frac{2\pi}{5} : 1$

Table 2.4: Direction-ratios of A type 2–fold symmetry axes e.g. $(A_1A_2)_2$ signifies the 2–fold axis joining the mid-point of A_1A_2 to the mid-point of the inverse edge $A_1'A_2'$.

2–fold symmetry axes	$X : Y : Z$
$(A_1A_4')_2$	$a - a\cos\frac{6\pi}{5} : -a\sin\frac{6\pi}{5} : 0$ $1 + \cos\frac{\pi}{5} : \sin\frac{\pi}{5} : 0$
$(A_2A_4')_2$	$a\cos\frac{2\pi}{5} - a\cos\frac{6\pi}{5} : a\sin\frac{2\pi}{5} - a\sin\frac{6\pi}{5} : 0$ $\cos\frac{2\pi}{5} + \cos\frac{\pi}{5} : \sin\frac{2\pi}{5} + \sin\frac{\pi}{5} : 0$
$(A_2A_5')_2$	$a\cos\frac{2\pi}{5} - a\cos\frac{8\pi}{5} : a\sin\frac{2\pi}{5} - a\sin\frac{8\pi}{5} : 0$ $0 : 1 : 0$
$(A_3A_5')_2$	$a\cos\frac{4\pi}{5} - a\cos\frac{8\pi}{5} : a\sin\frac{4\pi}{5} - a\sin\frac{8\pi}{5} : 0$ $-\cos\frac{\pi}{5} - \cos\frac{2\pi}{5} : \sin\frac{\pi}{5} + \sin\frac{2\pi}{5} : 0$
$(A_3A_1')_2$	$a\cos\frac{4\pi}{5} - a : a\sin\frac{4\pi}{5} : 0$ $-\cos\frac{\pi}{5} - 1 : \sin\frac{\pi}{5} : 0$

Table 2.5: Direction-ratios of A' type 2–fold symmetry axes e.g. $(A_1A_4')_2$ signifies the 2–fold axis joining the mid-point of A_1A_4' to the mid-point of the inverse edge $A_1'A_4$.

3–fold symmetry axes	$X : Y : Z$
$(PA_1A_2)_3$	$a + a\cos\frac{2\pi}{5} : a\sin\frac{2\pi}{5} : R + 2 \mid OA \mid$ $1 + \cos\frac{2\pi}{5} : \sin\frac{2\pi}{5} : 4\cos^3\frac{\pi}{5}$
$(PA_2A_3)_3$	$a\cos\frac{2\pi}{5} + a\cos\frac{4\pi}{5} : a\sin\frac{2\pi}{5} + a\sin\frac{4\pi}{5} : R + 2 \mid OA \mid$ $\cos\frac{2\pi}{5} - \cos\frac{\pi}{5} : \sin\frac{2\pi}{5} + \sin\frac{\pi}{5} : 4\cos^3\frac{\pi}{5}$
$(PA_3A_4)_3$	$a\cos\frac{4\pi}{5} + a\cos\frac{6\pi}{5} : a\sin\frac{4\pi}{5} + a\sin\frac{6\pi}{5} : R + 2 \mid OA \mid$ $-2\cos\frac{\pi}{5} : 0 : 4\cos^3\frac{\pi}{5}$
$(PA_4A_5)_3$	$a\cos\frac{6\pi}{5} + a\cos\frac{8\pi}{5} : a\sin\frac{6\pi}{5} + a\sin\frac{8\pi}{5} : R + 2 \mid OA \mid$ $-\cos\frac{\pi}{5} + \cos\frac{2\pi}{5} : -\sin\frac{\pi}{5} - \sin\frac{2\pi}{5} : 4\cos^3\frac{\pi}{5}$
$(PA_5A_1)_3$	$a\cos\frac{8\pi}{5} + a : a\sin\frac{8\pi}{5} : R + 2 \mid OA \mid$ $\cos\frac{2\pi}{5} + 1 : -\sin\frac{2\pi}{5} : 4\cos^3\frac{\pi}{5}$

Table 2.6: Direction-ratios of P type 3–fold symmetry axes e.g. $(PA_1A_2)_3$ signifies the 3–fold axis joining the centroid of the face PA_1A_2 into the centroid of the inverse face $P'A_1'A_2'$.

3-fold symmetry axes	$X : Y : Z$
$(A_1A_2A_4')_3$	$a + a\cos\frac{2\pi}{5} + a\cos\frac{\pi}{5} : a\sin\frac{2\pi}{5} + a\sin\frac{\pi}{5} : \mid OA \mid$ $1 + \cos\frac{2\pi}{5} + \cos\frac{\pi}{5} : \sin\frac{2\pi}{5} + \sin\frac{\pi}{5} : \frac{1}{2}$
$(A_2A_3A_5')_3$	$-a\cos\frac{\pi}{5} : 2a\sin\frac{2\pi}{5} + a\sin\frac{\pi}{5} : \mid OA \mid$ $-\cos\frac{\pi}{5} : 2\sin\frac{2\pi}{5} + \sin\frac{\pi}{5} : \frac{1}{2}$
$(A_3A_4A_1')_3$	$-2a\cos\frac{\pi}{5} - a : 0 : \mid OA \mid$ $-2\cos\frac{\pi}{5} - 1 : 0 : \frac{1}{2}$
$(A_4A_5A_2')_3$	$-a\cos\frac{\pi}{5} : -a\sin\frac{\pi}{5} - 2a\sin\frac{2\pi}{5} : \mid OA \mid$ $-\cos\frac{\pi}{5} : -\sin\frac{\pi}{5} - 2\sin\frac{2\pi}{5} : \frac{1}{2}$
$(A_5A_1A_3')_3$	$a\cos\frac{2\pi}{5} + a + a\cos\frac{\pi}{5} : -a\sin\frac{2\pi}{5} - a\sin\frac{\pi}{5} : \mid OA \mid$ $\cos\frac{2\pi}{5} + 1 + \cos\frac{\pi}{5} : -\sin\frac{2\pi}{5} - \sin\frac{\pi}{5} : \frac{1}{2}$

Table 2.7: Direction-ratios of A type 3-fold symmetry axes e.g. $(A_1A_2A_4')_3$ signifies the 3-fold axis joining the centroid of the face $A_1A_2A_4'$ into the centroid of the inverse face $A_1'A_2'A_4$.

oriented to these 2–fold axes, which implies the existence of three additional 3–fold axes equally oriented (allowing for negative direction) to them. This configuration is realised by the four diagonals of a cube plus the three axes passing through the cube centre parallel to the cube edges (Figure 2.9 a)). These three axes serve as 4–fold symmetry axes for the cube, so generating the octahedral group $\{432\}$. However, alternate corners of the cube delineate a regular tetrahedron (Figure 2.9 b)) for which these axes function only as 2–fold symmetry axes so generating the tetrahedral group $\{23\}$. It will be shown below that $\{23\}$ is a subgroup of $\{532\}$ i.e. a regular tetrahedron may be embedded within the regular icosahedron.

2.3 The Icosahedral Group

The icosahedral group $\{532\}$ is isomorphic with the alternating group A_5, which comprises 60 $(= \frac{1}{2}\, 5!)$ permutation operators. This representation allows us to write down immediately the cyclic subgroups of $\{532\}$ corresponding with the various symmetry axes listed below.

1. Six cyclic groups of order 5:

$$\left\{ (12345)\,,\, (12345)^2\,,\, (12345)^3\,,\, (12345)^4\,,\, I \right\};\ \begin{aligned} (12345)^2 &= (13524), \\ (12345)^3 &= (14253), \\ (12345)^4 &= (15432), \\ (12345)^5 &= I. \end{aligned} \qquad (2.3.1)$$

$$\left\{ (12354)\,,\, (12354)^2\,,\, (12354)^3\,,\, (12354)^4\,,\, I \right\};\ \begin{aligned} (12354)^2 &= (13425), \\ (12354)^3 &= (15243), \\ (12354)^4 &= (14532), \\ (12354)^5 &= I. \end{aligned} \qquad (2.3.2)$$

$$\left\{ (12534)\,,\,(12534)^2\,,\,(12534)^3\,,\,(12534)^4\,,\,I \right\};\ \begin{aligned}(12534)^2 &= (15423),\\ (12534)^3 &= (13245),\\ (12534)^4 &= (14352),\\ (12534)^5 &= I.\end{aligned} \tag{2.3.3}$$

$$\left\{ (15234)\,,\,(15234)^2\,,\,(15234)^3\,,\,(15234)^4\,,\,I \right\};\ \begin{aligned}(15234)^2 &= (12453),\\ (15234)^3 &= (13542),\\ (15234)^4 &= (14325),\\ (15234)^5 &= I.\end{aligned} \tag{2.3.4}$$

$$\left\{ (12435)\,,\,(12435)^2\,,\,(12435)^3\,,\,(12435)^4\,,\,I \right\};\ \begin{aligned}(12435)^2 &= (14523),\\ (12435)^3 &= (13254),\\ (12435)^4 &= (15342),\\ (12435)^5 &= I.\end{aligned} \tag{2.3.5}$$

$$\left\{ (14235)\,,\,(14235)^2\,,\,(14235)^3\,,\,(14235)^4\,,\,I \right\};\ \begin{aligned}(14235)^2 &= (12543),\\ (14235)^3 &= (13452),\\ (14235)^4 &= (15324),\\ (14235)^5 &= I.\end{aligned} \tag{2.3.6}$$

2. Ten cyclic groups of order 3:

$$\left\{ \begin{matrix} I\,,\,(1)(2)(345) \\ \quad,\,(1)(2)(354) \end{matrix} \right\},\ \left\{ \begin{matrix} I\,,\,(1)(3)(245) \\ \quad,\,(1)(3)(254) \end{matrix} \right\},$$

$$\left\{ \begin{matrix} I\,,\,(1)(4)(235) \\ \quad,\,(1)(4)(253) \end{matrix} \right\},\ \left\{ \begin{matrix} I\,,\,(1)(5)(234) \\ \quad,\,(1)(5)(243) \end{matrix} \right\},$$

$$\left\{ \begin{matrix} I\,,\,(2)(3)(145) \\ \quad,\,(2)(3)(154) \end{matrix} \right\},\ \left\{ \begin{matrix} I\,,\,(2)(4)(135) \\ \quad,\,(2)(4)(153) \end{matrix} \right\},$$

$$\left\{ \begin{matrix} I\,,\,(2)(5)(134) \\ \quad,\,(2)(5)(143) \end{matrix} \right\},\ \left\{ \begin{matrix} I\,,\,(3)(4)(125) \\ \quad,\,(3)(4)(152) \end{matrix} \right\},$$

$$\left\{ \begin{matrix} I\,,\ (3)(5)(124), \\ \qquad (3)(5)(142) \end{matrix} \right\}\,,\ \left\{ \begin{matrix} I\,,\ (4)(5)(123), \\ \qquad (4)(5)(132) \end{matrix} \right\}. \tag{2.3.7}$$

3. Fifteen cyclic groups of order 2:

$$\{\, I\,,\ (12)(34)(5)\,\}\,,\ \{\, I\,,\ (13)(24)(5)\,\}\,,\ \{\, I\,,\ (14)(23)(5)\,\},$$

$$\{\, I\,,\ (12)(35)(4)\,\}\,,\ \{\, I\,,\ (13)(25)(4)\,\}\,,\ \{\, I\,,\ (15)(23)(4)\,\},$$

$$\{\, I\,,\ (12)(45)(3)\,\}\,,\ \{\, I\,,\ (14)(25)(3)\,\}\,,\ \{\, I\,,\ (15)(24)(3)\,\},$$

$$\{\, I\,,\ (13)(45)(2)\,\}\,,\ \{\, I\,,\ (14)(35)(2)\,\}\,,\ \{\, I\,,\ (15)(34)(2)\,\},$$

$$\{\, I\,,\ (23)(45)(1)\,\}\,,\ \{\, I\,,\ (24)(35)(1)\,\}\,,\ \{\, I\,,\ (25)(34)(1)\,\}, \tag{2.3.8}$$

From these cyclic groups we may build up dihedral subgroups of three distinct types as already anticipated on geometrical grounds:

i) {52} type generated by (12345) and (14)(23)(5) subject to relations

$$(12345)^5 \;=\; [\,(14)(23)(5)\,]^2 \;=\; [\,(12345)\,\bullet\,(14)(23)(5)\,]^2 \;=\; I \tag{2.3.9}$$

corresponding with a 5–fold principal axis and five secondary 2–fold axes.

ii) {32} type generated by (123)(4)(5) and (23)(45)(1) with the relations

$$[\,(123)(4)(5)\,]^3 \;=\; [\,(23)(45)(1)\,]^2 \;=\; [\,(123)(4)(5)\,\bullet\,(23)(45)(1)\,]^2 \;=\; I \tag{2.3.10}$$

corresponding with a 3–fold principal axis and three secondary 2–fold axes.

iii) {22} type generated by (12)(34)(5) and (13)(24)(5) subject to relations

$$[\,(12)(34)(5)\,]^2 = [\,(13)(24)(5)\,]^2 = [\,(12)(34)(5) \bullet (13)(24)(5)\,]^2 = [\,(14)(23)(5)\,]^2 = I \tag{2.3.11}$$

as exhibited below by the first row of (2.3.12)

By contrast with {32} there exists a tetrahedral group {23} ($\equiv T$) within {532} having the following multiplication Table:

$$T = \left\{ \begin{array}{cccc} I & (12)(34)(5) & (13)(24)(5) & (14)(23)(5) \\ (123)(4)(5) & (134)(2)(5) & (243)(1)(5) & (142)(3)(5) \\ (132)(4)(5) & (234)(1)(5) & (124)(3)(5) & (143)(2)(5) \end{array} \right\} \tag{2.3.12}$$

generated by (123)(4)(5) and (12)(34)(5) with relations [3]

$$[\,(123)(4)(5)\,]^3 = [\,(12)(34)(5)\,]^2 = [\,(123)(4)(5)\,] \bullet (12)(34)(5)\,]^3 = [\,(134)(2)(5)\,]^3 = I. \tag{2.3.13}$$

By virtue of the 5–fold symmetry of the icosahedron there exists five such tetrahedral groups within {532} i.e. replacing (5) by (1), (2), (3), (4) in turns into formula (2.3.12).

We are now in a position to write out the coset decomposition of {532} with respect to T:

$$\begin{aligned} \{532\} &= T + (12345)\,T + (12345)^2\,T + (12345)^3\,T + (12345)^4\,T, \\ \{532\} &= T + T\,(12345) + T\,(12345)^2 + T\,(12345)^3 + T\,(12345)^4 \end{aligned} \tag{2.3.14}$$

so providing the group multiplication Tables 2.8 and 2.9. Note that

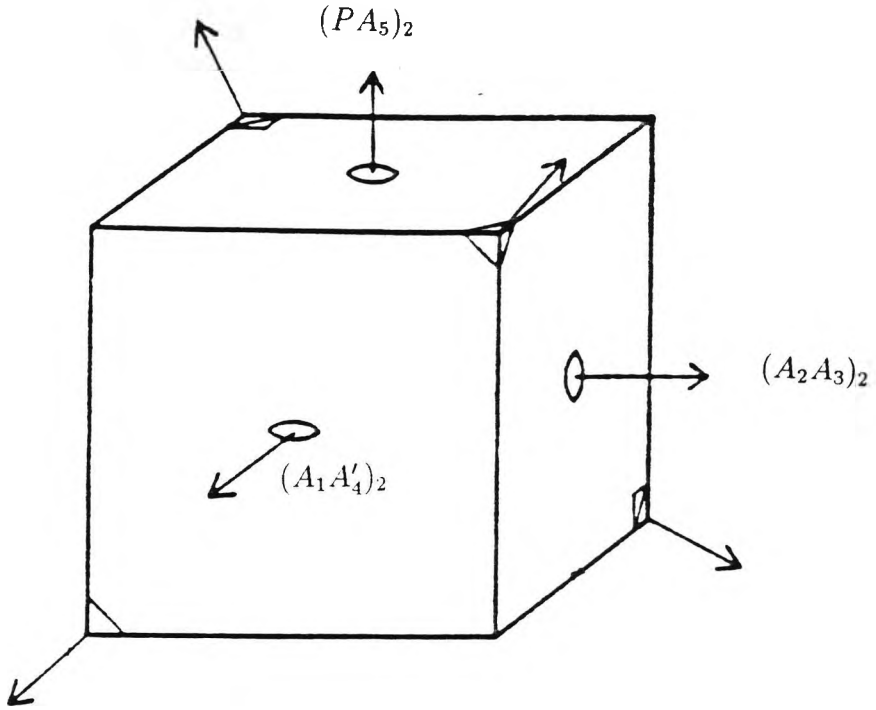

Figure 2.9: a) Delineation of a cube showing three 2–fold axis of symmetry plus four 3–fold axis of symmetry [4].

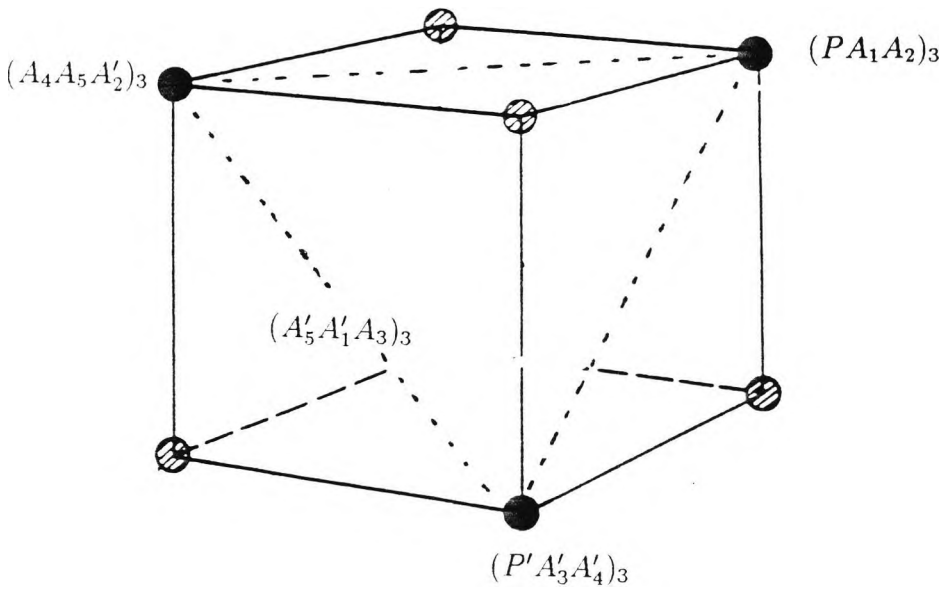

Figure 2.9 b) Four atoms lying at the corners of a cube can be transformed into each other by operations of the tetrahedral group. Note that the solid atom marked $(PA_1A_2)_3$ has an inverse marked by the shaded atom along the opposite diagonal.

$$(12345)\,T \neq T\,(12345)$$

showing that T is not an invariant subgroup of $\{532\}$ (consistent with the fact that $\{532\}$ is a simple group). In fact A_5 is a subgroup of the symmetry group S_5 as discussed in Appendix C.

2.4 Angles Associated With The Icosahedron

In this section we utilise our drs to explore two primary angles characteristic of the icosahedron

1. **angle subtended by an edge**: $2\,\phi$
2. **dihedral angle**: $\pi - 2\,\psi$.

The edge PA_1 subtends an angle $2\,\phi$ at O given by

$$\cos 2\phi = \frac{\vec{OP} \bullet \vec{OA}_1}{|\,OP\,| \bullet |\,OA_1\,|} = \frac{(PP')_5 \bullet (A_1A_1')_5}{|\,(PP')_5\,| \bullet |\,(A_1A_1')_5\,|}$$

$$\hookrightarrow \text{see Table 2.2} \hookleftarrow$$

$$= \frac{(0,0,1) \bullet (2,0,1)}{\sqrt{5}} = \frac{1}{\sqrt{5}} \quad . \tag{2.4.1}$$

This verifies the Coxeter formula

$$\cos\,\phi = \frac{\cos\,\frac{\pi}{p}}{\sin\,\frac{\pi}{q}} = \frac{\cos\,\frac{\pi}{3}}{\sin\,\frac{\pi}{5}} = \frac{\frac{1}{2}}{\sin\,\frac{\pi}{5}} \tag{2.4.2}$$

since

$$\cos\,2\,\phi = 2\,\cos^2\,\phi - 1 = \frac{2}{4\,\sin^2\,\frac{\pi}{5}} - 1 = \frac{1}{\sqrt{5}} \tag{2.4.3}$$

on noting

$$\sin^2 \frac{\pi}{5} = \frac{5 - \sqrt{5}}{8} \quad .$$

The two neighbouring faces PA_1A_2, $A_1A_2A_4'$ have normals defined by the 3–fold axes $(PA_1A_2)_3$, $(A_1A_2A_4')_3$–see Table 2.6 and Table 2.7.
These meet at an angle $2\,\psi$ given by

$$\cos 2\psi = \frac{(PA_1A_2)_3 \bullet (A_1A_2A_4')_3}{|(PA_1A_2)_3||(A_1A_2A_4')_3|}$$

$$= \frac{\left(1 + \cos\frac{2\pi}{5}, \sin\frac{2\pi}{5}, 4\cos^3\frac{\pi}{5}\right) \bullet \left(1 + \cos\frac{2\pi}{5} + \cos\frac{\pi}{5}, \sin\frac{2\pi}{5} + \sin\frac{\pi}{5}, \frac{1}{2}\right)}{\left(1 + \cos\frac{2\pi}{5}\right)^2 + \sin^2\frac{2\pi}{5} + \left(4\cos^3\frac{\pi}{5}\right)^2}$$

$$= \frac{\frac{5}{4}\left(\sqrt{5} + 2\right)}{\frac{3}{4}\left(2\sqrt{5} + 5\right)} = \frac{\sqrt{5}}{3} \quad .$$

(2.4.4)

This verifies the Coxeter formula

$$\cos\psi = \frac{\cos\frac{\pi}{5}}{\sin\frac{\pi}{3}} = \frac{\cos\frac{\pi}{5}}{\sqrt{3}/2} \tag{2.4.5}$$

since

$$\cos 2\psi = 2\cos^2\psi - 1 = 2 \bullet \frac{4\cos^2\frac{\pi}{5}}{3} - 1 = \frac{8\left(1 - \sin^2\frac{\pi}{5}\right) - 3}{3}$$

$$= \frac{5 - 8\sin^2\frac{\pi}{5}}{3} = \frac{5 - 8\left(\frac{5-\sqrt{5}}{8}\right)}{3} = \frac{\sqrt{5}}{3} \quad .$$

(2.4.6)

From this observation, we infer that (2.4.4) provides $\cos\phi$ for the dodecahedron and simultaneously (2.4.1) provides $\cos\psi$ for the dodecahedron as will be exploited on geometrical ground in the next chapter.

•	I	(12)(34)(5)	(13)(24)(5)	(14)(23)(5)	(123)(4)(5)	(134)(2)(5)
I	I	(12)(34)(5)	(13)(24)(5)	(14)(23)(5)	(123)(4)(5)	(134)(2)(5)
(12345)	(12345)	(135)(2)(4)	(14325)	(15)(24)(3)	(13245)	(14235)
(13524)	(13524)	(14523)	(152)(3)(4)	(25)(34)(1)	(14)(25)(3)	(15243)
(14253)	(14253)	(15324)	(345)(1)(2)	(12)(35)(4)	(15342)	(253)(1)(4)
(15432)	(15432)	(254)(1)(3)	(12354)	(13)(45)(2)	(354)(1)(2)	(12)(45)(3)

Table 2.8: The left coset decomposition of $\{532\}$ with respect to T.

(243)(1)(5)	(142)(3)(5)	(132)(4)(5)	(234)(1)(5)	(124)(3)(5)	(143)(2)(5)
(243)(1)(5)	(142)(3)(5)	(132)(4)(5)	(234)(1)(5)	(124)(3)(5)	(143)(2)(5)
(125)(3)(4)	(15)(34)(2)	(145)(2)(3)	(12435)	(13425)	(15)(23)(4)
(13452)	(235)(1)(4)	(15234)	(13)(25)(4)	(14352)	(245)(1)(3)
(14)(35)(2)	(12453)	(24)(35)(1)	(14532)	(153)(2)(4)	(12534)
(15423)	(13254)	(12543)	(154)(2)(3)	(23)(45)(1)	(13542)

Continuation of Table 2.8 along the row direction.

•	I	(12345)	(13524)	(14253)	(15432)
I	I	(12345)	(13524)	(14253)	(15432)
(12)(34)(5)	(12)(34)(5)	(245)(1)(3)	(14235)	(13254)	(153)(2)(4)
(13)(24)(5)	(13)(24)(5)	(14532)	(354)(1)(2)	(125)(3)(4)	(15234)
(14)(23)(5)	(14)(23)(5)	(13)(45)(2)	(12)(35)(4)	(25)(34)(1)	(15)(24)(3)
(123)(4)(5)	(123)(4)(5)	(13452)	(24)(35)(1)	(14325)	(154)(2)(3)
(134)(2)(5)	(134)(2)(5)	(12453)	(14352)	(254)(1)(3)	(15)(23)(4)
(243)(1)(5)	(243)(1)(5)	(145)(2)(3)	(12354)	(13)(25)(4)	(15342)
(142)(3)(5)	(142)(3)(5)	(23)(45)(1)	(135)(2)(4)	(12534)	(15243)
(132)(4)(5)	(132)(4)(5)	(345)(1)(2)	(12435)	(14)(25)(3)	(15423)
(234)(1)(5)	(234)(1)(5)	(13245)	(14)(35)(2)	(12543)	(152)(3)(4)
(124)(3)(5)	(124)(3)(5)	(14523)	(13542)	(253)(1)(4)	(15)(34)(2)
(143)(2)(5)	(143)(2)(5)	(12)(45)(3)	(235)(1)(4)	(13425)	(15324)

Table 2.9: The right coset decomposition of $\{532\}$ with respect to T.

Chapter 3

The Regular Dodecahedron

3.1 Introduction

In this chapter we study the underlying structure of the regular dodecahedron from the face perspective as this method of representation correlates with the vertex perspective of the regular icosahedron, which has been discussed with great clarity in the previous chapter. This study focuses on how the face perspective catered for the conclusive evidence of its icosahedral symmetry. To prove this, we implement a similar coordinate system for the regular dodecahedron as we did for the regular icosahedron.

3.2 Face Perspective

The regular dodecahedron is a complementary figure to the regular icosahedron, and it therefore has the same symmetry axes with the role of the vertices and faces interchanged. Accordingly there are six 5–fold axes joining the centres of opposite faces, ten 3–fold axes joining opposite vertices, and fifteen 2–fold symmetry axes

joining the mid-points of opposite edges. Also it has an inversion centre, O, which is the common point of intersection of all the axes.

We now introduce a rectangular coordinate system for the regular dodecahedron of edge length $2\,l$, starting with any face. This is a regular pentagon $A_1, \ldots, A_5$, centre A with circumradius a, as already illustrated in Figure 2.5, where we find that

$$2a \sin \frac{\pi}{5} = 2l \Longrightarrow a = \frac{l}{\sin \frac{\pi}{5}} \tag{3.2.1}$$

as in (2.1.3). Also we note from the isosceles triangle $A_1A_2A_3$ (Figure 3.1) that

$$| A_1A_3 | = 2 \mid A_1A_2 \mid \sin \frac{3\pi}{10} = 4l \sin \frac{3\pi}{10} \equiv 2\,d. \tag{3.2.2}$$

The edge A_1A_2 is shared with the pentagonal face $A_1A_2B_1B_2B_4'$ where B_1B_2 lies parallel to A_1A_2 (Figure 3.2) with $\mid B_1B_2 \mid$ given by (3.2.2). Accordingly there exists a second pentagon B_1, B_2, B_3, B_4, B_5, centre B, of circumradius b which is similar and similarly situated to the A-pentagon as depicted by the orthogonal projection of the A-pentagon upon the B-plane in Figure 3.3 (a).
Note from similar triangles that

$$\frac{| BB_1 |}{| B_1B_2 |} = \frac{| A^*A_1^* |}{| A_1^*A_2^* |} = \frac{| AA_1 |}{| A_1A_2 |} = \frac{a}{2\,l} \tag{3.2.3}$$

$$\Longrightarrow b \equiv | BB_1 | = | B_1B_2 | \bullet \frac{a}{2\,l} \quad .$$

Since $\mid B_1B_2 \mid$ is a diagonal of the face $A_1A_2B_1B_2B_4'$ we conclude that

$$\begin{aligned} b &= 2\,d \bullet \frac{a}{2\,l} = 4\,l \sin \frac{3\pi}{10} \bullet \frac{a}{2\,l} \\ &= 2\,a \sin \frac{3\pi}{10} = 2\,l \frac{\sin \frac{3\pi}{10}}{\sin \frac{\pi}{5}} \end{aligned} \tag{3.2.4}$$

Finally, the vertical separation between the pentagons may be calculated by reference to Figure 3.3 (b):

$$| AB |^2 = | A_1A_1^* |^2 = | A_1B_1 |^2 - | B_1A_1^* |^2 = 4\,l^2 - (b - a)^2$$

Substituting for l in terms of a from (3.2.1) and for b in terms of a from (3.2.4) gives rise to

$$\begin{aligned} | AB |^2 &= 4\left(a \sin^2 \frac{\pi}{5}\right)^2 - \left(2\,a \sin \frac{3\pi}{10} - a\right)^2 \\ &= 4\,a^2 \sin^2 \frac{\pi}{5} - 4\,a^2 \sin^2 \frac{3\pi}{10} + 4\,a^2 \sin \frac{3\pi}{10} - a^2 \\ &= 4\,a^2\left(\frac{5 - \sqrt{5}}{8}\right) - 4\,a^2\left(\frac{3 + \sqrt{5}}{8}\right) + 4\,a^2\left(\frac{1 + \sqrt{5}}{4}\right) - a^2 \\ &= a^2 \text{ (see Appendix D).} \end{aligned} \tag{3.2.5}$$

The pentagon $B_1, \ldots, B_5$, centre B, inverts into the parallel pentagon $B_1', \ldots, B_5'$, centre B', where B_4' has already been met as a corner of the face $A_1A_2B_1B_2B_4'$ (see Figure 3.4). Since O is equidistant from each vertex, we see (Figure 3.3 (b)) that

$$R^2 = | OA_1 |^2 = | OA |^2 + | AA_1 |^2 = | OA |^2 + a^2, \tag{3.2.6}$$

and also

$$R^2 = | OB_1 |^2 = | OB |^2 + | BB_1 |^2 = | OB |^2 + b^2, \tag{3.2.7}$$

where R denotes the circumradius of the dodecahedron. Equating (3.2.6), (3.2.7) for R^2 and bearing in mind $| OA | = | OB | + | BA |$ where a, b, $| AB |$ are known from (3.2.1), (3.2.4) and (3.2.5) provides

$$| OB |^2 = | OA |^2 + a^2 - b^2 = (| OB | + | BA |)^2 + a^2 - b^2$$

$$= |OB|^2 + |BA|^2 + 2\,|OB|\,|BA| + a^2 - b^2$$

$$= |OB|^2 + a^2 + 2a\,|OB| + a^2 - b^2$$

$$= |OB|^2 + 2a\,|OB| + 2a^2 - b^2$$

so that

$$|OB| = \frac{b^2 - 2a^2}{2\,|AB|} = \frac{4a^2 \sin^2 \frac{3\pi}{10} - 2a^2}{2a} = 2a \sin^2 \frac{3\pi}{10} - a$$

$$= 2a\left(\frac{3+\sqrt{5}}{8}\right) - a = \frac{(-1+\sqrt{5})}{4}a. \tag{3.2.8}$$

Now

$$|OA| = |OB| + |BA| = \frac{-1+\sqrt{5}}{4}a + a = \frac{3+\sqrt{5}}{4}a. \tag{3.2.9}$$

Utilising the expression (3.2.6) for R^2 now gives

$$R^2 = \left(2a \sin^2 \frac{3\pi}{10}\right)^2 + a^2 = 4a^2\left(\sin^2 \frac{3\pi}{10}\right)^2 + a^2$$

$$= 4a^2\left(\frac{3+\sqrt{5}}{8}\right)^2 + a^2 = 4a^2\left(\frac{14+6\sqrt{5}}{64}\right) + a^2$$

$$= \frac{(30+6\sqrt{5})\,a^2}{16} = \frac{(30+6\sqrt{5})}{16} \bullet \frac{l^2}{\sin^2 \frac{\pi}{5}}$$

i.e.

$$R^2 = \frac{(30+6\sqrt{5})\,l^2}{2\,(5-\sqrt{5})} = \frac{3 \bullet 2\,(3+\sqrt{5})\,l^2}{4} = \left(\sqrt{3}\left(\frac{1+\sqrt{5}}{2}\right)l\right)^2 \tag{3.2.10}$$

on solving a^2 in terms of l^2. The resulting R is equal to that classically available as displayed in Appendix A.

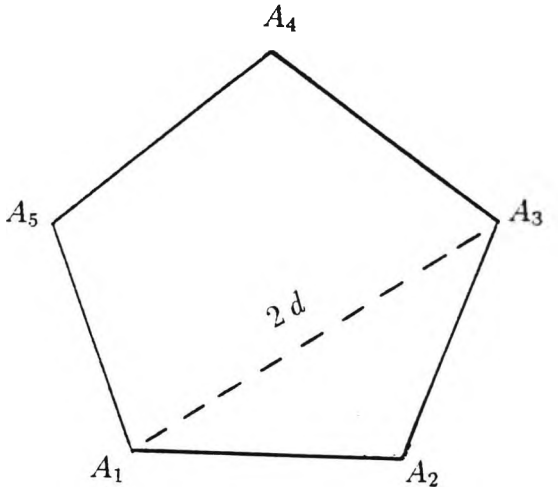

Figure 3.1: The aerial view of the dodecahedral pentagonal face showing A_1A_3 as diagonal of the face $A_1A_2 \ldots A_5$.

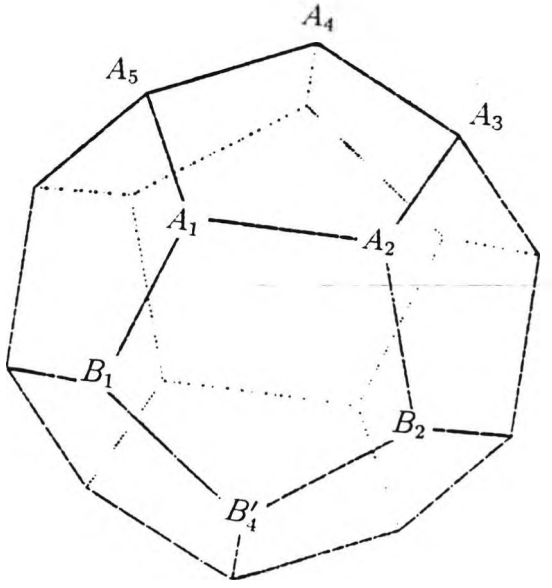

Figure 3.2: 'Wire' model of the regular dodecahedron. Note that the edge A_1A_2 lies parallel to B_1B_2 with A_1A_2 as the join of 2 adjacent faces $A_1A_2 \ldots A_5$ and $A_1A_2B_1B_2B_4'$.

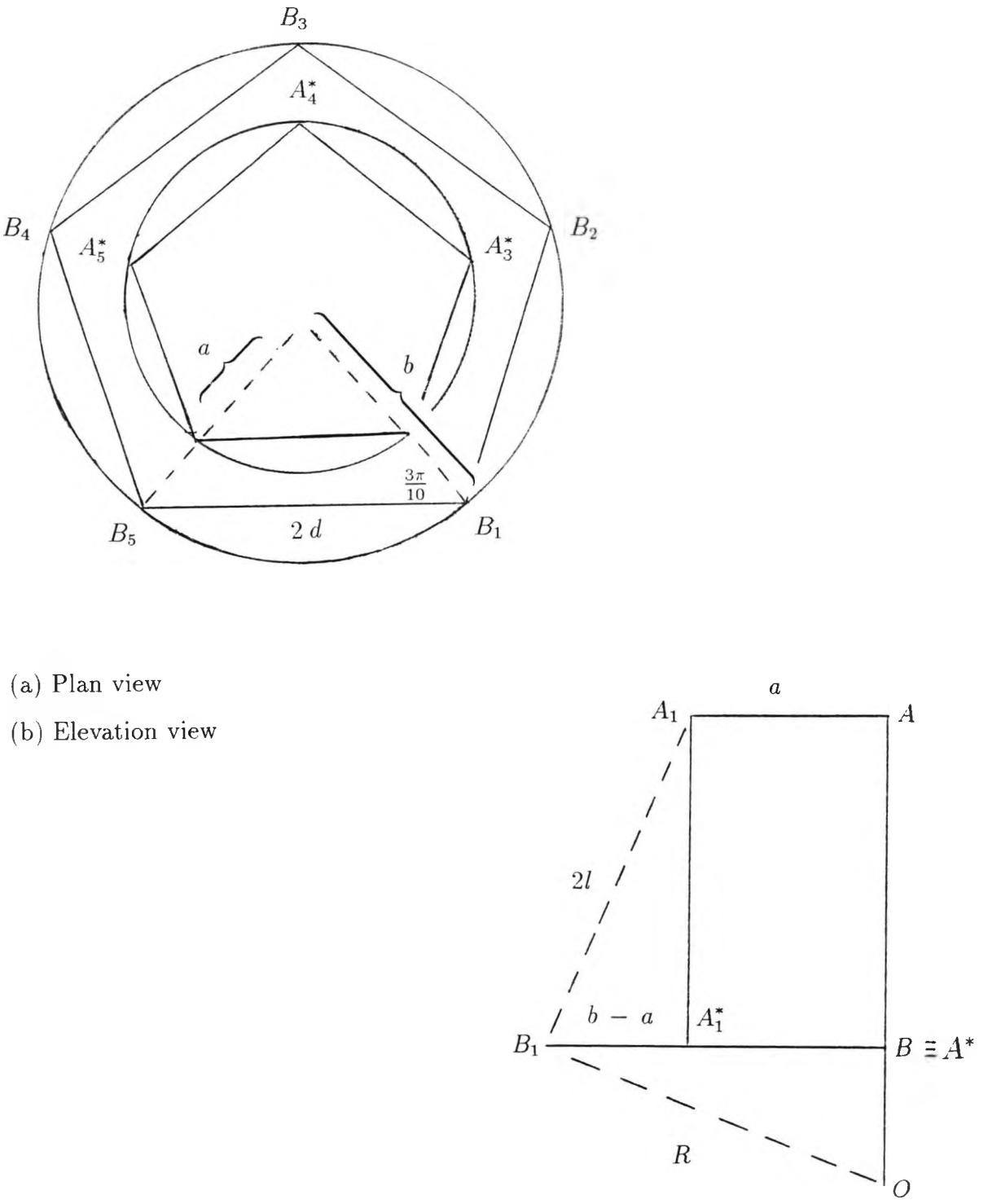

(a) Plan view

(b) Elevation view

Figure 3.3: Orthogonal projection of the A-dodecahedral pentagon onto the B-pentagonal plane.

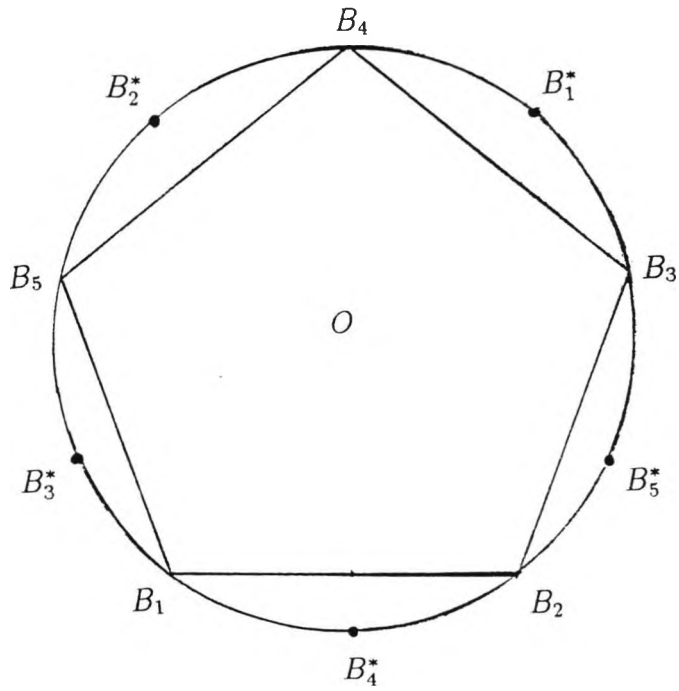

Figure 3.4: The points B_1^*, ...mark the inverses B_1', ...upon the B-pentagonal plane. The corresponding diagram for the A-plane has been given in Figure 2.8.

3.3 Rectangular Coordinate System

A suitable coordinate system may now be constructed with O as origin and OA as the positive z–axis. If so $z = \mid OA \mid$ for all points in the A–plane and $z = \mid OB \mid$ for all points in the B–plane. Vertices within the A–plane may be conveniently represented by the complex vectors

$$\vec{AA_1} = a\,e^{i0} \equiv a,\ \vec{AA_2} = a\,e^{i\frac{2\pi}{5}} \equiv a\left(\cos\frac{2\pi}{5} + i\,\sin\frac{2\pi}{5}\right), \ldots \qquad (3.3.1)$$

following (2.1.4), and within the B-plane by

$$\vec{BB_1} = b\,e^{i0} \equiv b,\ \vec{BB_2} = b\,e^{i\frac{2\pi}{5}} \equiv b\left(\cos\frac{2\pi}{5} + i\,\sin\frac{2\pi}{5}\right), \ldots \qquad (3.3.2)$$

Breaking down the complex numbers (3.3.1), (3.3.2) into their x, y components, we obtain the x, y, z coordinates of A_1, A_2, ..., B_1, B_2, ... as listed in Tables 3.1 and 3.2.

Since x, y, z inverts into $-x$, $-y$, $-z$ we immediately have the coordinates of A_1', ..., B_1'. Of course

$$A = (0, 0, \mid OA \mid),\ A' = (0, 0, - \mid OA \mid) \qquad (3.3.3)$$

Tables 3.3 and 3.4 list the direction-ratios (drs) of the ten 3–fold symmetry axes $(A_1A_1')_3 \ldots (B_1B_1')_3 \ldots$ which join the inverse pairs of vertices.
Similarly Tables 3.5, 3.6 and 3.7 list the drs of the fifteen 2–fold axes $(A_1A_2)_2 \ldots$ $(A_1B_1)_2 \ldots (B_1B_4')_2 \ldots$ which join the inverse pairs of mid-point of the edges.
Finally Table 3.8 lists the drs of the six 5–fold axes $(AA')_5$, $(F_1F_1')_5$, ... $(F_4F_4')_5$ which pass through the six face-centres A, F_1, F_2, ... F_4 and the the inverses A', F_1', F_2', ... F_4' where F_1, F_2 and F_3 are the centres of three faces which adjoin the face $A_1A_2A_3A_4A_5$ as shown (Figure 3.5).

A regular icosahedron may be embedded within the dodecahedron by joining adjacent face-centres. Thus $\mid AF_1 \mid$ becomes the edge length of the icosahedron. We may verify that

$$\frac{|\,OA\,|}{|\,AF_1\,|} = \frac{R_{ic}}{2\,l}$$

as expected where R_{ic} denotes the circumradius of the regular icosahedron, so providing a fresh confirmation of the embedding property.

3.4 Angles Associated With The Dodecahedron

The two neighbouring faces $A_1A_2A_3A_4A_5$, $A_1A_2B_1B_2B_4'$ have normals defined by the 5–fold axes $(AA')_5$, $(F_1F_1')_5$—see Table 3.8. These meet at an angle given by

$$\begin{aligned}
\cos\,2\,\psi &= \frac{\vec{OA}\,\bullet\,\vec{OF_1}}{|\,\vec{OA}\,|\,\bullet\,|\,\vec{OF_1}\,|} = \frac{(AA')_5\,\bullet\,(FF_1')_5}{|\,(AA')_5\,|\,\bullet\,|\,(FF_1')_5\,|} \\
&= \frac{(0,0,1)\,\bullet\,\left(2\,(\,5\,+\,2\sqrt{5}),2(5\,+\,3\sqrt{5})\,\sin\,\frac{\pi}{5},5\,+\,3\sqrt{5}\right)}{\sqrt{(10\,+\,4\sqrt{5})^2\,+\,(\,(10\,+\,6\sqrt{5})\,\sin\,\frac{\pi}{5})^2\,+\,(5\,+\,3\sqrt{5})^2}} \qquad (3.4.1) \\
&= \frac{5\,+\,3\sqrt{5}}{15\,+\,5\sqrt{5}} = \frac{1}{\sqrt{5}} \quad .
\end{aligned}$$

This verifies the Coxeter formula

$$\cos\,\psi = \frac{\cos\,\frac{\pi}{q}}{\sin\,\frac{\pi}{p}} = \frac{\cos\,\frac{\pi}{3}}{\sin\,\frac{\pi}{5}} = \frac{\frac{1}{2}}{\sin\,\frac{\pi}{5}}$$

since that

$$\cos\,2\,\psi = 2\,\cos^2\,\psi\,-\,1 = \frac{2}{4\,\sin^2\,\frac{\pi}{5}}\,-\,1 = \frac{1}{\sqrt{5}} \quad .$$

The edge A_1A_2 subtends an angle $2\,\phi$ at O given by

$$\cos 2\phi = \frac{\vec{OA_1} \bullet \vec{OA_2}}{|\vec{OA_1}| \bullet |\vec{OA_2}|} = \frac{(A_1A_1')_3 \bullet (A_2A_2')_3}{|(A_1A_1')_3| \bullet |(A_2A_2')_3|}$$

↪ see Table 3.3 ↩

$$= \frac{(4\sqrt{5}, 0, 5 + 3\sqrt{5}) \bullet (5 - \sqrt{5}, (10 + 2\sqrt{5}) \sin\frac{\pi}{5}, 5 + 3\sqrt{5})}{\sqrt{(30\sqrt{5} + 150)} \bullet \sqrt{(30\sqrt{5} + 150)}}$$

$$= \frac{50 + 50\sqrt{5}}{150 + 30\sqrt{5}} = \frac{\sqrt{5}}{3} \quad . \tag{3.4.2}$$

Again, this verifies the Coxeter formula

$$\cos\phi = \frac{\cos\frac{\pi}{p}}{\sin\frac{\pi}{q}} = \frac{\cos\frac{\pi}{5}}{\sin\frac{\pi}{3}} = \frac{\cos\frac{\pi}{5}}{\sqrt{3}/2}$$

since that

$$\cos 2\phi = 2\cos^2\phi - 1 = 2 \bullet \frac{4\cos^2\frac{\pi}{5}}{3} - 1 = \frac{8\left(\frac{3+\sqrt{5}}{8}\right) - 3}{3}$$

$$= \frac{\sqrt{5}}{3} \quad .$$

Of course, this equals the value of cos 2ψ given by (2.4.6). Therefore the observation that (2.4.4) provides cos ϕ for the dodecahedron whilst (2.4.1) provides cos ψ for the dodecahedron are hereby verified. In the light of this result, we confer that the icosahedral symmetry found in these two complementary solids paved a way to the configuration of C_{20} of the buckyball, as will be exploited in Part II.

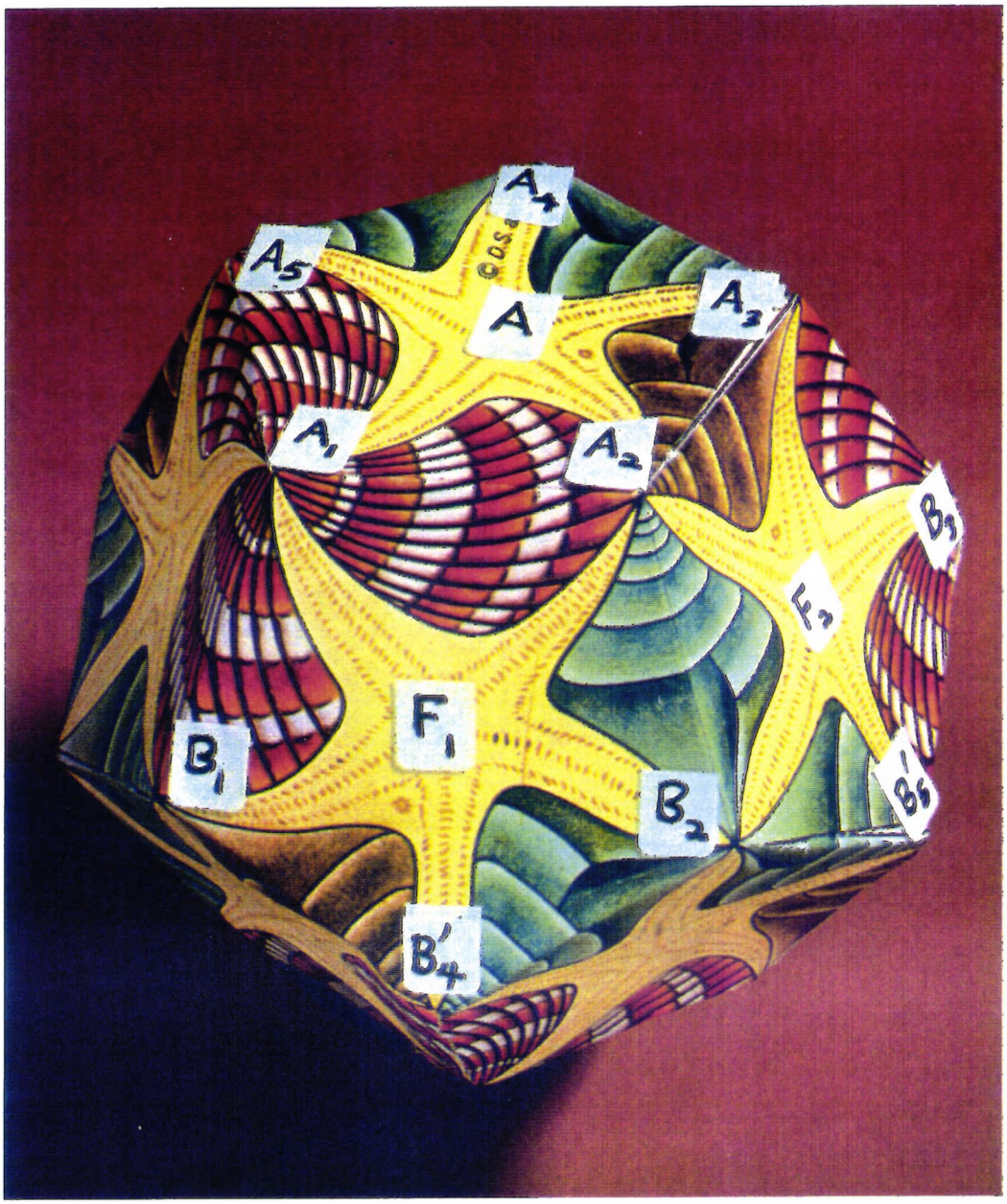

Figure 3.5: Photoprint of the regular dodecahedron which displays three of the five adjoining face-centres A, F_1, F_2, ..., F_4. The tesselation of this model is based upon Escher's drawing in [5].

Vertices	X, Y, Z	*Inverse Vertices*
A_1	$(a, 0, \mid OA \mid)$ $a\left(1, 0, \frac{3+\sqrt{5}}{4}\right)$	A_1'
A_2	$\left(a\cos\frac{2\pi}{5}, a\sin\frac{2\pi}{5}, \mid OA \mid\right)$ $a\left(\cos\frac{2\pi}{5}, \sin\frac{2\pi}{5}, \frac{3+\sqrt{5}}{4}\right)$	A_2'
A_3	$\left(a\cos\frac{4\pi}{5}, a\sin\frac{4\pi}{5}, \mid OA \mid\right)$ $a\left(-\cos\frac{\pi}{5}, \sin\frac{\pi}{5}, \frac{3+\sqrt{5}}{4}\right)$	A_3'
A_4	$\left(a\cos\frac{6\pi}{5}, a\sin\frac{6\pi}{5}, \mid OA \mid\right)$ $a\left(-\cos\frac{\pi}{5}, -\sin\frac{\pi}{5}, \frac{3+\sqrt{5}}{4}\right)$	A_4'
A_5	$\left(a\cos\frac{8\pi}{5}, a\sin\frac{8\pi}{5}, \mid OA \mid\right)$ $a\left(\cos\frac{2\pi}{5}, -\sin\frac{2\pi}{5}, \frac{3+\sqrt{5}}{4}\right)$	A_5'

Table 3.1: Coordinates Of The Vertices In The A-plane. Note that $a = l\csc\frac{\pi}{5}$ while $\mid OA \mid$ is effectively provided by formula (3.2.9).

Vertices	X, Y, Z	*Inverse Vertices*
B_1	$(b, 0, \mid OB \mid)$ $a\left(2 \sin \frac{3\pi}{10}, 0, \frac{-1+\sqrt{5}}{4}\right)$	B_1'
B_2	$\left(b\cos \frac{2\pi}{5}, b\sin \frac{2\pi}{5}, \mid OB \mid\right)$ $a\left(2 \sin \frac{3\pi}{10} \cos \frac{2\pi}{5}, 2 \sin \frac{3\pi}{10} \sin \frac{2\pi}{5}, \frac{-1+\sqrt{5}}{4}\right)$	B_2'
B_3	$\left(b\cos \frac{4\pi}{5}, b\sin \frac{4\pi}{5}, \mid OB \mid\right)$ $a\left(-2 \cos^2 \frac{\pi}{5}, 2\sin \frac{3\pi}{10} \sin \frac{\pi}{5}, \frac{-1+\sqrt{5}}{4}\right)$	B_3'
B_4	$\left(b\cos \frac{6\pi}{5}, b\sin \frac{6\pi}{5}, \mid OB \mid\right)$ $a\left(-2\cos^2 \frac{\pi}{5}, -2\sin \frac{3\pi}{10} \sin \frac{\pi}{5}, \frac{-1+\sqrt{5}}{4}\right)$	B_4'
B_5	$\left(b\cos \frac{8\pi}{5}, b\sin \frac{8\pi}{5}, \mid OB \mid\right)$ $a\left(2 \sin \frac{3\pi}{10} \cos \frac{2\pi}{5}, -2 \sin \frac{3\pi}{10} \sin \frac{2\pi}{5}, \frac{-1+\sqrt{5}}{4}\right)$	B_5'

Table 3.2: Coordinates Of The Vertices In The B-plane. Note that b, $\mid OB \mid$ are provided by formulae (3.2.4), (3.2.8) in terms of a.

3–fold symmetry axes	$X : Y : Z$
$(A_1A_1')_3$	$2a : 0 : 2 \mid OA \mid$ $2 : 0 : \frac{3+\sqrt{5}}{2}$
$(A_2A_2')_3$	$2a \cos \frac{2\pi}{5} : 2a \sin \frac{2\pi}{5} : 2 \mid OA \mid$ $2\cos \frac{2\pi}{5} : 2\sin \frac{2\pi}{5} : \frac{3+\sqrt{5}}{2}$
$(A_3A_3')_3$	$2a \cos \frac{4\pi}{5} : 2a \sin \frac{4\pi}{5} : 2 \mid OA \mid$ $-2\cos \frac{\pi}{5} : 2\sin \frac{\pi}{5} : \frac{3+\sqrt{5}}{2}$
$(A_4A_4')_3$	$2a \cos \frac{6\pi}{5} : 2a \sin \frac{6\pi}{5} : 2 \mid OA \mid$ $-2\cos \frac{\pi}{5} : -2\sin \frac{\pi}{5} : \frac{3+\sqrt{5}}{2}$
$(A_5A_5')_3$	$2a \cos \frac{8\pi}{5} : 2a \sin \frac{8\pi}{5} : 2 \mid OA \mid$ $2\cos \frac{2\pi}{5} : -2\sin \frac{2\pi}{5} : \frac{3+\sqrt{5}}{2}$

Table 3.3: Direction-ratios of A type 3–fold symmetry axes e.g. $(A_1A_1')_3$ signifies the 3–fold symmetry axis joining the vertex A_1 into its inverse A_1'.

3-fold symmetry axes	$X : Y : Z$
$(B_1B_1')_3$	$4a \sin \frac{3\pi}{10} : 0 : 2 \mid OB \mid$ $4 \sin \frac{3\pi}{10} : 0 : \frac{-1+\sqrt{5}}{2}$
$(B_2B_2')_3$	$4a \sin \frac{3\pi}{10} \cos \frac{2\pi}{5} : 4a \sin \frac{3\pi}{10} \sin \frac{2\pi}{5} : 2 \mid OB \mid$ $4 \sin \frac{3\pi}{10} \cos \frac{2\pi}{5} : 4 \sin \frac{3\pi}{10} \sin \frac{2\pi}{5} : \frac{-1+\sqrt{5}}{2}$
$(B_3B_3')_3$	$-4a \cos^2 \frac{\pi}{5} : 4a \sin \frac{3\pi}{10} \sin \frac{\pi}{5} : 2 \mid OB \mid$ $-4 \cos^2 \frac{\pi}{5} : 4 \sin \frac{3\pi}{10} \sin \frac{\pi}{5} : \frac{-1+\sqrt{5}}{2}$
$(B_4B_4')_3$	$-4a \cos^2 \frac{\pi}{5} : -4a \sin \frac{3\pi}{10} \sin \frac{\pi}{5} : 2 \mid OB \mid$ $-4 \cos^2 \frac{\pi}{5} : -4 \sin \frac{3\pi}{10} \sin \frac{\pi}{5} : \frac{-1+\sqrt{5}}{2}$
$(B_5B_5')_3$	$4a \sin \frac{3\pi}{10} \cos \frac{2\pi}{5} : -4a \sin \frac{3\pi}{10} \sin \frac{2\pi}{5} : 2 \mid OB \mid$ $4 \sin \frac{3\pi}{10} \cos \frac{2\pi}{5} : -4 \sin \frac{3\pi}{10} \sin \frac{2\pi}{5} : \frac{-1+\sqrt{5}}{2}$

Table 3.4: Direction-ratios of B type 3-fold symmetry axes e.g. $(B_1B_1')_3$ signifies the 3-fold axis joining the vertex B_1 into the inverse vertex B_1'.

2–fold symmetry axes	$X : Y : Z$
$(A_1A_2)_2$	$a + a\cos\frac{2\pi}{5} : a\sin\frac{2\pi}{5} : 2 \mid OA \mid$ $1 + \cos\frac{2\pi}{5} : \sin\frac{2\pi}{5} : \frac{3+\sqrt{5}}{2}$
$(A_2A_3)_2$	$a\cos\frac{2\pi}{5} - a\cos\frac{\pi}{5} : a\sin\frac{2\pi}{5} + a\sin\frac{\pi}{5} : 2 \mid OA \mid$ $\cos\frac{2\pi}{5} - \cos\frac{\pi}{5} : \sin\frac{2\pi}{5} + \sin\frac{\pi}{5} : \frac{3+\sqrt{5}}{2}$
$(A_3A_4)_2$	$-2a\cos\frac{\pi}{5} : 0 : 2 \mid OA \mid$ $-2\cos\frac{\pi}{5} : 0 : \frac{3+\sqrt{5}}{2}$
$(A_4A_5)_2$	$-a\cos\frac{\pi}{5} + a\cos\frac{2\pi}{5} : -a\sin\frac{\pi}{5} - a\sin\frac{2\pi}{5} : 2 \mid OA \mid$ $-\cos\frac{\pi}{5} + \cos\frac{2\pi}{5} : -\sin\frac{\pi}{5} - \sin\frac{2\pi}{5} : \frac{3+\sqrt{5}}{2}$
$(A_5A_1)_2$	$a\cos\frac{2\pi}{5} + a : -a\sin\frac{2\pi}{5} : 2 \mid OA \mid$ $\cos\frac{2\pi}{5} + 1 : -\sin\frac{2\pi}{5} : \frac{3+\sqrt{5}}{2}$

Table 3.5: Direction-ratios of A type 2–fold symmetry axes e.g. $(A_1A_2)_2$ signifies the 2–fold symmetry axis joining the mid-point of the edge A_1A_2 into the mid-point of inverse edge $A_1'A_2'$.

2–fold symmetry axes	$X : Y : Z$
$(A_1B_1)_2$	$\frac{(3+\sqrt{5})}{2}\,a : 0 : \mid OA \mid + \mid OB \mid$ $\frac{3+\sqrt{5}}{2} : 0 : \frac{(2+\sqrt{5})}{4}$
$(A_2B_2)_2$	$\frac{(1+\sqrt{5})}{4}\,a : (2+\sqrt{5})\,a \sin\frac{\pi}{5} : \mid OA \mid + \mid OB \mid$ $\frac{(1+\sqrt{5})}{4} : (2+\sqrt{5}) \sin\frac{\pi}{5} : \frac{(2+\sqrt{5})}{4}$
$(A_3B_3)_2$	$\frac{-(2+\sqrt{5})}{2}\,a : \frac{(3+\sqrt{5})}{2}a \sin\frac{\pi}{5} : \mid OA \mid + \mid OB \mid$ $\frac{-(2+\sqrt{5})}{2} : \frac{(3+\sqrt{5})}{2} \sin\frac{\pi}{5} : \frac{(2+\sqrt{5})}{4}$
$(A_4B_4)_2$	$\frac{-(2+\sqrt{5})}{2}\,a : \frac{-(3+\sqrt{5})}{2}\,a \sin\frac{\pi}{5} : \mid OA \mid + \mid OB \mid$ $\frac{-(2+\sqrt{5})}{2} : \frac{-(3+\sqrt{5})}{2} \sin\frac{\pi}{5} : \frac{(2+\sqrt{5})}{4}$
$(A_5B_5)_2$	$\frac{(1+\sqrt{5})}{4}\,a : -(2+\sqrt{5})\,a \sin\frac{\pi}{5} : \mid OA \mid + \mid OB \mid$ $\frac{(1+\sqrt{5})}{4} : -(2+\sqrt{5}) \sin\frac{\pi}{5} : \frac{(2+\sqrt{5})}{4}$

Table 3.6: Direction-ratios of AB type 2–fold symmetry axes e.g. $(A_1B_1)_2$ signifies the 2–fold symmetry axis joining the mid-point of the edge A_1B_1 into the mid-point of inverse edge $A_1'B_1'$.

2–fold symmetry axes	$X : Y : Z$
$(B_1B_4')_2$	$\frac{5+3\sqrt{5}}{4}\,a : \frac{1+\sqrt{5}}{2}\,a \sin\frac{\pi}{5} : 0$ $\frac{5+3\sqrt{5}}{4} : \frac{1+\sqrt{5}}{2}\sin\frac{\pi}{5} : 0$
$(B_2B_5')_2$	$0 : (3+\sqrt{5})\,a \sin\frac{\pi}{5} : 0$ $0 : 1 : 0$
$(B_3B_1')_2$	$\frac{-(5+3\sqrt{5})}{4}\,a : \frac{1+\sqrt{5}}{2}\,a \sin\frac{\pi}{5} : 0$ $\frac{-(5+3\sqrt{5})}{4} : \frac{1+\sqrt{5}}{2}\sin\frac{\pi}{5} : 0$
$(B_4B_2')_2$	$\frac{-(5+\sqrt{5})}{4}\,a : -(2+\sqrt{5})\,a \sin\frac{\pi}{5} : 0$ $\frac{-(5+\sqrt{5})}{4} : -(2+\sqrt{5})\sin\frac{\pi}{5} : 0$
$(B_5B_3')_2$	$\frac{5+\sqrt{5}}{4}\,a : -(2+\sqrt{5})\,a \sin\frac{\pi}{5} : 0$ $\frac{5+\sqrt{5}}{4} : -(2+\sqrt{5})\sin\frac{\pi}{5} : 0$

Table 3.7: Direction-ratios of B' type 2–fold symmetry axes e.g. $(B_1B_4')_2$ signifies the 2–fold symmetry axis joining the mid-point of the edge B_1B_4' into the mid-point of inverse edge $B_1'B_4$.

5–fold symmetry axes	$X : Y : Z$
$(AA')_5$	$0 : 0 : 2 \mid OA \mid$ $0 : 0 : 1$
$(F_1F_1')_5$	$\frac{5+2\sqrt{5}}{2}\, a : \frac{5+3\sqrt{5}}{2}\, a \sin \frac{\pi}{5} : 2 \mid OA \mid + \mid OB \mid$ $\frac{5+2\sqrt{5}}{2} : \frac{5+3\sqrt{5}}{2} \sin \frac{\pi}{5} : \frac{5+3\sqrt{5}}{4}$
$(F_2F_2')_5$	$\frac{-(5+\sqrt{5})}{4}\, a : (5 + 2\sqrt{5})\, a \sin \frac{\pi}{5} : 2 \mid OA \mid + \mid OB \mid$ $\frac{-(5+\sqrt{5})}{4} : (5 + 2\sqrt{5}) \sin \frac{\pi}{5} : \frac{5+3\sqrt{5}}{4}$
$(F_3F_3')_5$	$-2\, a(5 + 3\sqrt{5}) : 0 : 2 \mid OA \mid + \mid OB \mid$ $8 : 0 : -1$
$(F_4F_4')_5$	$\frac{-(5+\sqrt{5})}{4}\, a : -(5 + 2\sqrt{5})\, a \sin \frac{\pi}{5} : 2 \mid OA \mid + \mid OB \mid$ $\frac{-(5+\sqrt{5})}{4} : -(5 + 2\sqrt{5}) \sin \frac{\pi}{5} : \frac{5+3\sqrt{5}}{4}$
$(F_5F_5')_5$	$\frac{5+2\sqrt{5}}{2}\, a : \frac{-(5+3\sqrt{5})}{2}\, a \sin \frac{\pi}{5} : 2 \mid OA \mid + \mid OB \mid$ $\frac{5+2\sqrt{5}}{2} : \frac{-(5+3\sqrt{5})}{2} \sin \frac{\pi}{5} : \frac{5+3\sqrt{5}}{4}$

Table 3.8: Direction-ratios of 5–fold symmetry axes e.g. $(AA')_5$ signifies the 5–fold symmetry axis joining the centroid of the pentagonal face A into the centroid of the inverse face A'.

Part II

FULLERENES

Chapter 4

C_{60}: Buckminsterfullerene

Φ Φ ——————————————————————————— Φ Φ

4.1 Introduction

With the advanced role of science in today's world we gain more knowledge of carbon, its existence and properties than we could ever imagine. Though we cannot detect it directly, its atoms are in every cell of our bodies, which makes carbon at the heart of all that sustains life on earth. In 1985 Kroto, Smalley et al. [6], on the basis of spectroscopic evidence, deduced the existence of a new carbon molecule C_{60} diffused through interstellar space. They also proposed that the molecule had an essentially spherical shape, the "buckyball", previously unknown to carbon chemistry. A few years later Krätschmer, Huffman et al. [7] produced C_{60} crystals in the laboratory, which opened the way to an explosion of experimental and theoretical research which still continues. Some mathematical features of buckyballs will be explored in this thesis, building upon the work of Part I.

The carbon atom has four valence electrons, which are available to form directed pair-bonds with neighbouring carbon atoms in symmetrical configurations. In diamond, for instance, each carbon atom lies at the centroid of a regular tetrahedron defined by its four nearest neighbours (Figure 4.1), and this pattern is

repeated in space to produce the diamond crystal. The C–C bond arises from two paired electrons, one from each atom, which oscillate between them to produce an attractive force according to the rules of quantum mechanics. This is the covalent bond of theoretical chemistry.

For some structures, only three of the valence electrons are utilised to form directed pair-bonds e.g. graphite. Here each carbon atom lies at the centroid of an equilateral triangle defined by its three nearest neighbours, so providing

$$OA = OB = OC = 1.420(4)\ \mathring{A} \tag{4.1.1}$$

showing an intermediate bond strength between $d(6{:}5)$ and $d(6{:}6)$. This pattern is repeated to produce the two-dimensional hexagonal layers as depicted in Figure 4.2 (a). The fourth valence electron (π - electron) breaks free from its atom and moves parallel to the layers so helping to

(i) *maintain the layers as planes and*

(ii) *stabilise them into an equilibrium stacking characteristic of the graphite crystal.*

Diamond and graphite were the only structures for pure carbon known before 1985. In that year, as already mentioned, the buckyball configuration was envisaged. This has 60 carbon atoms arranged symmetrically on the surface of a sphere of radius $R \sim 3.550(10)\ \mathring{A}$ [7,8], as depicted by the vertex points of a black-and-white football model covered by 12 regular spherical pentagons and 20 (slightly distorted) regular hexagons in Figure 4.3 (a). Equivalently we may imagine a regular icosahedron truncated at the the vertices, so providing a pentagonal-hexagonal framework as depicted in Figure 4.3 (b). Now two fundamental questions which arise from this model remain to be considered.

1. Must there be only 12 regular pentagons and 20 regular hexagons?

2. Is there a unique symmetrical arrangement of 60 equivalent carbon atoms on the surface of a sphere?

The first question is intimately connected with Euler's formula. Let the faces of a polyhedron comprise p pentagons and h hexagons only. Then

$$F = p + h. \tag{4.1.2}$$

Since the pentagons contribute $5p$ edges, whilst the hexagons contribute $6h$ edges, therefore

$$E = \frac{(5p + 6h)}{2} \tag{4.1.3}$$

due to each edge being counted twice. Likewise, since each vertex is common to three edges it follows that

$$V = \frac{(5p + 6h)}{3} \quad . \tag{4.1.4}$$

Euler's formula now gives

$$2 = F + V - E = (p + h) + \left(\frac{5p + 6h}{3}\right) - \left(\frac{5p + 6h}{2}\right)$$

$$= \frac{6(p + h) + 2(5p + 6h) - 3(5p + 6h)}{6} = \frac{p}{6}$$

so that $p = 12$.

This result imposes no mathematical constraint on h. However, as will be shown later, we must choose $h = 20$ or $h = 0$ to ensure a spherical configuration.

4.2 Geometrical Construction of C_{60}

Because the structural principle underlying C_{60} is in line with the geodesic dome created by the American architect Buckminster Fuller, who based it upon a hexagonal and pentagonal framework, this spherical configuration has been termed

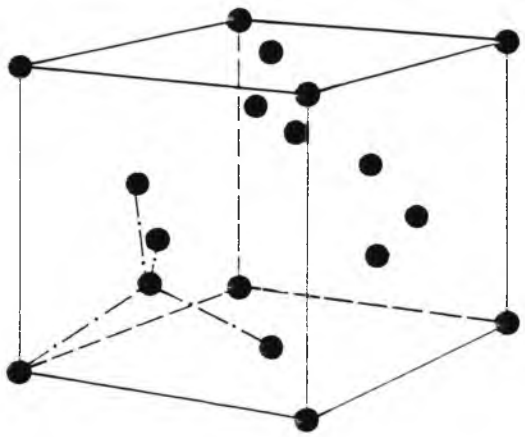

Figure 4.1: The carbon-bonding structure of a diamond. Each cluster of carbon is depicted at four vertices of the regular tetrahedron.

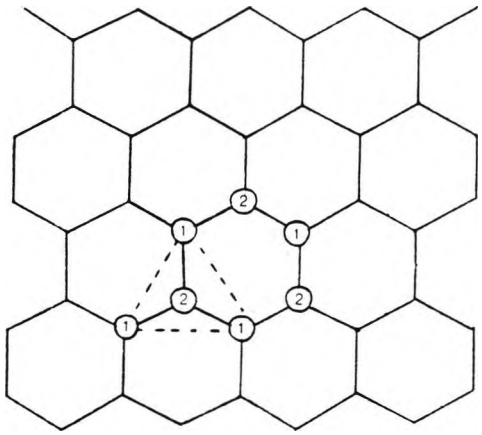

(a) Note that the three neighbouring vertices to

(2) form an equilateral triangle [9]

(b) Here $OA = OB = OC = d(6{:}6)$, i.e. a hexagonal-hexagonal boundary. Corresponding chemical data yields $d(6{:}6) = 1.420$ Å; with $A\hat{O}B = B\hat{O}C = C\hat{O}A = 120^0$.

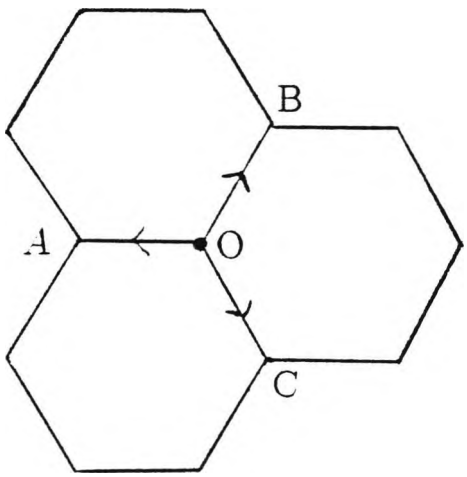

Figure 4.2: Planar configuration of graphite layer.

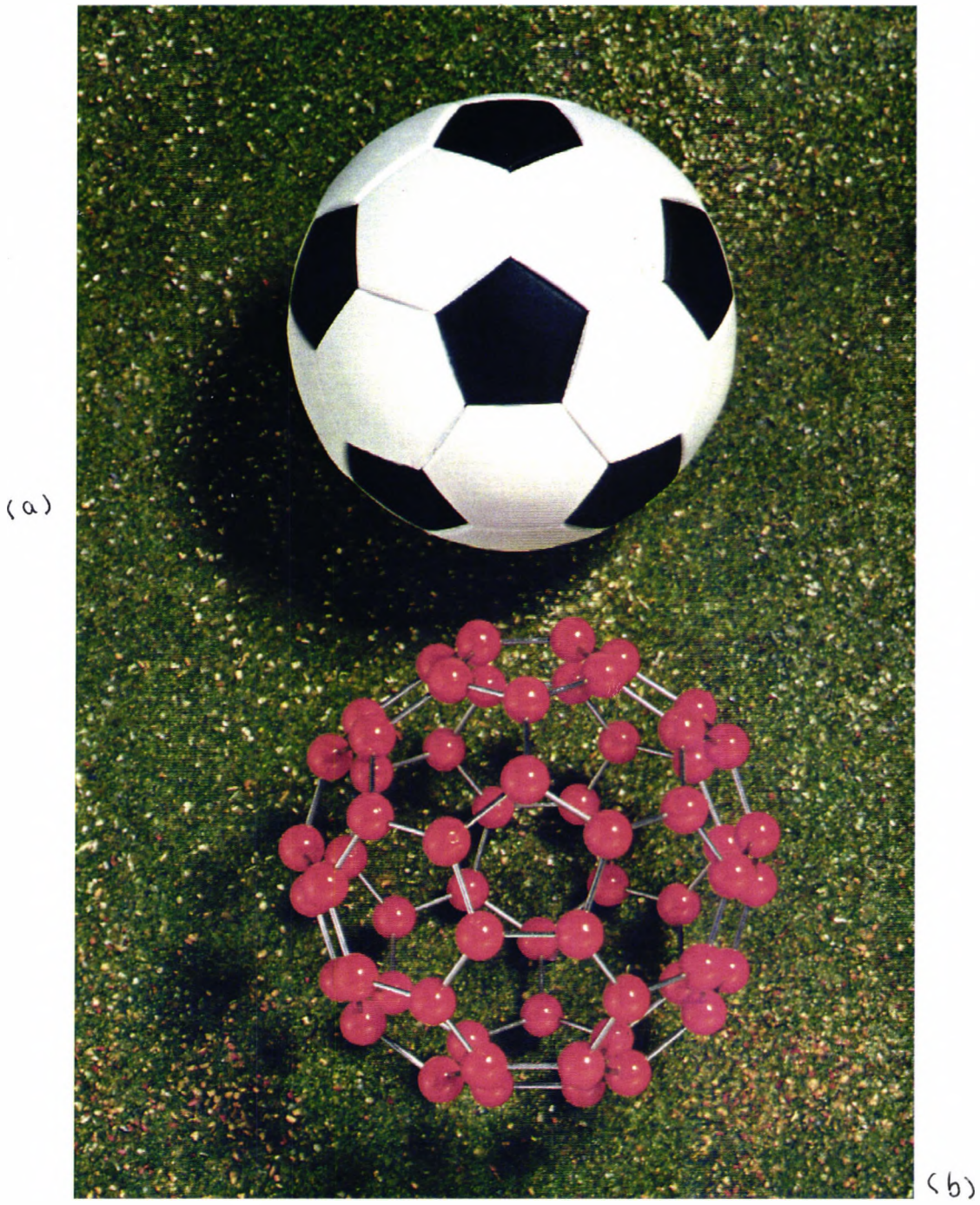

Figure 4.3: Idealized structures of C_{60} displayed by (a) a black-and-white football model (b) lattice model showing a pentagonal-hexagonal pattern on the surface of a sphere.

"buckminsterfullerene" or buckyball for short. By the same token we refer to the chemical compound composed of C_{60} molecules as fullerene.

A useful starting point for buckyball analysis is the regular icosahedron of edge length $2l$ to be determined. This has a circumsphere of radius R—which passes through all the vertices. Any vertex P is chosen as the pole vertex i.e. has coordinates $(0,\ 0,\ R)$ relative to the rectangular cartesian system introduced in Part I. Now replace P by a shallow spherical cap of depth

$$h = f\,R \tag{4.2.1}$$

where f is a non-dimensional parameter approximately within the interval $0.01 \leq f \leq 0.142$. A regular pentagon $p_1, p_2, \ldots, p_5$, centre P_0, is then inscribed in the latitude circle of radius $p \equiv |\ P_0p_1\ |$ where P_0 marks the projection of P upon the latitude plane. If so

$$|\ Op_1\ |^2 = |\ OP_0\ |^2 + |\ P_0p_1\ |^2$$

i.e.

$$R^2 = (R - h)^2 + p^2$$

so giving

$$p \simeq R\sqrt{2f} \tag{4.2.2}$$

on neglecting $\bigcirc\,(f^2)$ in comparison with $\bigcirc\,(f)$. See Figure 4.4 for details.

We may choose p_1 so that it is located in the XOZ-plane i.e. plane of *great circle* passing through P and the neighbouring icosahedral vertex A_1 (Figure 4.5). By analogy with the pentagon $A_1, A_2, \ldots, A_5$ (Chap. 2), vertices of the latitude pentagon (Figure 4.6) may be conveniently represented by the complex vectors

$$\vec{P_Op_1} = p\,e^{i0},\ \vec{P_Op_2} = p\,e^{i\frac{2\pi}{5}}, \ldots \tag{4.2.3}$$

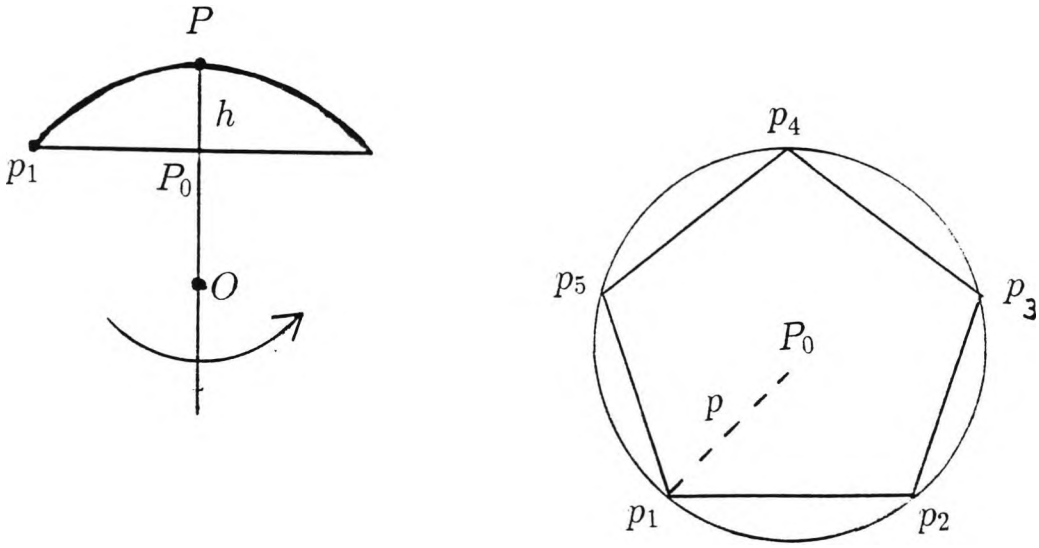

Figure 4.4: Spherical pentagon with latitude circle of radius p

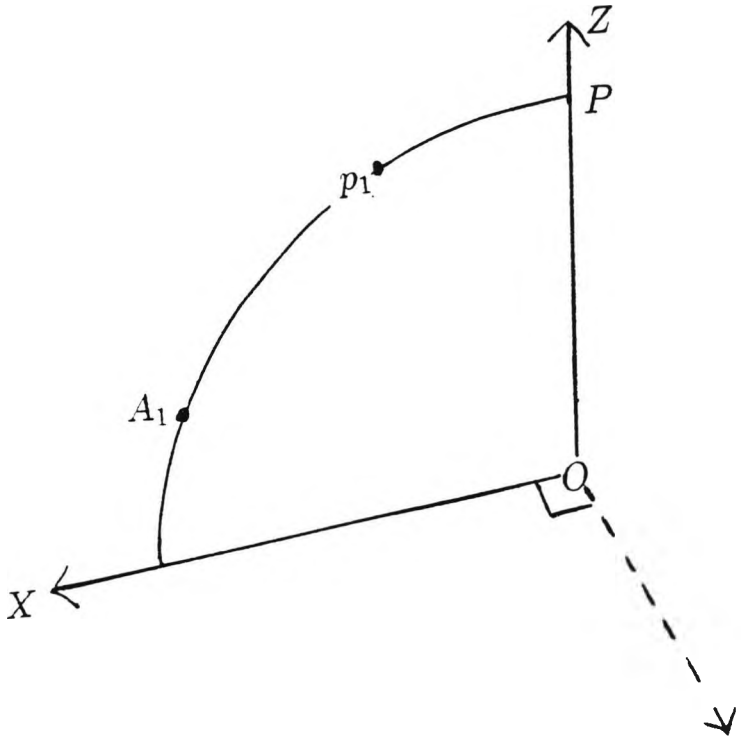

Figure 4.5: A convenient location of p_1 on the *great circle*, which pass through pole vertex P into the neighbouring icosahedral vertex A_1.

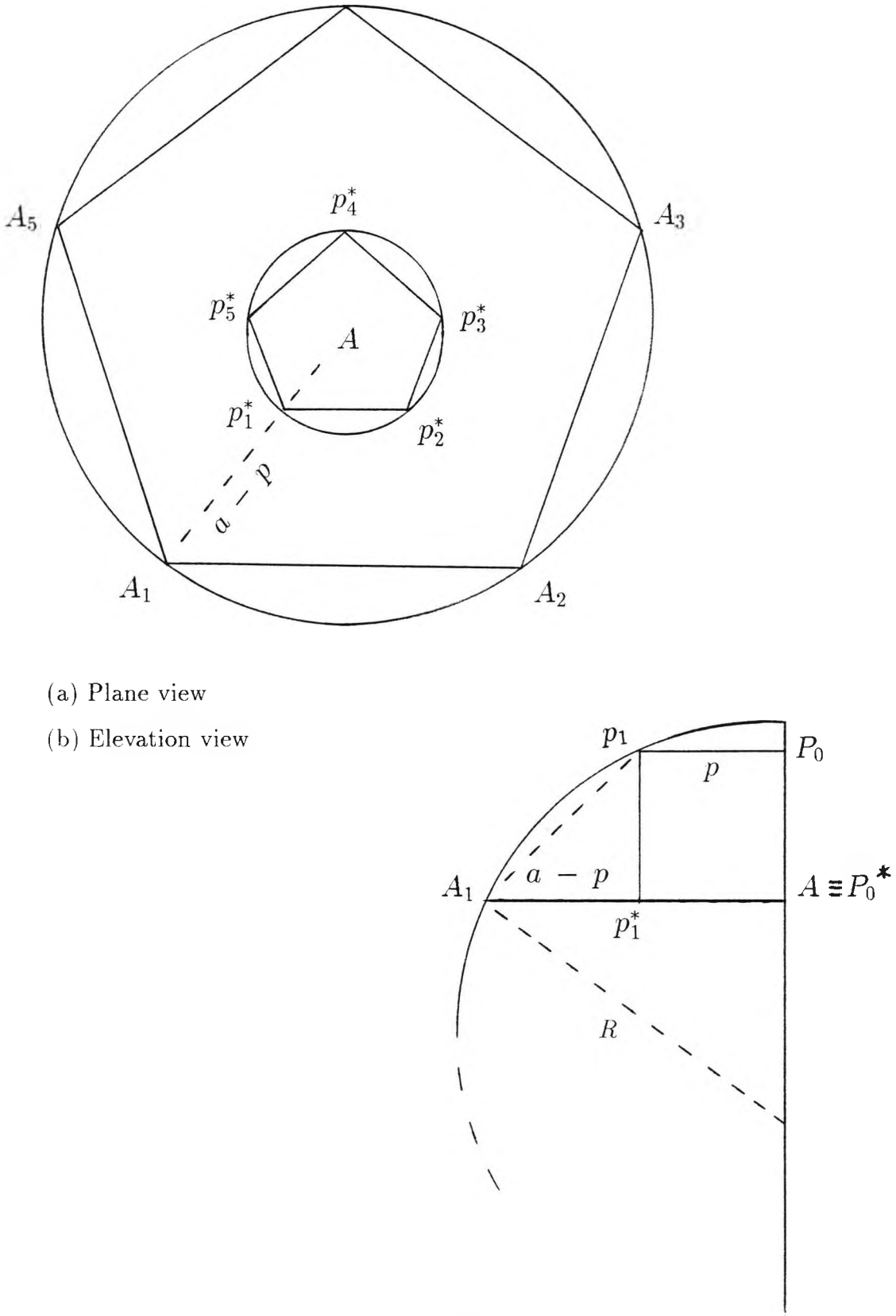

(a) Plane view

(b) Elevation view

Figure 4.6: Orthogonal projection of parallel latitude pentagons.

which provide the x, y coordinates of $p_1, p_2, \ldots, p_5$ respectively as listed in Appendix E. If so. then the x, y coordinates of $p_1, p_2, \ldots, p_5$ are the same as $A_1, A_2, \ldots, A_5$ (see Table 2.1) with a replaced by p. Of course all the vertices have the same z-coordinate given by

$$| OP_0 | = | OP | - | PP_0 | = R - h \simeq R(1 - f). \tag{4.2.4}$$

The pentagon has a side of length

$$\begin{aligned} d(6:5) &= | p_1 - p_2 | = 2 | P_0 - p_1 | \sin \frac{\pi}{5} \\ &= 2p \sin \frac{\pi}{5} = 2R\sqrt{2f} \sin \frac{\pi}{5} \end{aligned} \tag{4.2.5}$$

which brings out the dependence of $d(6{:}5)$ upon R and f. Note that the football model of course depicts a spherical pentagon, with $| p_1 - p_2 |$ replaced by $| p_1 \overset{\frown}{-} p_2 |$ i.e. arc length of *great circle* joining p_1 and p_2. A rough calculation of the ratio $| p_1 \overset{\frown}{-} p_2 | / | p_1 - p_2 |$ is given in Appendix F showing it to be $\simeq 1.02$ for the natural buckyball.

The remaining 11 spherical pentagons may be constructed by symmetry operations upon the pole pentagon as explained in Chap. 5. An immediate consequence is the automatic appearance of 20 spherical hexagons carved out from the 20 spherical triangles of the original icosahedral circumsphere. Hence we have deduced the football model by imposing spherical symmetry upon a hexagon-pentagon framework. This model provides a useful visual supplement to the truncated icosahedron model often pictured by (see Figure 4.3). Of course the latter model is more realistic since C–C bonds appear as straight lines rather than as arc of circles.

4.3 Preliminary Perspective of C_{60}

Clearly the buckyball is a spherical variant of the graphite layer in which hexagonal distortion arises consequent upon the necessary presence of pentagons. To examine

this in detail, refer to Figure 4.7 which exhibits a vertex O and its three neighbouring vertices A, B, C. Note that we write

$$OA = OB = d(6:5),\ OC = d(6:6) \tag{4.3.1}$$

since OA, OB form hexagonal-pentagonal boundaries whilst OC forms a hexagonal-hexagonal boundary. Chemical data [16] yield

$$d(6:5) = 1.455(12)\ \mathring{A},\ d(6:6) = 1.391(18)\ \mathring{A} \tag{4.3.2}$$

showing that the pure hexagonal bond is stronger than its neighbours. A further effect is the slight distortion of the hexagon from regularity due to sides of alternating length.

Note that the pentagon remains perfectly regular since all its sides have d(6:5) character, with $A\hat{O}B = 108.0(1)^0$. Finally, as in graphite, each buckyball atom donates a valence electron to the molecule as a whole (π-electron), which becomes available for electrical conduction when the molecules crystallise into a lattice. See Figure 4.8 for details.

In Chap.5 we compute the coordinates of neighbouring vertices in a buckyball. This enables us to determine d(6:6) as a function of the shallowness parameter f for a given R. Utilising (4.2.5), we obtain the ratio $\delta \equiv d(6{:}6)\ /\ d(6{:}5)$ as a function of f without reference to R. Some choice of δ will be considered in relation to possible buckyball configurations.

Figure 4.7: Two distinct carbon bonds d(6:6) and d(6:5) in bucky ball. Carbon atom at O has three directed bonds linking it with nearest neighbours A,B,C. Here hexagons cannot be perfectly regular, since d(6:5)≠ d(6:6) by virtue of the following chemical data: d(6:5)=1.455(12) °A, d(6:6)=1.391(18) °A. We also note $A\hat{O}B$=108.0(1)°, $A\hat{O}C$=$B\hat{O}C$= 120.0(1)°.

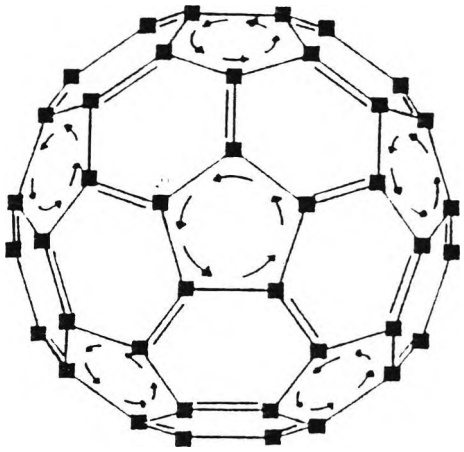

Figure 4.8: The fourth valence electron of the carbon atom is utilised as the double bond, which enhances the strength of the pure hexagonal bond [17]. The arrow $\longrightarrow$ corresponds to double bond emanating from a pentagon, five from each pentagon.

Chapter 5

Bonding Structure of C_{60}, C_{20} and Graphite

5.1 Determination of Pentagon Coordinates

The P-pentagon (p_1, p_2, ..., p_5) has five nearest neighbouring pentagons centred respectively upon the five icosahedral vertices A_1, A_2, ..., A_5 (see Figure 4.6), in particular the A_1-pentagon with vertices a_{11}, a_{12}, ..., a_{15}. The vertex a_{11} lies upon the *great circle* joining P and A_1 (Figure 5.1), being located approximately as close as to p_1 as its home neighbours p_2, p_5 i.e. the a_{11}-atom is available to provide a third pair-bond for the p_1-atom chemically required. Accordingly we write

$$d(6:6) = | p_1 - a_{11} | \tag{5.1.1}$$

where the coordinates of p_1 have already been determined as a function of the shallowness parameter f. However, it remains to compute those of a_{11}.

Note that a rotation through π about the axis $(PA_1)_2$, see Table 2.3 for its direction-ratios (drs), transforms P into A_1 (Figure 5.2). The same rotation trans-

Figure 5.1: Note that a_{11} is the nearest vertex to p_1 in A_1-pentagon, joining two neighbouring icosahedral vertices P and A_1.

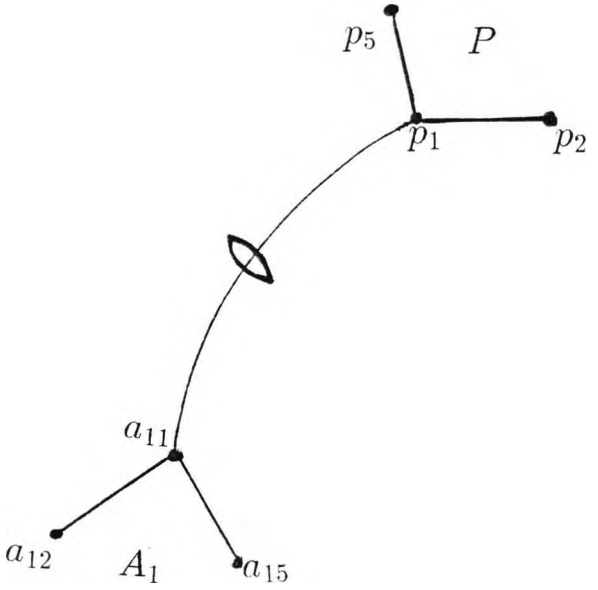

Figure 5.2: Transformation of icosahedral vertex P into icosahedral vertex A_1 by rotation through π about $(PA_1)_2$ generates a 2-fold symmetry axis passing through O and the mid-point of PA_1.

transforms p_1 into a_{11}, and more generally

$$p_1,\ p_2,\ \ldots,\ p_5 \longrightarrow a_{11},\ a_{12},\ \ldots,\ a_{15}$$

This transformation may be implemented mathematically by a rotation operator symbolised $M\ (h\ k\ l;\theta)$ where h, k, l are the drs of the axis and θ is the angle of rotation [9].

To construct $M\ (h\,k\,l;\theta)$ we transform from the original rectangular coordinates x, y, z to new rectangular cartesian coordinates X, Y, Z defined by

$$OZ \parallel h:k:l,\ OX \parallel l:O:\overline{h},\ OY \parallel \overline{h}k:h^2+l^2:\overline{k}l \tag{5.1.2}$$

which we may describe by the axis transformation matrix

$$(XYZ \mid xyz) = \frac{1}{NS}\begin{pmatrix} lN & 0 & \overline{hN} \\ \overline{hk} & S^2 & \overline{kl} \\ hS & kS & lS \end{pmatrix};S = \left(l^2+h^2\right)^{1/2},$$

$$N = \left(h^2+k^2+l^2\right)^{1/2} \tag{5.1.3}$$

Note that $(XYZ \mid xyz)$ is an orthogonal matrix, so that $(XYZ \mid xyz)^{-1} = (xyz \mid XYZ)$ = transpose of $(XYZ \mid xyz)$. If so, M provides a rotation through θ about OZ, i.e. it takes the simple form

$$M_Z\,(0\,0\,1;\theta) = \begin{pmatrix} \cos\theta & \overline{\sin\theta} & 0 \\ \sin\theta & \cos\theta & 0 \\ 0 & 0 & 1 \end{pmatrix}. \tag{5.1.4}$$

Now

$$M\,(h\ k\ l;\theta)\begin{pmatrix} x \\ y \\ z \end{pmatrix} = (xyz \mid XYZ)\ M_Z\,(0\,0\,1;\theta)\ (XYZ \mid xyz)\begin{pmatrix} x \\ y \\ z \end{pmatrix}$$

showing that

$$M\ (h\ k\ l;\theta)\ =\ (x\ y\ z\ \mid\ XYZ)\ M_Z\ (0\ 0\ 1;\theta)\ (XYZ\ \mid\ x\ y\ z) \tag{5.1.5}$$

$$= \cos\theta \begin{pmatrix} 1 & 0 & 0 \\ 0 & 1 & 0 \\ 0 & 0 & 1 \end{pmatrix} + \frac{\sin\theta}{N} \begin{pmatrix} 0 & \overline{l} & k \\ l & 0 & \overline{h} \\ \overline{k} & h & 0 \end{pmatrix} + \frac{1-\cos\theta}{N^2} \begin{pmatrix} h^2 & hk & hl \\ hk & k^2 & kl \\ hl & kl & l^2 \end{pmatrix}.$$

Substituting $h = 1$, $k = 0$, $l = 2\cos\frac{\pi}{5}$ and $\theta = \pi$ into (5.1.5) gives the matrix expression

$$M\ =\ \cos\theta \begin{pmatrix} \frac{-\sqrt{5}}{5} & 0 & \frac{2\sqrt{5}}{5} \\ 0 & -1 & 0 \\ \frac{2\sqrt{5}}{5} & 0 & \frac{\sqrt{5}}{5} \end{pmatrix}. \tag{5.1.6}$$

Note as expected that

(a) $M\ (h\ k\ l;0) = 1$ for any h, k, l

(b) $M\ (0\ 0\ 1;\theta) = M_Z\ (0\ 0\ 1;\theta)$.

It may readily verified that

$$M\,(x\ ,\ y\ ,\ z)_P\ =\ (x\ ,\ y\ ,\ z)_{A_1} \tag{5.1.7}$$

where

$$(x\ ,\ y\ ,\ z)_P\ =\ (0\ ,\ 0\ ,\ R)\,,$$

$$(x\ ,\ y\ ,\ z)_{A_1}\ =\ \left(a\ ,\ 0\ ,\ \frac{a}{2}\right). \tag{5.1.8}$$

If so, then

$$M\,(x\,,\,y\,,\,z)_{p_1} \;=\; (x\,,\,y\,,\,z)_{a_{11}}$$

$$= R\left(\frac{-\sqrt{10}}{5} + \frac{2\sqrt{5}}{5}(1 - f)\,,\,0\,,\,\frac{2\sqrt{10\,f}}{5} + \frac{\sqrt{5}}{5}(1 - f)\right) \tag{5.1.9}$$

since

$$(x\,,\,y\,,\,z)_{p_1} \;=\; R\left(\sqrt{2f}\,,\,0\,,\,1 - f\right). \tag{5.1.10}$$

Proceeding in a similar way with p_2, p_3, p_4 and p_5, we then arrive at all the coordinates of the corresponding vertices a_{12}, a_{13}, a_{14} and a_{15}, for $0.01 \leq \mathrm{f} \leq 0.142$. Therefore

$$d(6:6) \;= |\; p_1 \;-\; a_{11} \;|$$

$$= R \;\left|\left(\frac{-\sqrt{10}}{5} + \frac{2\sqrt{5}}{5}(1 - f) - \sqrt{2f}\right)^2 + \left(\frac{2\sqrt{10\,f}}{5} + \frac{\sqrt{5} - 5}{5}(1 - f)\right)^2\right| \tag{5.1.11}$$

so providing

$$\delta \;\equiv\; \frac{d(6:6)}{d(6:5)} \;=\; \frac{|\; p_1 \;-\; a_{11} \;|}{|\; p_1 \;-\; p_2 \;|}$$

$$= \frac{\left|\left(\frac{-\sqrt{10}}{5} + \frac{2\sqrt{5}}{5}(1 - f) - \sqrt{2f}\right)^2 + \left(\frac{2\sqrt{10\,f}}{5} + \frac{\sqrt{5}-5}{5}(1 - f)\right)^2\right|}{2\,\sqrt{2f}\,\sin\frac{\pi}{5}} \tag{5.1.12}$$

This formula enables δ to be readily calculated for any choice of f.

5.2 Relation of d(6:5) and R for a given f

Table A, accompanied by FORTRAN program, in Appendix G lists δ as a function of f, starting with $f_0 = 0.010$, and increasing in units of $\Delta f = 0.001$ until $f_{max} = 0.141$. Note that $\delta_0 = 4.814$ showing, as may be seen directly from Figure 5.3, that the pentagons become vanishingly small compared with the hexagons in the limit of a shallow cap. We start with $f_0 = 0.010$ since $\delta = \infty$ when $f = 0$.

At the other extreme, $\delta = 0$ at which point the hexagons become vanishingly small compared with the pentagons, i.e. the dodecahedron circumsphere may be produced from a buckyball by a continuous expansion of the buckyball pentagons–see Figure 5.4 for details. This will be further discussed below as a possible model for C_{20}. Two intermediate values of δ are of interest:

(i) $\delta_g = 1.00$ at $f_g = 0.059$ i.e. the case of undistorted hexagons since now $d(6{:}5) = d(6{:}6)$, so to speak mimicking the graphite configuration.

To examine this further, we rewrite (4.2.5) as

$$\frac{d(6:5)}{R_g} = 2\sqrt{2\,f_g}\,\sin\frac{\pi}{5} = 0.404 \tag{5.2.1}$$

which provides a relation between d(6:5) and R corresponding with f_g (Figure 5.5). A suitable choice for d(6:5) would be the graphite bond length $d(6{:}5) = 1.420(4)$ $\mathring{A}$, which gives $R_g = 3.520(4)$ $\mathring{A}$. This approximates tolerably to the observed radius, $R \sim 3.550(10)$ $\mathring{A}$–see reference [7,8], suggesting that a minimization of hexagonal distortion is the essential factor in producing the buckyball dimensions.

(ii) $\delta_n = 0.956$ corresponding with $f_n = 0.061$ as obtained from (4.3.2), i.e. the natural buckyball configuration.

As before, we note

$$\frac{d(6:5)}{R_n} = 2\sqrt{2\,f_n}\,\sin\frac{\pi}{5} = 0.411. \tag{5.2.2}$$

Choosing $d(6{:}5) = 1.455(12)$ $\mathring{A}$ as in (4.3.2) now yields $R = 3.540(8)$ $\mathring{A}$ which approximates closely to the observed radius. This encouraging result demonstrates the essential soundness of our mathematical model.

As regards the choice $\delta = 0$ mentioned earlier ($f_{max} = 0.141$ from Figure 5.6), we have the relation

$$\frac{d(6:5)}{R_{max}} = 2\sqrt{2\, f_{max}}\, \sin\frac{\pi}{5} = 0.624. \tag{5.2.3}$$

Accordingly as with (i), we choose $d(6{:}5) = 1.420(5)$ $\mathring{A}$ which yields $R_{max} = 2.276(16)$ $\mathring{A}$ for the C_{20} molecule.

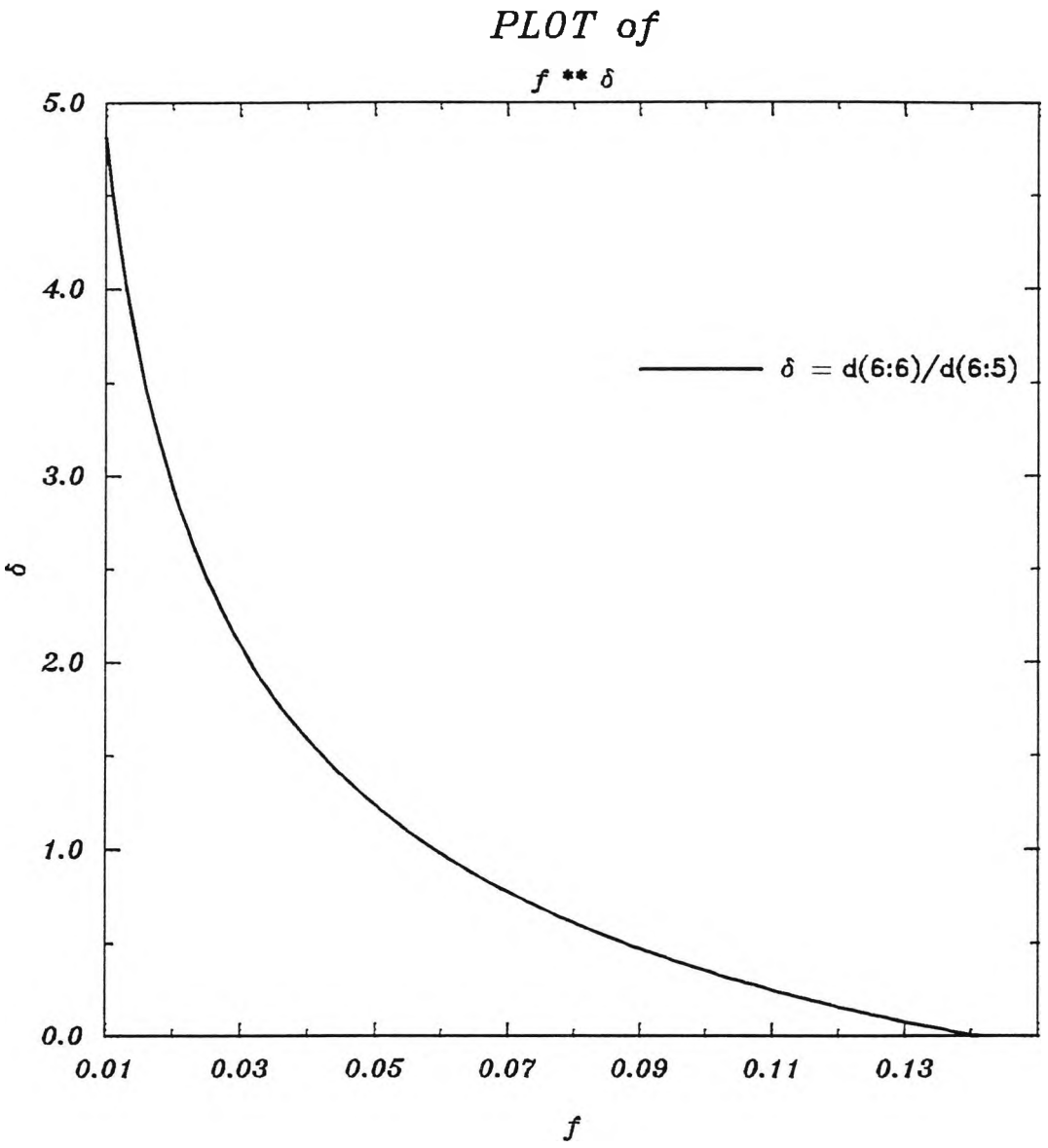

Figure 5.3: Profile of δ exhibiting its decrease as f reaches its limiting value. This is the stage when the sphere is fully covered by regular pentagons.

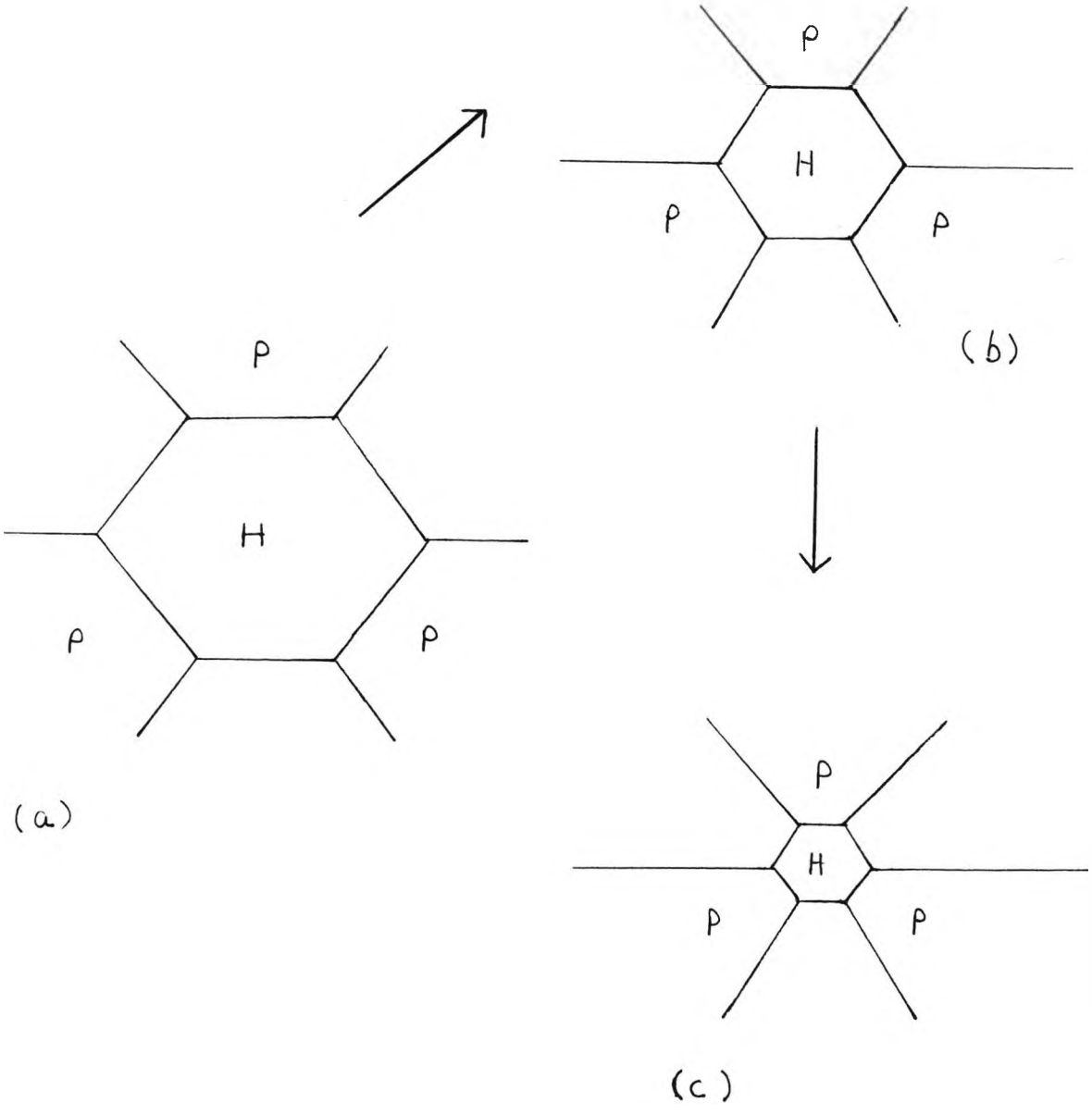

Figure 5.4: Three essential phases of the geometrical formulation which give rise to the dodecahedron circumsphere, arising from (a) buckyball pentagon, then (b) expansion of the pentagons accompanied by a reduction of hexagons, and finally (c) the circumsphere consists entirely of regular pentagons (schematic picture).

Here

$$\lambda = \frac{d(6:5)}{R}$$

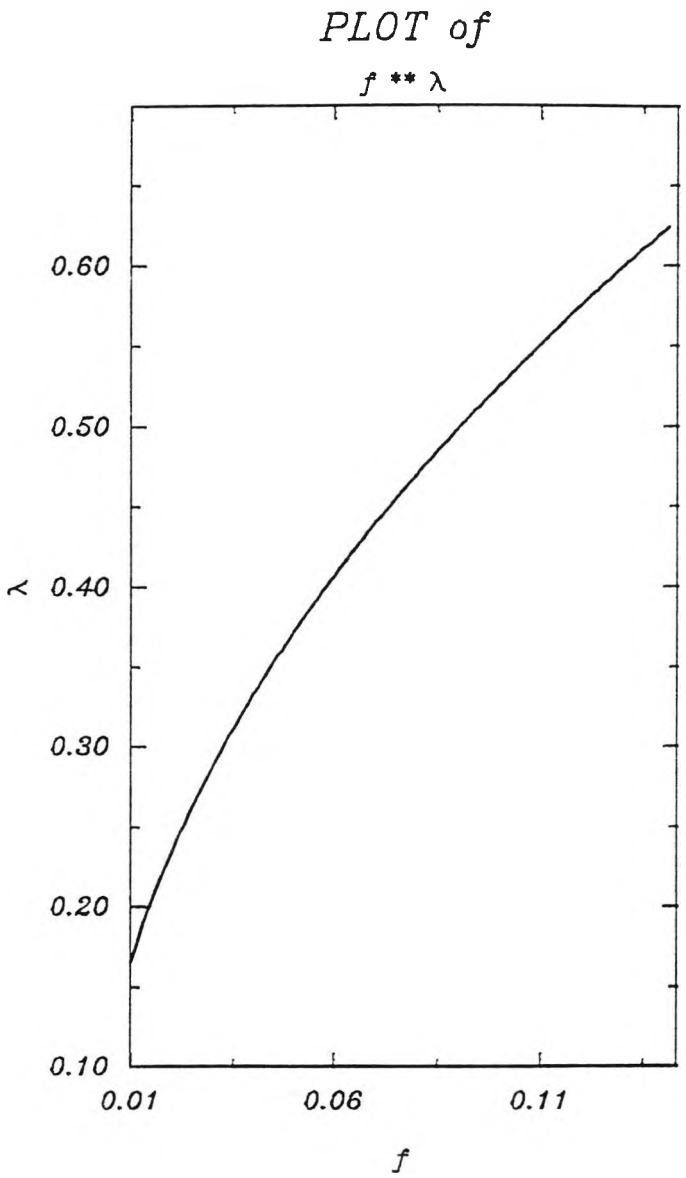

Figure 5.5: Profile of λ as given in (4.2.5) showing changing pentagonal pattern as f varies up to the possible maximum.

Here

$$\sigma = \frac{d(6:6)}{R}$$

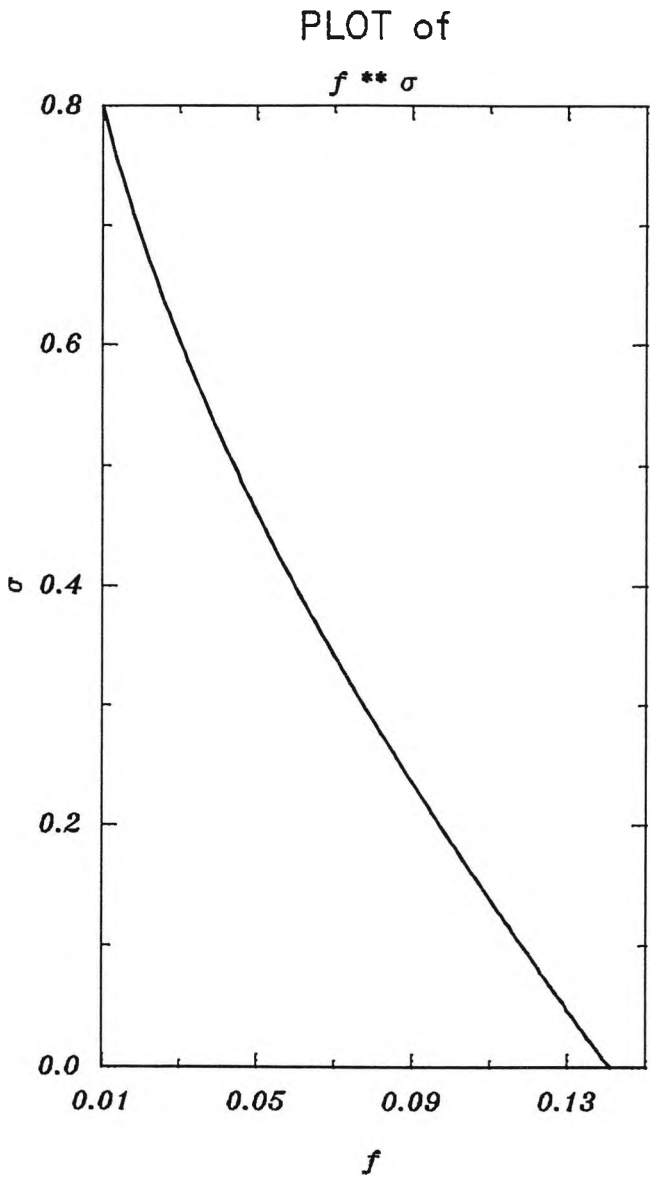

Figure 5.6: Profile of σ (as indicated above) showing changing hexagonal pattern as f varies up to the possible maximum.

Chapter 6

Possibility Of Inserting More Hexagons

6.1 Construction Of C_{80} and C_{70}

We now show how to construct models for the molecules C_{80} and C_{70} starting with the buckyball model for C_{60}. First choose an equatorial plane for the buckyball as that plane bisects the axis PP' joining the centre P of any spherical pentagon with centre P' of its inverse pentagon. If so the equatorial circle lies mid-way between the five pentagons surrounding P and those surrounding P', being therefore straddled by an equatorial belt of ten hexagons as depicted in Figure 6.1 (a). Figure 6.1 (b) shows a schematic picture of the equatorial belt, from which we find that

(i) each P is surrounded by 5 H's,

(ii) each H is surrounded by 3 P's and 3 H's.

Imagine this belt cut out from the buckyball, duplicated into a similar belt of twenty hexagons, and re-introduced as shown in Figure 6.2 (a). Now each P is once again surrounded by 5 H's whilst each H is surrounded either by

(i) 1 P and 4 H's or

(ii) 2 P's and 3 H's or

(iii) 5 H's.

as may be readily verified by a schematic picture in Figure 6.2 (b). Clearly the original buckyball has now been converted into a prolate spheroid of axial ratio $(2R+d)$ / $2R$ where d signifies the distance between two parallel edges of a hexagon. Note the insertion of 20 additional hexagonal vertices along the equatorial belt i.e. 20 carbon atoms have been added to the buckyball so providing a model for C_{80}, though the existence of C_{80} as a chemical has not been confirmed yet.

The construction of C_{70} is slightly more difficult. We imagine the equatorial belt cut out as before, but now only alternate hexagons are duplicated to form a serrated belt of 15 hexagons as depicted in Figure 6.3 (b). This is re-introduced as shown in Figure 6.3 (a), giving rise to 10 additional hexagonal vertices along the equatorial belt, i.e. 10 carbon atoms have been added to the buckyball yielding a model for C_{70}. As before each P is surrounded by 5 H's. However, each H is now surrounded either by

(i) 1 P and 4 H's or

(ii) 2 P and 3 H's.

Accordingly, this duplication transformed the original buckyball into a prolate spheroid of axial ratio $(2R + \frac{d}{2})$ / $2R$. Traces of C_{70} exist according to spectroscopic evidence. This is believed to adopt the structure of a rugby-ball illustrated in Figure 6.4. Note that the equatorial plane appears as a symmetry plane (mirror reflection) for C_{70}, replacing the inversion centre apparents in C_{60} and C_{80}.

Our construction for C_{80} may be extended to cover carbon molecules of the form $C_{60+20\,n}$; n = 1,2, ...

Similarly the mechanism which we implement for C_{70} may be extended to cover carbon molecules of the form $C_{70+20\,m}$; m = 0,1,2, ...

These are all prolate spheroids of increasing axial ratio, eventually becoming cigar-shaped cages of possible chemical importance [19]. Accordingly this suggests that it

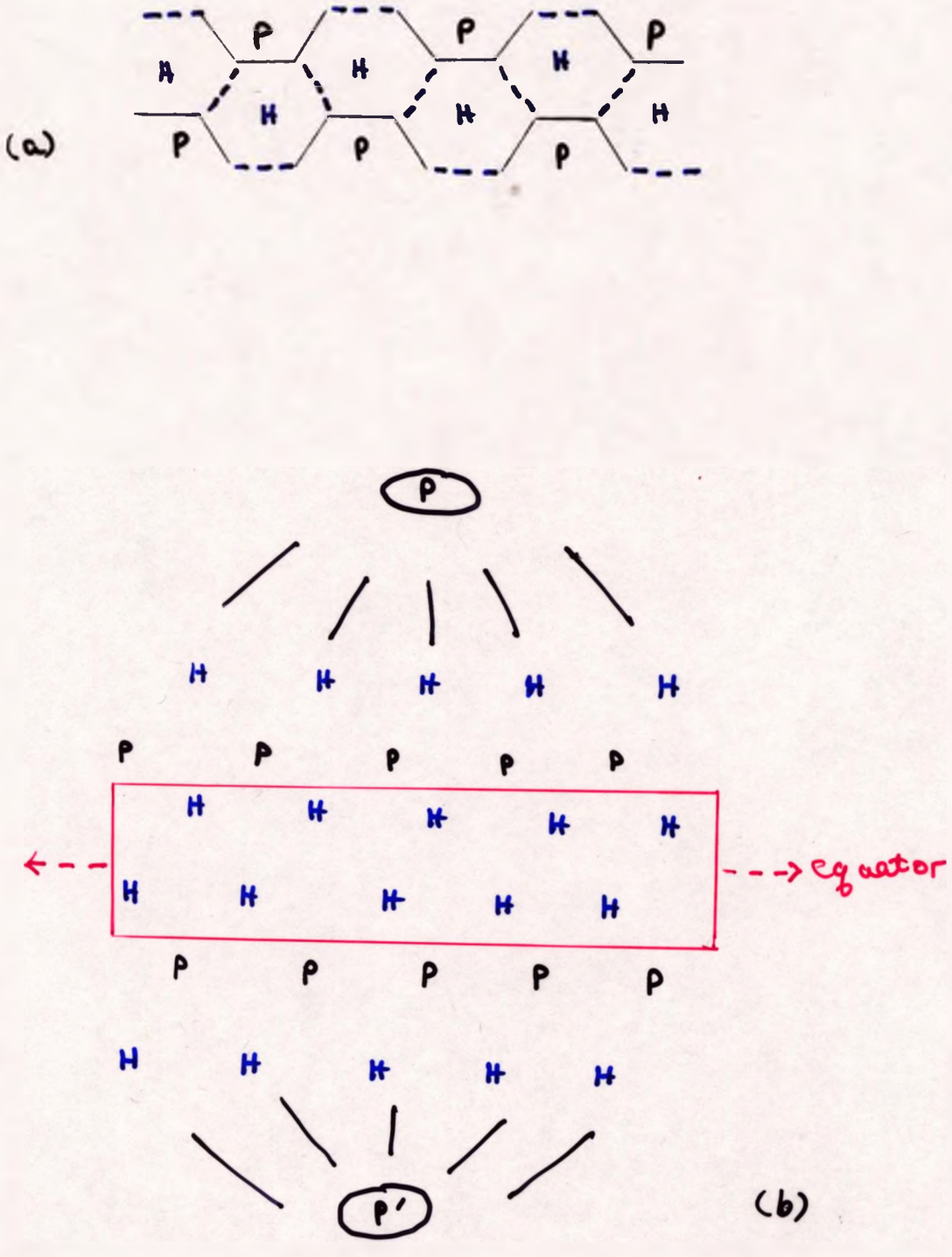

Figure 6.1: (a) Profile of C_{60} exhibiting part of the tessellation of hexagons (H's) and pentagons (P's) on the equatorial belt. (b) Schematic picture exhibiting a projective global view of pentagon-hexagon configuration. Here (P), (P') indicates the pole pentagons. Note that these are inverses with respect to the centre O (not shown).

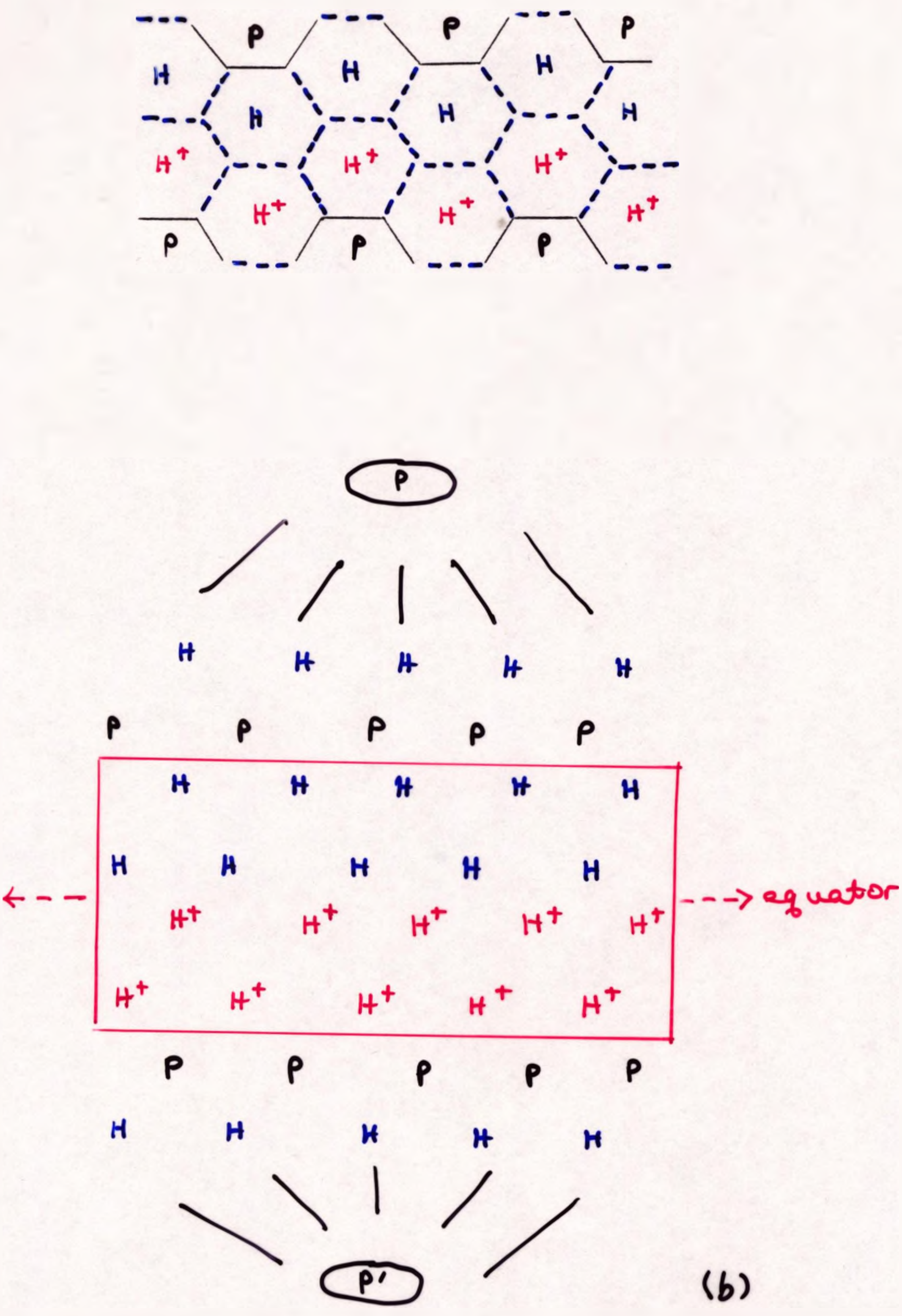

Figure 6.2: (a) Profile of C_{80} exhibiting part of the tessellation of hexagons and pentagons on the equatorial belt. (b) Schematic picture exhibiting a projective global view of pentagon-hexagon configuration. Here H^+ denotes an additional hexagon. For the symbolisms excluding H^+, see Figure 6.1 (b).

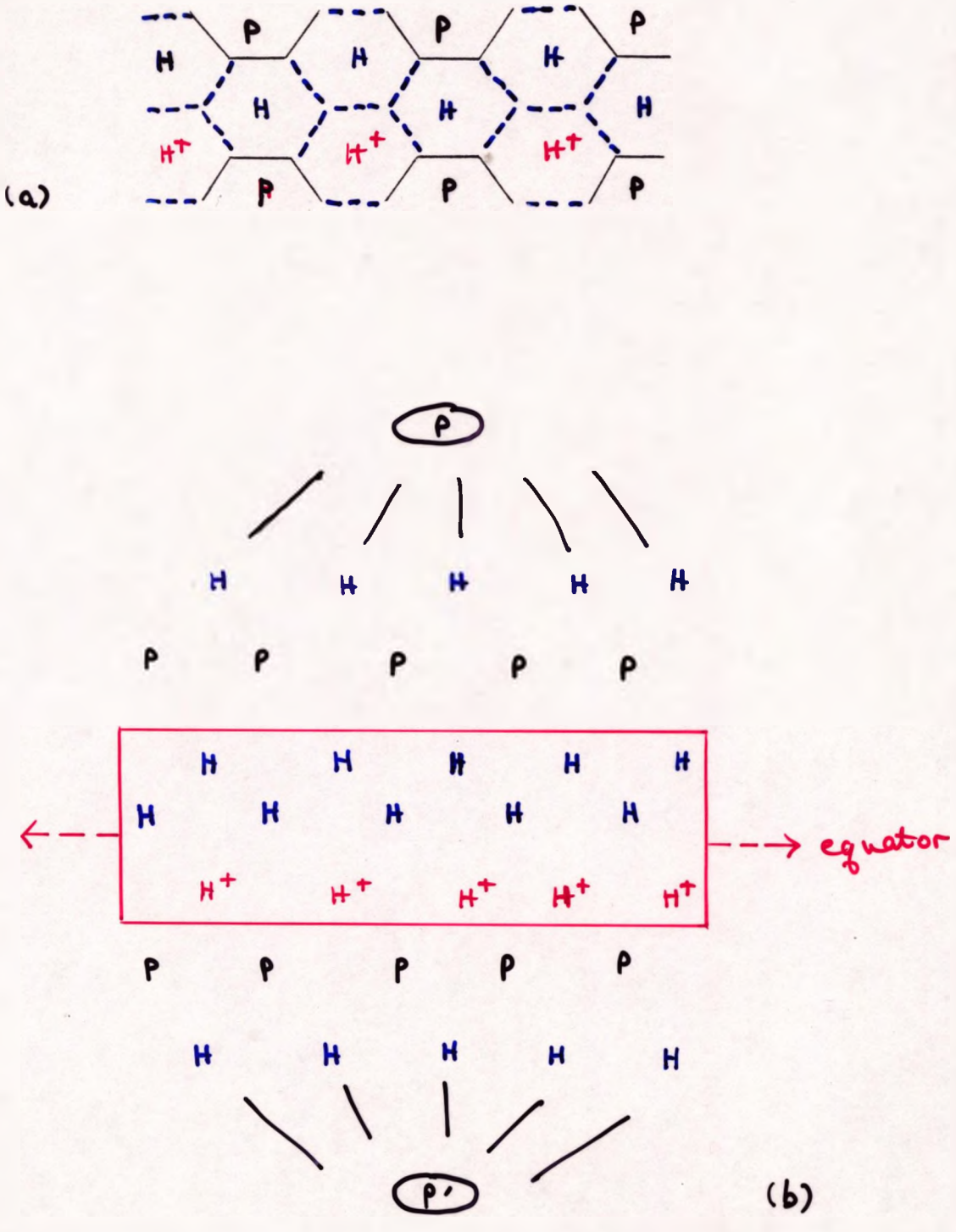

Figure 6.3: (a) Profile of C_{70} exhibiting part of the tessellation of hexagons and pentagons on the equatorial belt. (b) Schematic picture exhibiting a projective global view of pentagon-hexagon configuration. For the symbolisms, see Figure 6.2.

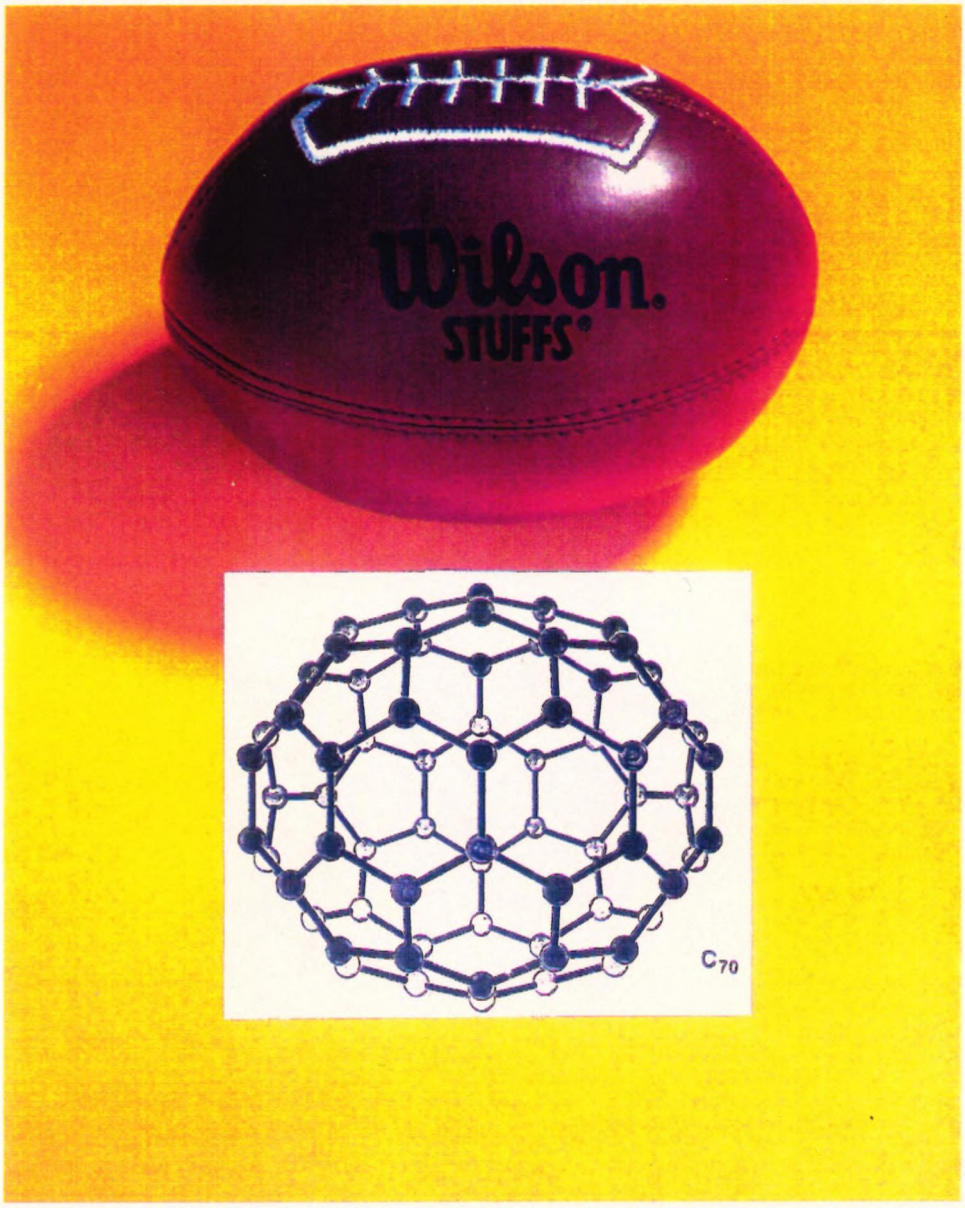

Figure 6.4: Proposed structure of C_{70} resembling a rugby-ball. The lattice model depicted below [18] shows the atomic pattern on the molecular cages.

it is best to regard the growth to concentric tubular cages as an essential mechanism for giant fullerenes.

6.2 Axial Ratio Of Prolate Spheroids

To determine the axial ratio of C_{80}, we observe that

$$d \;=\; 2\,d(6:6)\,\sin\frac{\pi}{3} \;=\; \sqrt{3}\,d(6:6) \;=\; 2.460\;\mathring{A} \tag{6.2.1}$$

bearing in mind the chemical bond-length in (4.1.1) which applies to a regular hexagon. If so,

$$\delta_{80} \;=\; \frac{2R\,+\,d}{2R} \;=\; \frac{2R_n\,+\,\sqrt{3}\,d(6:6)}{2R_n} \;=\; 1.347\;\mathring{A} \tag{6.2.2}$$

where R_n has been mentioned earlier in (5.2.2). This enables us to compute the obvious changes in the z-coordinate of the pole pentagons for C_{80} since the x, y-coordinates are restored as in C_{60}. Thus the z-coordinate is given by

$$R\,-\,h\,+\,\frac{d}{2} \;=\; R\,-\,f\,R\,+\,d(6:6)\,\sin\frac{\pi}{3} \tag{6.2.3}$$

where R, h and f are touched in Chap. 4 respectively.

For C_{70}, we proceed in a similar way so that

$$\delta_{70} \;=\; \frac{2R\,+\,\frac{d}{2}}{2R} \;=\; \frac{2R_n\,+\,\frac{\sqrt{3}}{2}\,d(6:6)}{2R_n} \;=\; 1.174\;\mathring{A} \tag{6.2.4}$$

by virtue of (6.2.1). As a result this yields the z-coordinate as

$$R\,-\,h\,+\,\frac{d}{4} \;=\; R\,-\,f\,R\,+\,\frac{1}{2}\,d(6:6)\,\sin\frac{\pi}{3}. \tag{6.2.5}$$

6.3 Point Group Features Of C_{60}, C_{80} and C_{70}

It has already been noted that the regular icosahedron conforms to the point-group symmetry 532. However this must be expanded into $\overline{5}\,\overline{3}\,\frac{2}{m}$ since its centre O is an inversion centre. Note that $\overline{5}$ signifies a 5–fold inversion axis, $\overline{3}$ signifies a 3–fold inversion axis, and $\frac{2}{m}$ signifies a 2–fold axis accompanied by a transverse symmetry plane.

To understand this further, we start with

$$\{5\} + J\{5\} = \{\overline{5}\} \tag{6.3.1}$$

since this group corresponds with the symmetry $\overline{5}$ on utilising (16) of [page 29, 4]. Then combine this decomposition with

$$\{23\} + J\{23\} = \{\overline{3}\,\frac{2}{m}\} \tag{6.3.2}$$

as follows from the fact that the tetrahedral group $\{23\}$ is a subgroup of $\{52\}$, introduced in Chap. 2.

Also $\{532\}$ contains a subgroup of $\{32\}$ which expands into

$$\{32\} + J\{32\} = \{3\,m\} + J\{3\,m\} = \{\overline{3}\,\frac{2}{m}\} \tag{6.3.3}$$

in line with (42) of [page 34, 4]. A combination of (6.3.1) with (6.3.3) yields

$$\{532\} + J\{532\} = \left\{\overline{5}\,\overline{3}\,\frac{2}{m}\right\} \tag{6.3.4}$$

which may be realised by a stereogram depicted in Figure 6.5.

Clearly the buckyball model for C_{60} conforms to the same symmetry arising from its method of construction, touched in Chap. 5. Five symmetry planes pass through PP', and one of these is displayed in Figure 6.6.

C_{80} retains PP' as a 5–fold symmetry axis, but it has no others. Reference to Figure 6.2 shows that it also retains the five symmetry planes passing through PP'

so providing the dihedral group

$$\{5\} + D\{5\} = \{5m\}; \tag{6.3.5}$$

i.e. more explicitly

$$\left\{ \begin{array}{c} I, C, C^2, \ldots C^4 \\ D, DC, DC^2, \ldots DC^4 \end{array} \right\}; C^5 = D^2 = (DC)^2 = I. \tag{6.3.6}$$

consistent with the demarcation implemented in (33) of [page 32, 4]. Since O still functions as an inversion centre, its presence expands $5m$ into $\overline{5}\frac{2}{m}$ (Figure 6.7) so that

$$\{52\} + J\{52\} = \{5m\} + J\{5m\} = \{\overline{5}\frac{2}{m}\} \tag{6.3.7}$$

may be generated and therefore confirming the existence of five 2–fold axes located in the equatorial plane–a feature not so easy to see directly.

C_{70} also retains PP' as a 5–fold symmetry axis, together with the five symmetry planes passing through PP' (Figure 6.3). However, O is no longer an inversion centre. Instead, the equatorial plane becomes a symmetry plane, so that $5m$ now expands into $\frac{5}{m}2m$ i.e. each symmetry plane through PP' intersects the equatorial plane in a 2–fold axis. Reference to Figure 6.8 shows the construction of the crystallographic point group

$$\{52\} + M\{52\} = \{5m\} + M\{5m\} = \{\frac{5}{m}2m\}$$

corresponding with the symmetry $\frac{5}{m}2m$.

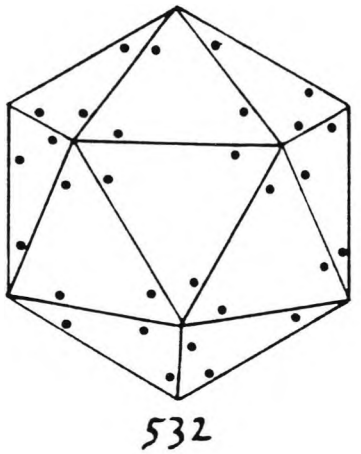

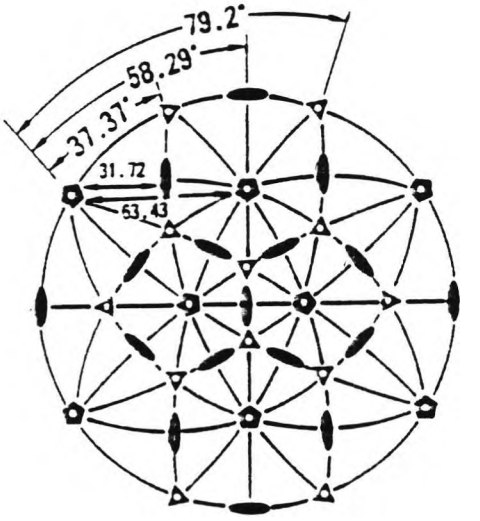

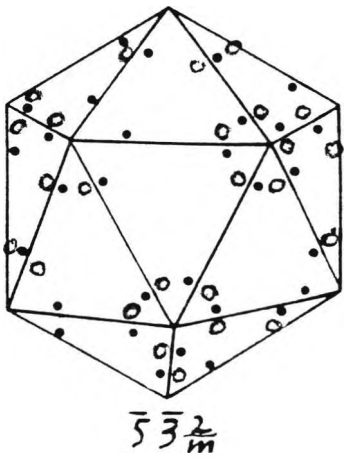

Figure 6.5: The symmetry $\bar{5}\bar{3}\frac{2}{m}$ may be realised by the atomic pattern on the regular icosahedron and its derivation from the stereogram of symmetry 532.

Figure 6.6: Note that the dotted line marks a symmetry plane passing through PP' and intersecting the equatorial plane.

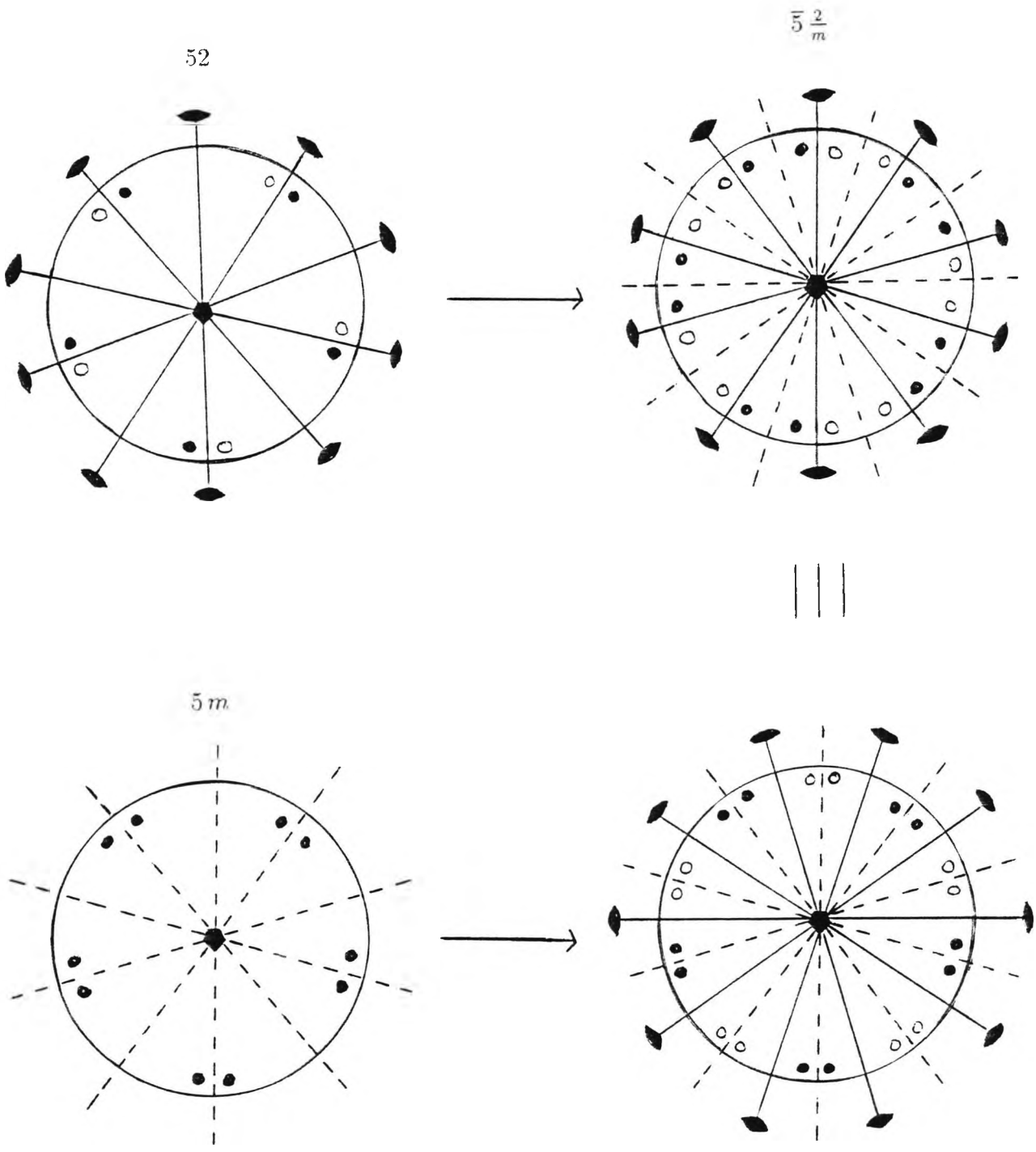

Figure 6.7: The symmetry $\bar{5}\frac{2}{m}$ is generated either by combining 52 or $5m$ with an inversion centre, thereby automatically introducing each horizontal axis lying perpendicular to a vertical mirror.

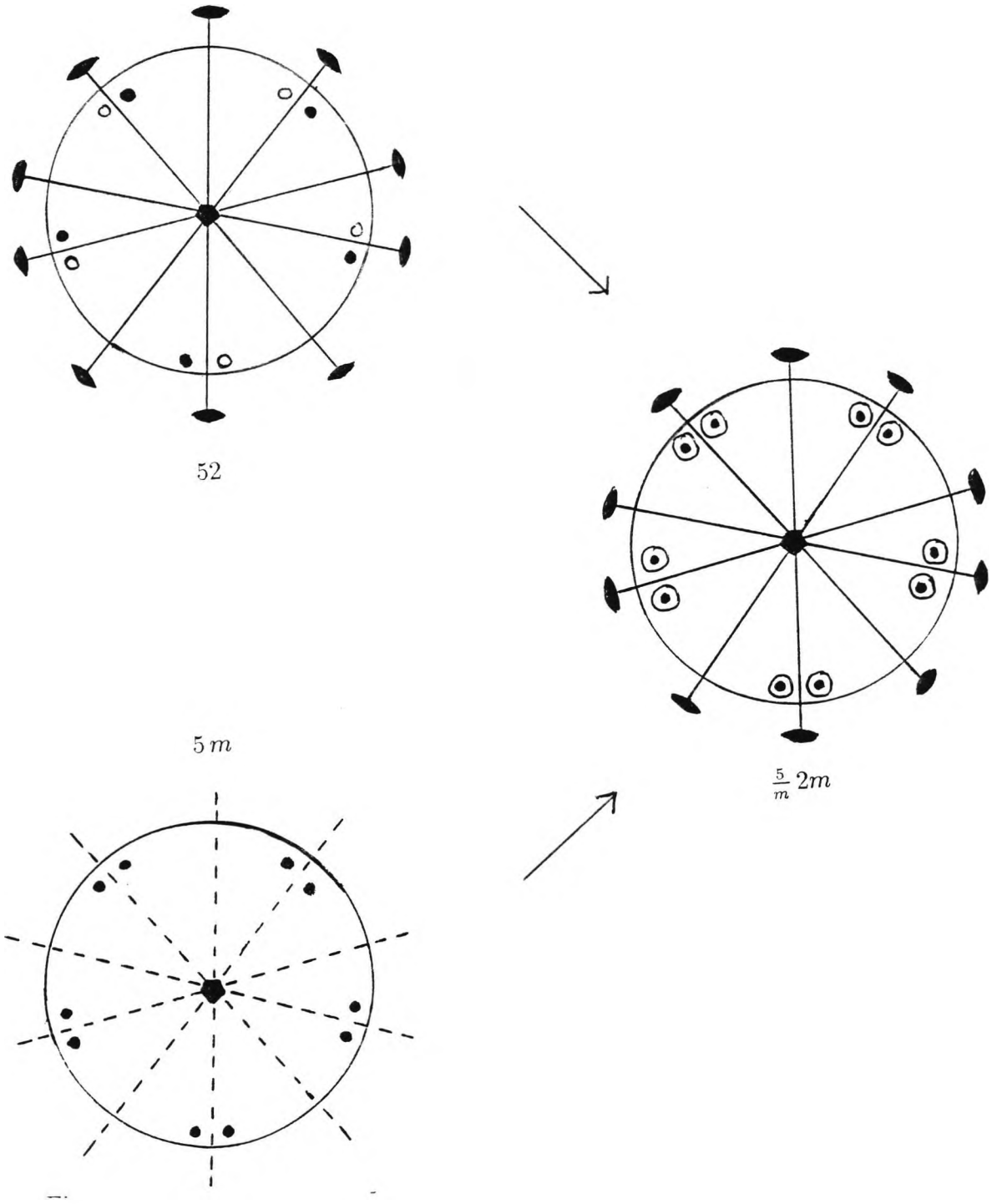

Figure 6.8: The symmetry $\frac{5}{m}2m$ is obtained either by combining 52 or $5\,m$ with a transverse mirror plane, thereby introducing the presence of both vertical mirrors and horizontal 2–fold axes.

Appendix A

The facts that

- for a given *surface area*, the sphere has a *greater volume* than any $\{p,q\}$;
- for a given *volume*, the sphere has a *smaller surface area* than any $\{p,q\}$,

there being no other possibilities, may be readily confirmed by evaluating the following numerical value for each $\{p,q\}$.

Regular Solid	$\{p,q\}$ *symbolism*	$\frac{S}{l^2} = F \bullet p \cot \frac{\pi}{p}$	$\frac{V}{l^3} = \frac{F \bullet p \cos \frac{\pi}{q}}{3 \tan^2 \frac{\pi}{p}}$
Tetrahedron	{3,3}	6.928	0.667
Cube	{4,3}	24.00	4.00
Octahedron	{3,4}	13.856	1.886
Icosahedron	{3,5}	34.641	5.393
Dodecahedron	{5,3}	82.583	18.944

Table showing the value of $\frac{S}{l^2}$ and $\frac{V}{l^3}$ for each $\{p,q\}$.

Regular Solid	$\{p,q\}$ *symbolism*	$\frac{R_{in}}{l} = \frac{1}{k} \cot \frac{\pi}{p} \cos \frac{\pi}{q}$	$\frac{\sigma}{l} = \left(\frac{F \bullet p \cot \frac{\pi}{p}}{4\pi}\right)^{1/2}$
Tetrahedron	{3,3}	0.408	0.743
Cube	{4,3}	1.00	1.382
Octahedron	{3,4}	0.816	1.050
Icosahedron	{3,5}	0.144	1.660
Dodecahedron	{5,3}	0.213	2.564

Table showing the value of $\frac{R_{in}}{l}$ and $\frac{\sigma}{l}$ for each $\{p,q\}$.

Regular Solid	$\{p,q\}$ *symbolism*	$\frac{\rho}{l} = \left(\frac{F \bullet p}{k} \cot^2 \frac{\pi}{p} \cos \frac{\pi}{q}\right)^{1/3}$
Tetrahedron	{3,3}	2.828
Cube	{4,3}	2.884
Octahedron	{3,4}	2.792
Icosahedron	{3,5}	3.741
Dodecahedron	{5,3}	5.687

Table showing the value of $\frac{\rho}{l}$ for each $\{p,q\}$.

Regular Solids	$\{p,q\}$ Symbolism	$\frac{\sigma}{R_{in}} = k\left(\frac{F \bullet p}{4\pi}\frac{\tan\frac{\pi}{p}}{\cos^2\frac{\pi}{q}}\right)^{1/2}$	$\frac{R_{in}}{\rho} = \frac{1}{k^{2/3}}\left(\frac{4\pi}{F \bullet p}\frac{\cos^2\frac{\pi}{q}}{\tan\frac{\pi}{p}}\right)^{1/3}$
Tetrahedron	{3,3}	1.819	0.671
Cube	{4,3}	1.382	0.806
Octahedron	{3,4}	1.286	0.846
Icosahedron	{3,5}	1.098	0.196
Dodecahedron	{5,3}	1.151	0.190

Table showing the value of $\frac{\sigma}{R_{in}}$ and $\frac{R_{in}}{\rho}$ for each $\{p,q\}$.

Appendix B

It appears that formulae (2.1.6), (2.1.10) and (2.1.11) can be achieved directly by utilising a fundamental but essential lemma as exhibited below:

Lemma 1 *The mathematical expression $v_1 = v_2$ is obeyed by a regular icosahedron and not for every regular solids, where*

$$v_1 = \frac{\left(1 - 2\sin^2\theta\right)^2}{4\sin^2\theta - 1}; \quad v_2 = \sin^2\theta - \sin^2\frac{\theta}{2}$$

Proof: Suppose $v = \sin^2\theta$, then

$$v_1 = \frac{\left(1 - 2\sin^2\theta\right)^2}{4\sin^2\theta - 1} = \frac{(1-2v)^2}{4v-1}. \tag{1}$$

Now utilising $2\sin^2\theta = 1 - \cos 2\theta$ so that $\sin^2\frac{\theta}{2} = \frac{(1-\cos 2\bullet\frac{\theta}{2})}{2} = \frac{1-\cos\theta}{2}$, we have

$$v_2 = \sin^2\theta - \sin^2\frac{\theta}{2} = v - \frac{1}{2}(1 - \cos\theta) = v - \frac{1}{2} + \frac{1}{2}\cos\theta. \tag{2}$$

Writing $\cos\theta = 1 - \left(\sin^2\theta\right)^{1/2}$ gives

$$v_2 = v - \frac{1}{2} + \frac{1}{2}(1 - v)^{1/2} \tag{3}$$

on substituting once again $v = \sin^2\theta$. Equating formula (1) with (3) now yields

$$\frac{1 - 4v + 4v^2}{4v - 1} = v - \frac{1}{2} + \frac{1}{2}(1 - v)^{1/2},$$

thus enabling us to write

$$1 - 4v + 4v^2 = (4v - 1)\left(v - \frac{1}{2} + \frac{1}{2}(1 - v)^{1/2}\right)$$

so that

$$1 - 4v + 4v^2 = 4v^2 - 2v + 2v(1 - v)^{1/2} - v + \frac{1}{2} - \frac{1}{2}(1 - v)^{1/2}. \quad (4)$$

Eliminating v^2, v from (4) gives

$$\begin{aligned} \frac{1}{2} - 4v + 4v^2 &= 4v^2 - 3v + 2v(1 - v)^{1/2} - \frac{1}{2}(1 - v)^{1/2}, \\ 1 - 8v + 8v^2 &= 8v^2 - 6v + 4v(1 - v)^{1/2} - (1 - v)^{1/2}, \\ 1 - 2v &= (4v - 1)(1 - v)^{1/2} \end{aligned} \quad (5)$$

on multiplying across by 2 to both sides. As a consequence, we arrive at

$$v\left(16v^2 - 20v + 5\right) = 0 \Longrightarrow 16v^2 - 20v + 5 = 0 \quad (6)$$

From formula (6) $b^2 > 4ac$ i.e. $(-20)^2 > 4\,(16)\,(5)$, we deduce

$$\begin{aligned} v &= \frac{20 \pm \sqrt{(-20)^2 - 4\,(16)\,(5)}}{2\,(16)} = \frac{20 \pm \sqrt{400 - 320}}{32} \\ &= \frac{20 \pm 4\sqrt{5}}{32} = \frac{5 \pm \sqrt{5}}{8} \end{aligned} \quad (7)$$

Bearing in mind $v = \sin^2\theta$, two special cases arise:

(i)

$$\sin^2\theta = \frac{5 - \sqrt{5}}{8}$$

(ii)

$$\sin^2 \theta = \frac{5 + \sqrt{5}}{8}$$

Substituting v into (1) we obtain

$$v_1 = \frac{1}{4}$$

which implies $\theta = \frac{\pi}{5}, \frac{3\pi}{5}, \ldots$

We ruled out case (ii) since $v_1 \neq v_2$.

Appendix C

Though the representation of S_5, the symmetry group of order 5, has been explored extensively in many group theory books, it is necessary to include the remaining 60 permutational operators since the other 60 elements have been enumerated while generating the icosaheral group $\{532\}$ in Chapter 2. This is essential for the validity of the statement embodied in the text. So we write down the faithful representation of S_5 by means of cosets decomposition of the alternating group A_5 as follows:

$$S_5 = A_5 + (12)(3)(4)(5)\,A_5 = A_5 + A_5\,(12)(3)(4)(5). \qquad (1)$$

However, the faithful representations of (a) are not in the same order as the representation of (b).

It may be readily verified that A_5 is the invariant subgroup of S_5 where 10 of the elements are best regarded as 2–fold symmetry axes, 20 of the elements as 3–fold symmetry axes, and 30 of the elements as 4–fold symmetry axes. For brevity, we list down all the 60 elements in chains of tables as shown in the next pages.

•	I	(12)(34)(5)	(13)(24)(5)	(14)(23)(5)
(12)(3)(4)(5)	(12)(3)(4)(5)	(34)(1)(2)(5)	(1324)(5)	(1423)(5)

•	(123)(4)(5)	(243)(1)(5)	(142)(3)(5)	(132)(4)(5)
(12)(3)(4)(5)	(23)(1)(4)(5)	(1342)(5)	(14)(2)(3)(5)	(13)(2)(4)(5)

•	(234)(1)(5)	(124)(3)(5)	(143)(2)(5)	(12345)
(12)(3)(4)(5)	(1234)(5)	(24)(1)(3)(5)	(1432)(5)	(2345)(1)

•	(135)(2)(4)	(14325)	(15)(24)(3)	(13245)
(12)(3)(4)(5)	(1352)(4)	(143)(25)	(1524)(3)	(13)(245)

•	(14235)	(125)(3)(4)	(15)(34)(2)	(145)(2)(3)
(12)(3)(4)(5)	(14)(235)	(25)(3)(4)(1)	(152)(34)	(1452)(3)

•	(12435)	(13425)	(15)(23)(4)	(13524)
(12)(3)(4)(5)	(2435)(1)	(134)(25)	(1523)(4)	(135)(24)

•	(14523)	(152)(3)(4)	(25)(34)(1)	(14)(25)(3)
(12)(3)(4)(5)	(145)(23)	(15)(2)(3)(4)	(125)(34)	(1425)(3)

•	(15243)	(13452)	(235)(1)(4)	(15234)
(12)(3)(4)(5)	(243)(15)	(1345)(2)	(1235)(4)	(15)(234)

•	(235)(1)(4)	(15234)	(13)(25)(4)	(14352)
(12)(3)(4)(5)	(1235)(4)	(15)(234)	(1325)(4)	(1435)(2)

•	(245)(1)(3)	(14253)	(15324)	(345)(1)(2)
(12)(3)(4)(5)	(1245)(3)	(14)(253)	(153)(24)	(12)(345)

•	(12)(35)(4)	(15342)	(253)(1)(4)	(14)(35)(2)
(12)(3)(4)(5)	(1)(2)(4)(35)	(1534)(2)	(1253)(4)	(142)(35)

•	(12453)	(24)(35)(1)	(14532)	(153)(2)(4)
(12)(3)(4)(5)	(2453)(1)	(124)(35)	(1453)(2)	(1532)(4)

•	(12534)	(15432)	(254)(1)(3)	(12354)
(12)(3)(4)(5)	(2534)(1)	(1543)(2)	(1254)(3)	(2354)(1)

•	(13)(45)(2)	(354)(1)(2)	(12)(45)(3)	(15423)
(12)(3)(4)(5)	(132)(45)	(12)(354)	(1)(2)(3)(45)	(154)(23)

•	(13254)	(12543)	(154)(2)(3)	(23)(45)(1)
(12)(3)(4)(5)	(13)(254)	(2543)(1)	(1542)(3)	(123)(45)

Appendix D

In Appendix D we illustrate the irrational values of each mathematical expressions that has significant role in Chapters 2 and 3. These expressions not only simplify the calculation but effectively display that they are applicable to the physical features of the regular icosahedron and the regular dodecaheron and no others.
The symbolism which is used in the next table is written as follows:

a. Argand diagram describing the root of the quintic equation

b. $\sin^2 \frac{\pi}{5} = \frac{1 - \cos \frac{2\pi}{5}}{2}$

c. $\cos^2 \frac{\pi}{5} + \sin^2 \frac{\pi}{5} = 1$

d. $\sin^2 \frac{\pi}{5} - \sin^2 \frac{\pi}{10} = \frac{1}{4}$

e. $\cos^2 \frac{2\pi}{5} = 1 - \sin^2 \frac{2\pi}{5}$

f. $\cos^2 \frac{\pi}{10} + \sin^2 \frac{\pi}{10} = 1$

g. $\sin^2 \frac{2\pi}{5} = 4 \sin^2 \frac{\pi}{5} \cos^2 \frac{\pi}{5}$

Trigonometric Identities	*Equivalent Identities*	*Irrational Value*	*Method Of Derivation*
$\cos \frac{2\pi}{5}$		$\frac{\sqrt{5}-1}{4}$	a
$\cos \frac{\pi}{5}$		$\frac{1+\sqrt{5}}{4}$	a
$\sin^2 \frac{\pi}{5}$	$\cos^2 \frac{3\pi}{10}$	$\frac{5-\sqrt{5}}{8}$	b
$\cos^2 \frac{\pi}{5}$	$\sin^2 \frac{3\pi}{10}$	$\frac{3+\sqrt{5}}{8}$	c
$\sin^2 \frac{\pi}{10}$	$\cos^2 \frac{2\pi}{5}$	$\frac{3-\sqrt{5}}{8}$	d , e
$\cos^2 \frac{\pi}{10}$	$\sin^2 \frac{2\pi}{5}$	$\frac{5+\sqrt{5}}{8}$	f , g

Table of trigonometric identities for comparable angular measurement $\frac{\pi}{5}$, $\frac{2\pi}{5}$ and $\frac{3\pi}{10}$.

Appendix E

As already been invoked earlier in the text, the derivation of the x, y, z coordinates of the vertices p_1, p_2, p_3, p_4 and p_5 associated with the pole pentagon of the buckyball are displayed below for some f between the interval $0.01 \leq f \leq 0.142$. The corresponding values are listed in double precision to ensure exact accuracy. For instance when $f = 0.1000000\text{D-}01$ (meaning 0.01 to 7 decimal places) p_1, p_2, p_3, p_4 and p_5 are read in the following sequence:

$$\begin{aligned} \text{1st row} &\longmapsto p_1 \\ \text{2nd row} &\longmapsto p_2 \\ \text{3rd row} &\longmapsto p_3 \\ \text{4th row} &\longmapsto p_4 \\ \text{5th row} &\longmapsto p_5. \end{aligned}$$

The algorithms that we utilised are based on [10]–[15]

Appendix E.1

f	x	y	z
0.1000000D-01	0.1414214D+00	0.0000000D+00	0.9900000D+00
0.1000000D-01	0.4370160D-01	0.1344997D+00	0.9900000D+00
0.1000000D-01	-0.1144123D+00	0.8312539D-01	0.9900000D+00
0.1000000D-01	-0.1144123D+00	-0.8312539D-01	0.9900000D+00
0.1000000D-01	0.4370160D-01	-0.1344997D+00	0.9900000D+00
0.1010000D-01	0.1421267D+00	0.0000000D+00	0.9899000D+00
0.1010000D-01	0.4391957D-01	0.1351705D+00	0.9899000D+00
0.1010000D-01	-0.1149829D+00	0.8353998D-01	0.9899000D+00
0.1010000D-01	-0.1149829D+00	-0.8353998D-01	0.9899000D+00
0.1010000D-01	0.4391957D-01	-0.1351705D+00	0.9899000D+00
0.1020000D-01	0.1428286D+00	0.0000000D+00	0.9898000D+00
0.1020000D-01	0.4413645D-01	0.1358380D+00	0.9898000D+00
0.1020000D-01	-0.1155507D+00	0.8395253D-01	0.9898000D+00
0.1020000D-01	-0.1155507D+00	-0.8395253D-01	0.9898000D+00
0.1020000D-01	0.4413645D-01	-0.1358380D+00	0.9898000D+00
0.1030000D-01	0.1435270D+00	0.0000000D+00	0.9897000D+00
0.1030000D-01	0.4435228D-01	0.1365023D+00	0.9897000D+00
0.1030000D-01	-0.1161158D+00	0.8436305D-01	0.9897000D+00
0.1030000D-01	-0.1161158D+00	-0.8436305D-01	0.9897000D+00
0.1030000D-01	0.4435228D-01	-0.1365023D+00	0.9897000D+00
0.1040000D-01	0.1442221D+00	0.0000000D+00	0.9896000D+00
0.1040000D-01	0.4456706D-01	0.1371633D+00	0.9896000D+00
0.1040000D-01	-0.1166781D+00	0.8477159D-01	0.9896000D+00
0.1040000D-01	-0.1166781D+00	-0.8477159D-01	0.9896000D+00
0.1040000D-01	0.4456706D-01	-0.1371633D+00	0.9896000D+00
0.1050000D-01	0.1449138D+00	0.0000000D+00	0.9895000D+00
0.1050000D-01	0.4478082D-01	0.1378212D+00	0.9895000D+00
0.1050000D-01	-0.1172377D+00	0.8517818D-01	0.9895000D+00
0.1050000D-01	-0.1172377D+00	-0.8517818D-01	0.9895000D+00
0.1050000D-01	0.4478082D-01	-0.1378212D+00	0.9895000D+00
0.1060000D-01	0.1456022D+00	0.0000000D+00	0.9894000D+00
0.1060000D-01	0.4499355D-01	0.1384759D+00	0.9894000D+00
0.1060000D-01	-0.1177947D+00	0.8558282D-01	0.9894000D+00
0.1060000D-01	-0.1177947D+00	-0.8558282D-01	0.9894000D+00
0.1060000D-01	0.4499355D-01	-0.1384759D+00	0.9894000D+00
0.1070000D-01	0.1462874D+00	0.0000000D+00	0.9893000D+00
0.1070000D-01	0.4520529D-01	0.1391276D+00	0.9893000D+00
0.1070000D-01	-0.1183490D+00	0.8598557D-01	0.9893000D+00
0.1070000D-01	-0.1183490D+00	-0.8598557D-01	0.9893000D+00
0.1070000D-01	0.4520529D-01	-0.1391276D+00	0.9893000D+00
0.1080000D-01	0.1469694D+00	0.0000000D+00	0.9892000D+00
0.1080000D-01	0.4541604D-01	0.1397762D+00	0.9892000D+00
0.1080000D-01	-0.1189007D+00	0.8638644D-01	0.9892000D+00
0.1080000D-01	-0.1189007D+00	-0.8638644D-01	0.9892000D+00
0.1080000D-01	0.4541604D-01	-0.1397762D+00	0.9892000D+00
0.1090000D-01	0.1476482D+00	0.0000000D+00	0.9891000D+00
0.1090000D-01	0.4562581D-01	0.1404218D+00	0.9891000D+00
0.1090000D-01	-0.1194499D+00	0.8678545D-01	0.9891000D+00
0.1090000D-01	-0.1194499D+00	-0.8678545D-01	0.9891000D+00
0.1090000D-01	0.4562581D-01	-0.1404218D+00	0.9891000D+00
0.1100000D-01	0.1483240D+00	0.0000000D+00	0.9890000D+00
0.1100000D-01	0.4583463D-01	0.1410645D+00	0.9890000D+00
0.1100000D-01	-0.1199966D+00	0.8718264D-01	0.9890000D+00
0.1100000D-01	-0.1199966D+00	-0.8718264D-01	0.9890000D+00
0.1100000D-01	0.4583463D-01	-0.1410645D+00	0.9890000D+00
0.1110000D-01	0.1489966D+00	0.0000000D+00	0.9889000D+00
0.1110000D-01	0.4604250D-01	0.1417042D+00	0.9889000D+00
0.1110000D-01	-0.1205408D+00	0.8757803D-01	0.9889000D+00
0.1110000D-01	-0.1205408D+00	-0.8757803D-01	0.9889000D+00
0.1110000D-01	0.4604250D-01	-0.1417042D+00	0.9889000D+00
0.1120000D-01	0.1496663D+00	0.0000000D+00	0.9888000D+00
0.1120000D-01	0.4624943D-01	0.1423411D+00	0.9888000D+00
0.1120000D-01	-0.1210826D+00	0.8797164D-01	0.9888000D+00
0.1120000D-01	-0.1210826D+00	-0.8797164D-01	0.9888000D+00
0.1120000D-01	0.4624943D-01	-0.1423411D+00	0.9888000D+00

```
0.1419000D+00 -0.4309867D+00 -0.3131301D+00  0.8581000D+00
0.1419000D+00  0.1646223D+00 -0.5066552D+00  0.8581000D+00
0.1420000D+00  0.5329165D+00  0.0000000D+00  0.8580000D+00
0.1420000D+00  0.1646803D+00  0.5068337D+00  0.8580000D+00
0.1420000D+00 -0.4311385D+00  0.3132405D+00  0.8580000D+00
0.1420000D+00 -0.4311385D+00 -0.3132405D+00  0.8580000D+00
0.1420000D+00  0.1646803D+00 -0.5068337D+00  0.8580000D+00
```

Appendix E.2

Appendix F

For comparison of efficiency in regards to calculating the bond-length, we generate the following formula embodied earlier in Chap. 4

$$| P \overset{\frown}{-} p_1 | = \theta R \tag{1}$$

where

$$\theta = \tan^{-1} \frac{p}{R(1 - f)} = \tan^{-1} \frac{R\sqrt{2f}}{R(1 - f)}$$

and for sufficiently small θ

$$\frac{\sqrt{2f}}{1 - f} \sim \sqrt{2f}\,(1 + f) + \bigcirc\left(f^2\right). \tag{2}$$

Also

$$\begin{aligned} | P - p_1 | &= \sqrt{h^2 + p^2} = \sqrt{R^2 f^2 + 2f R^2} = \sqrt{R^2 (f^2 + 2f)} \\ &= R\sqrt{2f}\left(1 + \frac{f}{2}\right)^{1/2} \sim R\sqrt{2f}\left(1 + \frac{f}{4}\right), \end{aligned} \tag{3}$$

such that f that generates

$$\frac{| P \overset{\frown}{-} p_1 |}{| P - p_1 |} = \frac{1 + f}{1 + \frac{f}{4}} \sim 1 + \frac{3f}{4} + \bigcirc\left(f^2\right) \tag{4}$$

is 0.0519826. From this result, we deduce that spherical symmetry is as significant as the straight line nature of the bond-length since the difference between them is relatively small.

Appendix G

The algorithm of the Fortran program which we utilise in calculating the ratio $\delta \equiv \frac{d(6:6)}{d(6:5)}$ of the two characteristics C–C bond lengths as a function of shallownesss parameter f is illustrated in the next three pages. To start with

1. Fix the circumsphere radius R.

2. For $0.01 \leq f \leq 0.142$, calculate radius p as in (4.2.2) of the latitude circle since each of x, y coordinates of the pole pentagon may be expressed in terms of p where p.

3. Iterate the case for k=0 and k=1 since k enters into the angle of rotation about the pole pentagon.
   If k=0 then

   (a) calculate x, y and z coordinates for p_1 of the pole pentagons, defined in terms of column vector v(1,1), v(2,1) and v(3,1).

   (b) perform a matrix multiplication of 3 X 3 matrix M (constitute of the direction ratios H:K:L) with the column vector in (a). This provides coordinates of a_{11}.

   (c) substract the x, y and z coordinates of p_1, thereby giving rise to the bond length d(6:6). For brevity, a variable name sigma is assigned to d(6:6).

   (d) proceed to the case k=1.

   If k=1 then

   (a) same statements as in (a) for k=0.

(b) compute the distance $\mid p_1 - p_2 \mid$ as depicted in (4.2.5) which provides the bond length d(6:5). Again for brevity, a variable name lambda is assigned to d(6:5). Then ratio of interest δ i.e sigma/lambda (corresponding with the Fortran variable name) is derived.

4. Repeat the same process until arriving at the limiting value of f i.e. $f = 0.142$.

Finally, Table A displays the numerical results which have significant role in analysing some models of the buckyball configuration.

Appendix G

```
c                     PROGRAM carbon.f
c
c     input:
c             f - non-dimensional parameter between the interval
c                 0.010 and 0.142
c
c            pi - angle calculated in radian
c
c     output:
c             p - circumradius of the latitude circle forming the
c                 base of the spherical pole pentagon
c
c         sigma - carbon bond joining two neighbouring spherical
c                 regular pentagon---"d(6:6) without
c                 reference to R(radius of the buckyball)"
c
c        lambda - carbon bond joining two neigbouring atoms within
c                 spherical regular pentagon---"d(6:5) without
c                 reference to R(radius of the buckyball)"
c
c         delta - ratio of d(6:6) to d(6:5)
c
c     subroutine required:  vector,matvec,difvec
c
c           function used:  dist1
c
c     This program determines the value of f as a function parameter R
c     in which delta=0.956, delta for natural buckyball;
c              delta=1.000, delta for graphite layer;
c              delta=0.000, delta for dodecahedron.
c
c-----------------------------------------------------------------------72
c
      double precision p,pi,x,y,z,b1,b2,b3,b(3,1),m(3,3),v(3,1),l(3,1),
     +                 theta,dcos,dsin,datan,dist1,sigma,lambda,delta
      common b1,b2,b3
      real f
      integer k
c
      pi=4.0d0*datan(1.0d0)
      write(*,'(11x,"f",13x,"d",11x,"d(6:6)",8x,"d(6:5)")')
      write(*,'(37x,"w/o R",9x,"w/o R")')
c
        do 20 f=0.010,0.142,0.001
              p=sqrt(2.0d0*dble(f))
        do 30 k=0,1
        theta=((pi*dble(k))*2.0d0)/5.0d0
        if(theta.eq.0.0d0)then
            x=p*dcos(0.0d0)
            y=p*dsin(0.0d0)
            z=1.0d0-dble(f)
            call vector(x,y,z,v)
            call matvec(m,v,l)
            call difvec(l,v,b)
            sigma=dist1(b1,b2,b3)
         else
            x=p*dcos(theta)
            y=p*dsin(theta)
            z=1.0d0-dble(f)
            lambda=(2.0d0*sqrt(2.0d0*dble(f)))*dsin(pi/5.0d0)
             delta=sigma/lambda
         end if
   30    continue
         write(6,33)f,delta,sigma,lambda
   33    format(4(F14.3))
   20   continue
```

```
       stop
       end
c
c-----------------------------------------------------------------------
c
       subroutine vector(x,y,z,v)
       double precision x,y,z,v(3,1)
       integer n
c
c      This subprogram stores the x,y,z coordinate of p1 and etc as
c      one dimensional array v(n,1)
c
       do 50 n=1,3
         if(n.eq.1)then
            v(n,1)=x
         else if(n.eq.2)then
            v(n,1)=y
         else
            v(n,1)=z
         end if
    50 continue
       return
       end
c
c-----------------------------------------------------------------------
c
       subroutine matvec(m,v,l)
       double precision m(3,3),v(3,1),l(3,1)
       integer i
c
c      This subprogram computes the matrix multiplication:l=m*v by
c      incorporating the direction-ratios H:K:L as matrix m, so
c      providing e.g. the coordinate transformation of p1 into a11
c
       do 50 i=1,2
       m(i,i+1)=0.0d0
       m(i+1,i)=0.0d0
    50 continue
       m(2,2)=-1.0d0
       m(1,1)=(-(5.0d0)**0.5)/5.0d0
       m(1,3)=(2.0d0*((5.0d0)**0.5))/5.0d0
       m(3,1)=(2.0d0*((5.0d0)**0.5))/5.0d0
       m(3,3)=((5.0d0)**0.5)/5.0d0
       l(1,1)=m(1,1)*v(1,1)+m(1,2)*v(2,1)+m(1,3)*v(3,1)
       l(2,1)=m(2,1)*v(1,1)+m(2,2)*v(2,1)+m(2,3)*v(3,1)
       l(3,1)=m(3,1)*v(1,1)+m(3,2)*v(2,1)+m(3,3)*v(3,1)
       return
       end
c
c-----------------------------------------------------------------------
c
       subroutine difvec(l,v,b)
       double precision v(3,1),l(3,1),b(3,1),b1,b2,b3
       common b1,b2,b3
c
c      Here we calculates the difference between the x,y,z
c      coordinates of p1 and the corresponding x,y,z
c      coordinates of a11
c
       b(1,1)=l(1,1)-v(1,1)
       b(2,1)=l(2,1)-v(2,1)
       b(3,1)=l(3,1)-v(3,1)
           b1=b(1,1)
           b2=b(2,1)
           b3=b(3,1)
       return
```

```
      end
c
c-------------------------------------------------------------------
c
      double precision function dist1(b1,b2,b3)
      double precision b1,b2,b3
c
c     Here we calculates the bond length d(6:6)
c
      dist1=sqrt((b1)**2+(b2)**2+(b3)**2)
      return
      end
```

Appendix G

Table A

f	δ	d(6:6) w/o R	d(6:5) w/o R
0.010	4.814	0.800	0.166
0.011	4.517	0.788	0.174
0.012	4.257	0.775	0.182
0.013	4.028	0.763	0.190
0.014	3.823	0.752	0.197
0.015	3.639	0.741	0.204
0.016	3.473	0.730	0.210
0.017	3.321	0.720	0.217
0.018	3.182	0.710	0.223
0.019	3.054	0.700	0.229
0.020	2.935	0.690	0.235
0.021	2.825	0.681	0.241
0.022	2.723	0.671	0.247
0.023	2.627	0.662	0.252
0.024	2.537	0.653	0.258
0.025	2.453	0.645	0.263
0.026	2.373	0.636	0.268
0.027	2.298	0.628	0.273
0.028	2.227	0.619	0.278
0.029	2.159	0.611	0.283
0.030	2.095	0.603	0.288
0.031	2.034	0.595	0.293
0.032	1.975	0.587	0.297
0.033	1.919	0.580	0.302
0.034	1.866	0.572	0.307
0.035	1.815	0.565	0.311
0.036	1.766	0.557	0.315
0.037	1.719	0.550	0.320
0.038	1.674	0.542	0.324
0.039	1.630	0.535	0.328
0.040	1.589	0.528	0.333
0.041	1.548	0.521	0.337
0.042	1.509	0.514	0.341
0.043	1.472	0.507	0.345
0.044	1.435	0.501	0.349
0.045	1.400	0.494	0.353
0.046	1.366	0.487	0.357
0.047	1.333	0.480	0.360
0.048	1.301	0.474	0.364
0.049	1.270	0.467	0.368
0.050	1.240	0.461	0.372
0.051	1.211	0.454	0.375
0.052	1.182	0.448	0.379
0.053	1.154	0.442	0.383
0.054	1.127	0.436	0.386
0.055	1.101	0.429	0.390
0.056	1.076	0.423	0.393
0.057	1.051	0.417	0.397
0.058	1.027	0.411	0.400
0.059	1.003	0.405	0.404
0.060	0.980	0.399	0.407
0.061	0.957	0.393	0.411
0.062	0.935	0.387	0.414
0.063	0.914	0.381	0.417
0.064	0.893	0.375	0.421
0.065	0.872	0.370	0.424
0.066	0.852	0.364	0.427
0.067	0.832	0.358	0.430
0.068	0.813	0.353	0.434
0.069	0.794	0.347	0.437
0.070	0.776	0.341	0.440
0.071	0.758	0.336	0.443
0.072	0.740	0.330	0.446
0.073	0.723	0.325	0.449

Table A

0.074	0.706	0.319	0.452
0.075	0.689	0.314	0.455
0.076	0.673	0.308	0.458
0.077	0.656	0.303	0.461
0.078	0.641	0.297	0.464
0.079	0.625	0.292	0.467
0.080	0.610	0.287	0.470
0.081	0.595	0.282	0.473
0.082	0.580	0.276	0.476
0.083	0.566	0.271	0.479
0.084	0.552	0.266	0.482
0.085	0.538	0.261	0.485
0.086	0.524	0.255	0.488
0.087	0.510	0.250	0.490
0.088	0.497	0.245	0.493
0.089	0.484	0.240	0.496
0.090	0.471	0.235	0.499
0.091	0.459	0.230	0.502
0.092	0.446	0.225	0.504
0.093	0.434	0.220	0.507
0.094	0.422	0.215	0.510
0.095	0.410	0.210	0.512
0.096	0.398	0.205	0.515
0.097	0.387	0.200	0.518
0.098	0.375	0.195	0.520
0.099	0.364	0.190	0.523
0.100	0.353	0.185	0.526
0.101	0.342	0.181	0.528
0.102	0.331	0.176	0.531
0.103	0.320	0.171	0.534
0.104	0.310	0.166	0.536
0.105	0.300	0.161	0.539
0.106	0.289	0.157	0.541
0.107	0.279	0.152	0.544
0.108	0.269	0.147	0.546
0.109	0.260	0.143	0.549
0.110	0.250	0.138	0.551
0.111	0.240	0.133	0.554
0.112	0.231	0.128	0.556
0.113	0.222	0.124	0.559
0.114	0.212	0.119	0.561
0.115	0.203	0.115	0.564
0.116	0.194	0.110	0.566
0.117	0.185	0.105	0.569
0.118	0.177	0.101	0.571
0.119	0.168	0.096	0.574
0.120	0.159	0.092	0.576
0.121	0.151	0.087	0.578
0.122	0.143	0.083	0.581
0.123	0.134	0.078	0.583
0.124	0.126	0.074	0.585
0.125	0.118	0.069	0.588
0.126	0.110	0.065	0.590
0.127	0.102	0.060	0.592
0.128	0.094	0.056	0.595
0.129	0.087	0.052	0.597
0.130	0.079	0.047	0.599
0.131	0.071	0.043	0.602
0.132	0.064	0.039	0.604
0.133	0.056	0.034	0.606
0.134	0.049	0.030	0.609
0.135	0.042	0.025	0.611
0.136	0.035	0.021	0.613
0.137	0.027	0.017	0.615
0.138	0.020	0.013	0.618
0.139	0.013	0.008	0.620

0.140	0.006	0.004	0.622
0.141	0.000	0.000	0.624

Table A

References And Bibliography

[1] H.S.M Coxeter (1969). *Introduction to GEOMETRY* second edition, Wiley.

[2] Polya And Szego (1969). *Parametric Inequalities*, Dover.

[3] D.R. Nelson and B.I. Halperin(1985). *Pentagonal and Icosahedral Order in Rapidly Cooled Metals*, Science 229, 233–238.

[4] M.A. Jaswon and M.A. Rose (1983). *CRYSTAL SYMMETRY: Theory of Colour Crystallography*, Ellis Horwood Series.

[5] D. Schattschneider (1990). *Visions of Symmetry: Notebooks, Periodic Drawings, and Related Work of M.C. Escher*, W.H. Freeman and company.

[6] H. Kroto et al. (1985). *C_{60}: Buckminsterfullerene*, Nature 318, 162–163.

[7] W. Krätschmer et al. (1990). *Solid C_{60}: a new form of carbon*, Nature 347, 354–357.

[8] G.S. Hammond and V.J. Kuck (1991). *Fullerenes:Synthesis, Properties, and Chemistry of Large Carbon Clusters*, 108–113, ACS Symposium Series.

[9] M.A. Jaswon (1965). *Mathematical Crystallography*, Longmans.

[10] R.H. Hammond (1987). *Introduction to FORTRAN 77 and The Personal Computer*, McGraw Hill.

[11] H. Balfour and D.H. Marwick (1979). *Programming in Standard FORTRAN 77*, Heinemann Educational Books.

[12] D. Topham (1990). *The First Book of UNIX*, Howard W. Sams and Company.

[13] D.M. Monro (1989). *A Crash Course in FORTRAN 77*, Edward Arnold.

[14] W.H. Press et al. (1992). *Numerical Recipes: The Art of Scientific Computing (Fortan Version)*, Cambridge University Press.

[15] I.O. Angell and G. Griffith (1977) *High-resolution Computer Graphics Using FORTRAN 77*, Macmillan.

[16] H. Kroto. *Crystal Structure and Bonding of Ordered* C_{60}., Nature 353, 147–149.

[17] H. Kroto. *Space, Stars,* C_{60} *and Soot*, Nature 242, 1139–1142.

[18] W. Krätschmer et al. (1990). *Characterization of the Soluble All-Carbon Molecules* C_{60} *and* C_{70}., J. Phys. Chemistry 94, 8630–8633.

[19] M. Ge and K. Sattler (1993). *Vapor-Condensation Generation and STM Analysis of Fullerene Tubes*, Science 260, 515-518.

[20] T. Fujiwara (1989). *Introduction to Quasicrystals*, Proceedings of the 12th Taniguchi Symposium, Japan, Springer Verlag.

[21] Felix Klein (1913). *Lectures on the Icosahedron and the Solution of Equation of the Fifth Degree*, Dover.

[22] F.C. Frank (1952). *Supercooling of Liquids*, Proc. R. Soc. London Ser. A215, 43–46.

[23] D. Schechtman et al. (1984). Phys. Rev. Lett. 53, 43–46.

[24] Marko V. Jarič (1988). *Introduction to Quasicrystals*, Volume 1, Academic Press.

[25] Marko V. Jarič (1988). *Mathematical Quasicrystals*, Volume 2, Academic Press.

[26] News Reports (1993). *Going Back to the Future With Small Synthetic Compounds*, Science 260, 910–911.

[27] BBC Horizon Series (Transcripts of Programme Transmitted 20th Jan. 1992). *Molecules with Sunglasses*, 1–26.

[28] R.F. Curl and R.E.Smalley (1991). *Fullerenes*, Scientific American, 32–41.

[29] P. Fowler (1991). *Aromaticity Revisited*, Nature 350, 20–21.